ALLOGRAFT MINERALIZED BONE PARTICLE/POLYURETHANE COMPOSITES FOR BONE TISSUE ENGINEERING

By

JERALD E. DUMAS

Dissertation

Submitted to the Faculty of the

Graduate School of Vanderbilt University

for the degree of

DOCTOR OF PHILOSOPHY

in

Chemical Engineering

December, 2010

Nashville, Tennessee

Approved:

Professor Peter Cummings

Professor Douglass LeVan

Professor G. Kane Jennings

Professor Ginger Holt

Professor Todd Boyce

Professor Scott Guelcher

To the late Walter and Emma Dumas.

To the Henry (late) and Lois White.

All for saying yes.

ACKNOWLEDGEMENTS

This thesis would not have been possible without the kind support of my thesis advisor, Dr. Scott Guelcher . I would like to thank him for his guidance, mentorship and for providing the opportunity to pursue a new research direction. I gratefully acknowledge my thesis committee members, Dr. Peter Cummings, Dr. Kane Jennings, Dr. Douglas LeVan, Dr. Todd Boyce and Dr. Ginger Holt for their support, informative discussions, and valuable suggestions.

I would also like to thank all of my collaborators and funding sources with whom I have worked with.

I am grateful for the membersof family (parents: Jed and Jean Dumas) and my friends for their support.

LIST OF FIGURES

Figure 1.1: Diagram of long bone. 3
Figure 1.2: Critical Cells involved in bone formation and resorption. 5
Figure 1.3: Reaction between a polyester triol and triisocyanate that produces a polyurethane. 12
Figure 2.1: Compressive properties of PUR/HA and PUR/TCP composites. 25
Figure 2.2A: SEM images of HA70, HA79, TCP70, and TCP70 composites. 26
Figure 2.3: In vitro degradation of PUR/HA and PUR/TCP composites. 27
Figure 2.4: Proliferation of 2T3 cells seeded on the surface of PUR/HA and PUR/TCP composites. 28
Figure 2.5: DNA amount of 2T3 cells cultured on PUR/HA and PUR/TCP composites surfaces. 28
Figure 2.6: Osteogenic differentiation of 2T3 cells seeded on PUR/HA and PUR/TCP composites. 29
Figure 2.7: X-rays of PUR/HA and PUR/TCP composites at week 4 after implantation in the distal femur of Sprague-Dawley rats. 30
Figure 2.8: Micro CT of PUR/HA and PUR/TCP composites at week4. 30
Figure 2.9: Histological pictures (HE staining) of PUR/HA and PUR/TCP composites at week 4. 32
Figure 2.10: Histological pictures (TRAP staining) of PUR/HA and PUR/TCP composites at week 4. 32
Figure 3.1: Characterization of rabbit mineralized particles. 51
Figure 3.2: Results from a fluorescein isothiocyanate (FITC) assay. 53
Figure 3.3: IR spectra of 6C3G1L600-SDBP composite (blue) and mineralized bone particles (red). 54
Figure 3.4: Distribution of allograft bone composites. 56
Figure 3.5: Radiographs of extracted rabbit distal femurs. 57
Figure 3.6: Histology at 2 weeks for 6C3G1L300-SDBP treatment group. 60
Figure 3.7: Low magnification (1.25X) histological sections of all treatment groups at 6 weeks. 61
Figure 3.8: Remodeling of allograft bone particles in 6C3G1L600-SDBP treatment group. 62
Figure 3.9: Histomorphometry of AMBP/PUR composites implanted *in vivo*. 63
Figure 3.10: The process of creeping substitution is accelerated by the presence of a continuous, percolated bone phase. 67
Figure 3.11: Low magnification histology (2.5x). 69
Figure 4.1: A schematic of the synthesis of injectable MBP/PUR composites. 91

Figure 4.2: Scanning electron microscopy images of allograft bone particles. 98
Figure 4.3: SDMBP/PUR scaffold porosity as a function of water concentration at varying concentrations of DMAEE. 101
Figure 4.4: Compressive stress–strain curves for the 38%, 47%, and 60% porosity scaffolds fabricated from SDMBP. 102
Figure 4.5: Compressive strengths of dry and wet 50 wt% (36 vol%) SDMBP/PUR scaffolds at porosities ranging from 30% to 60%. 103
Figure 4.6: Compressive moduli of dry and wet 50 wt% (36 vol%) SDMBP/PUR foam scaffolds at varying porosities. 103
Figure 4.7: Scanning electron microscopy images of SDMBP/PUR scaffolds. 105
Figure 4.8: The tack-free and working times of 50wt% SDMBP/PUR scaffolds with varying TEDA concentrations. 106
Figure 4.9: Initial dynamic viscosity of injectable MBP/PUR composites measured using an AR-G2 (TA Instruments) rheometer. 107
Figure 4.10: In vitro degradation of SDMBP/PUR scaffolds as a function of porosity. .108
Figure 4.11: Microcomputed tomography images of human-SDMBP/PUR bone void filler injected into plug defects in the distal femurs of athymic rats 109
Figure 4.12: Thin decalcified sections of the composite bone void filler injected in bilateral femoral plug defects in rats 110
Figure 4.13: Histology of implant of wounds closed after 15 minutes. 111
Figure 4.14: Histology of areas of new bone formation. 112
Figure 5.1: In vitro release kinetics of rhBMP-2 from BVF composite with 50% porosity and 47% AMBP 130
Figure 5.2: Surgical photos from the NZW rabbit calvaria CSD study 131
Figure 5.3: X-rays of rabbit calvaria at 6 and 12 weeks. 132
Figure 5.4: X-ray of (A) collagen with rhBMP-2 and (B) BVF composite with the incorporation of rhBMP-2 at 6 weeks. 133
Figure 5.5: Percent of defect area filled and density measurements as measure by CTAn software. 134
Figure 5.6: Percent of defect area filled and density measurements as measure by CTAn software. 135
Figure 5.7: Histology of untreated calvarium defect. 137
Figure 5.8: Histology of Norain treatment group in the calvarium defect 137
Figure 5.9: Histology of BVF composite treatment group in the calvarium defect at 6 weeks. 138
Figure 5.10: Histology of BVF composite treatment group at 12 weeks. 139
Figure 5.11: Histology of BVF composite treatment group with the incorporation of rhBMP-2 at 6 weeks. 139
Figure 5.12: Histology of collagen treatment group with the incorporation of rhBMP-2 at 6 weeks. 140

Figure 5.13: High magnification histology of BVF treatment group with the incorporation of rhBMP-2 at 6 weeks. 140
Figure 5.14: Histomorphometry of the BVF treatment groups. 141
Figure 6.1: Mechanical properties of AMBP/PUR putty system. 152
Figure 6.2: μCT images of AMBP/PUR composites. 155
Figure 6.3: Histology from the ABMP/PUR putty treatment group with no rhBMP-2. . 156
Figure 6.4: Critical interactions of AMBP/PUR putty. 158

LIST OF TABLES

Table 1.1: Cell types involved during bone repair. 6
Table 1.2: Terms used to describe biomaterials in bone tissue engineering. 7
Table 2.1: CaP treatment groups. 21
Table 3.1: AMBP/PUR composite formulations. 49
Table 3.2: Mechanical and swelling properties of bone/polymer composites. 55
Table 3.3: Takayanagi model calculations for compressive modulus of bone/polymer composites. 73
Table 4.1: Molecular Weight Distribution of Lysine Triisocyanate-Poly(Ethylene Glycol) Prepolymer. 96
Table 4.2: Characterization of Polyester Macrotriol. 96
Table 4.3: Characterization of Bovine and Human Allograft Bone Particles. 98
Table 5.1: Treatment groups for in vivo rabbit calvaria study. 129
Table 6.1: Treatment groups of *in vivo* rabbit study. 153
Table 7.1: Summary of PUR Composites 162

Table of Contents

DEDICATION ii

ACKNOWLEDGEMENTS iii

LIST OF FIGURES iv

LIST OF TABLES vii

CHAPTER I. 1

Introduction 1

Musculoskeletal Diseases 1

Bone Biology 1

Remodeling after Injury 5

Treatment 6

Polyurethanes 11

Research Objective 13

RERFENCES 15

CHAPTER II. 18

Synthesis, characterization, and remodeling of calcium phosphate (CaP)/PUR implants 18

Introduction 18

Materials and Methods 20

Results 24

Discussion 33

Conclusions 36

REFERENCES 37

CHAPTER III 41

Synthesis, characterization and remodeling of allograft mineralized bone particle/polyurethane implants in a rabbit distal femur model 41

Introduction 41

Materials and Methods 45

Results 50

Discussion 63
Conclusions 75
REFERENCES 76
CHAPTER IV. 83
Synthesis, characterization, and remodeling of porous allograft mineralized bone particle/polyurethane bone void filler in a rat model 83
Introduction 83
Methods and Materials 86
Results 94
Discussion 113
Conclusions 119
REFERENCES 120
CHAPTER V. 123
Remodeling of allograft mineralized bone particle/polyurethane bone void filler composite with recombinant human bone morphogenetic protein (rhBMP-2) in a rabbit calvarium model 123
Introduction 123
Materials and Methods 126
Results 130
Discussion 141
Conclusion 144
REFERENCES 145
CHAPTER VI. 149
Low-porosity injectable allograft bone/polymer biocomposites incorporating rhBMP-2 149
Introduction 149
Materials and Methods 150
Results 154
Discussion 156
Conclusions 158
REFERENCES 160
CHAPTER VII. 162

Conclusions 162

CHAPTER I.

Introduction

Musculoskeletal Diseases

Musculoskeletal disorders are a common occurrence throughout the United States as they can derive from several factors such as osteoporosis, arthritis, injuries, and infantile developmental conditions. Of self-reported primary medical conditions of adults in 2005, 48.3% involve a musculoskeletal disorder creating a huge impact on the economy due to lost work days[1-3]. This number is expected to grow as the U.S. population continues to age[1]. Former president George W. Bush declared the years of 2002-2011 as the United States Bone and Joint Decade in March 2002[1]. The challenge of developing strategies to combat this multifaceted problem crosses all scientific disciplines. In this work, a novel biomaterial for bone tissue engineering will be discussed as a treatment to help alleviate the burden of musculoskeletal diseases globally.

Bone Biology

Bone is a dynamic tissue that fulfills a critical role in the proper function of the body. As a major part of the skeletal system, bone has five major functions[4]: support, protection, movement, hematopoiesis, and mineral/energy storage. Bone forms the framework of the body that supports and protects the organs and soft tissues. In conjunction with muscle contraction, bones are levers that allow for movement around

joints. Red bone marrow cells in conjunction with platelets are formed within bone. Furthermore, bone stores both calcium and phosphorus that can be released as needed to other locations in the body[5,6]. Bone can also store energy as adipose cells of yellow bone marrow are also able to store energy within lipids.

There are four major categories of bone[4]: long, short, flat, and irregular. Long bones are typically found in the appendages, while short bones are found in small, compact spaces in the body. The shaft of long bones consists of the diaphysis, and each end of the bone is referred to as the epiphysis. These regions comprise of either cancellous (spongy) and cortical (compact) bone. Cortical bone surrounds cancellous bone in both epiphyseal regions. Cancellous bone, which contains red bone marrow, is a cell-rich region and it constantly undergoes remodeling[7]. The diaphysis, separated from the epiphysis by the epiphyseal line, contains the medullary cavity that has yellow blood marrow and nutrient vessels within it. The inner wall of this cavity is lined with a layer of connective tissue called the endosteum, and the outer wall is similarly covered with dense regular connective tissue to form the periosteum[4]. Cortical bone has a compressive strength and modulus in the range of 130-180 MPa and 12-18 GPa, respectively[8,9]. In contrast, cancellous bone has a compressive strength and modulus range of 4-12 MPa and 0.1-0.5 GPa, respectively. Flat bones are found around the skull and ribs. Odd shaped bones such as vertebrae comprise the irregular bones.

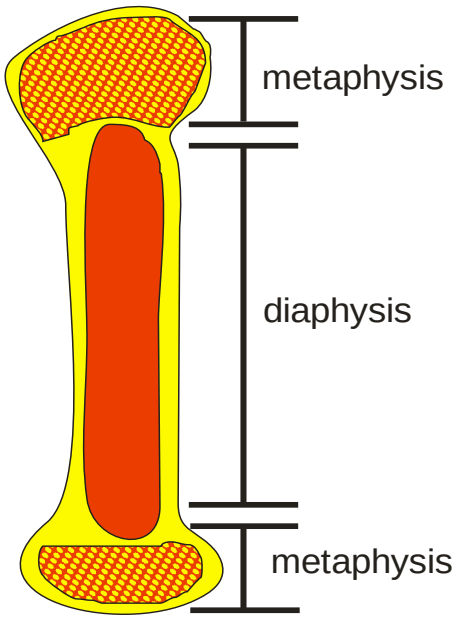

Figure I.1: Diagram of long bone.

Bone is a natural composite matrix that comprises of 70-80 wt% inorganic material, 20 wt% organic material, and a remaining balance of water[6,10,11]. Although cells and blood vessels comprise bone, the actual bone matrix is more than 90% of the total tissue[6]. Collagens are the predominant organic component in the bone matrix, which contribute to the tensile strength and flexibility of bone[6,11]. Growth factors such as bone morphogenetic protein, a protein that controls and supports the activity of bone cells, are also found in the bone matrix. Collagen in encompassed by the mineral of the inorganic matrix, containing apatite, carbonate ions, and acid phosphate groups[6]. The mineral phase of the bone matrix is responsible its hardness and stiffness[7,11]as well as its ion storage capabilities[5,6]. These ions are important in key biochemical reactions such as nerve conduction and muscle contraction[6].

Multiple cells are involved in bone formation; however, osteoblasts, osteoclasts, and osteocytes are three essential cells that have a direct role in maintaining critical balance of bone remodeling. Osteoblasts derive from ostoprogenitor cells that are found in bone canals, endosteum, and periosteum[6]. They are bone forming cells that are responsible for synthesis of the bone matrix as well as the regulation of the mineralization process[6,10,12]. By tightly aligning themselves on the surface of new bone, osteoblasts deposit new mineral. The unmineralized organic matrix that is secreted by the osteoblasts is called osteoid[6,7]. Osteoid is composed of 90% type I collagen and other bone proteins such as lipids[7]. Once surrounded by newly formed mineral matrix, osteoblasts differentiate into osteocytes, which form more than 90% of the cell population in adult bone[6,12]. Their oval shapes allow them to have contact with other cells, providing an intricate communication system throughout bone [7,12]. This communication system allows them to conduct cell-mediated mineral exchange as well as ion exchange[6,12]. Osteoclasts, the largest of the bone cells, are responsible for the resorption of bone. Stimulated monocytes are fused together to form multi-nucleated osteoclasts, which can have three to twenty nuclei[6]. Osteoclasts have ruffled borders which gives them increased surface area to resorb bone. Osteoclasts bind themselves to the surface of bone and pump transport protons into the sealed space reducing the pH from 7 to 4, which solubilizes the bone mineral[6]. Osteoclasts have the capability to divide into mononuclear cells once it has completed its resorption activity[6].

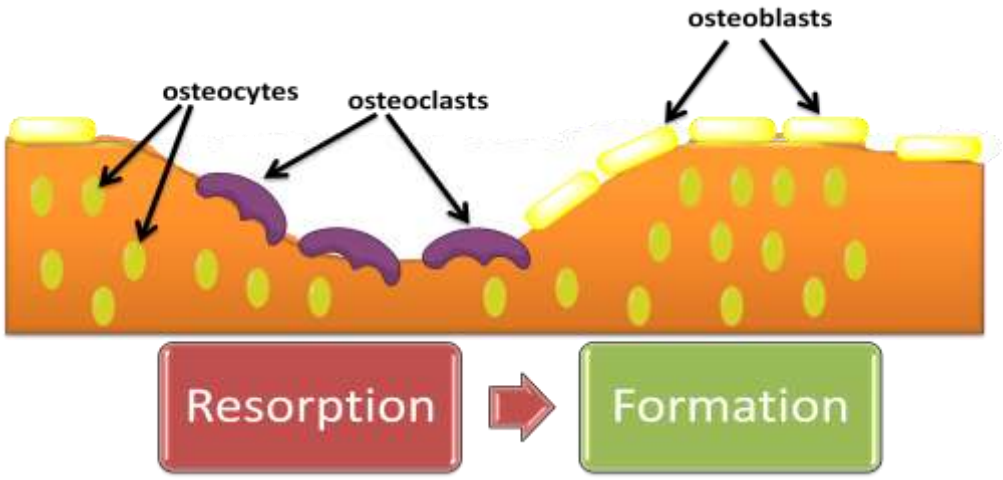

Figure I.2: Critical Cells involved in bone formation and resorption.

Remodeling after Injury

The healing mechanism of bone is dependent upon the site and type of injury. The healing of long bone fractures provides a generic process of the bone healing, which occurs in three overlapping phases: the early inflammatory stage, the repair stage, and the late remodeling stage[7]. In the early inflammatory stage, inflammatory cells such as monocytes and macrophages, invade the bone defect. Granulation tissue, temporary connective tissue, along with vascular tissue is formed and mesenchymal cells begin to migrate to the defect[7,13]. Fibroblasts begin to lay down stroma, and a callus, a mineralized collagen matrix, is formed around the repair site. The callus eventually transitions to woven bone, which is immature bone with randomly arranged collagen bundles. Woven bone is weak with respect to mature bone due to its lack of collagen organization[11,13,14]. During the late remodeling stage, woven bone is replaced with mature and subsequently strength is restored. The remodeling is guided by mechanical stress, and the duration of this stage can be from months to years[7,13].

Table I.1: Cell types involved during bone repair.

cell type	function
osteoblasts	responsible for the production of the bone matrix
osteoclasts	multinucleated giant cells with resorbing activity of mineralized tissue
osteocytes	mature osteoblasts within the bone matrix; responsible for bone maintenance
fibroblasts	responsible for synthesizing cartilage and extracellular matrix
monocytes	precursors to macrophages that are part of an immune response
macrophages	mononuclear cells that remove dead cell material
mesenchymal stem cells	undifferentiated cells that are precursors to the ostoblast cell type

Treatment

Substantial bone defects typically require treatment to facilitate proper healing. Furthermore, critical size defects will not heal without the aid of a biomaterial. Such biomaterials facilitate new bone formation via the following mechanisms: osteogenesis, osteoinduction, and osteoconduction. Osteogenesis involves the direct formation of bone matrix by osteoblasts already present in the biomaterial. Osteoinductive biomaterials stimulate bone formation via paracine signaling, communication of cells within the same proximity, from bone growth factors that are incorporated in the biomaterial. A biomaterial that acts as a scaffold, supporting cell adhesion, for new bone formation is osteoconductive. Biomaterials may possess a combination of these mechanisms.

Table I.2: Terms used to describe biomaterials in bone tissue engineering.

term	definition
biocompatibility	the lack of immunogenic response
osteoconductivity	the quality of a porous interconnected structure that permits new cells to attach, proliferate, and migrate
osteoinductivity	possessing the necessary proteins and growth factors that induce the progression of precursors toward osteblast lineage
osteointegration	a newly formed intimate bond with the implant and material

Bone derived graft is a common treatment that is used to treat defects. There are three categories of bone grafts: autograft, allograft, and xenograft. Autograft bone, considered the gold standard of treating bone defect, is a graft that is transplanted from one site to another site of the same individual. In general, autograft bone is considered to be osteogenic, but this is highly dependent upon the source of the autograft. Factors such as health and quality of bone can significantly affect the remodeling properties of autograft[15]. Cancellous autograft is porous and contains abundant host vessels and osteoblasts[16]. In contrast, cortical autograft is less porous and contains less osteoblasts than cancellous autograft, making it less osteogenic[15]. However, the strategy of using vascularized cortical autograft improves the osteogenic properties of the graft as it more resembles natural bone[15]. As more studies continue to show the safety of allograft bone[17], allograft bone is becoming an attractive option to treat defects. Allograft bone does not remodel via osteogenesis; however, it possesses osteoinductive properties with appropriate processing. Osteoinductive proteins can still be present in allograft

demineralized bone matrix (DBM) with the appropriate sterilization and storage techniques[17,18]. Cortical allograft bone is only osteoconductive as it has few cells or bone matrix proteins within its mineral matrix[7,15]. However, it possesses high initial strength due to its mineral content. Xenograft bone is transplanted between different species. Several studies have shown that xenograft bone is biocompatible as well as osteoconductive[19-21].

Bone Derived Graft Substitutes

As an alternative to bone grafts, several substitutes have been developed to mimic the properties of autograft. Thus, graft substitutes should be biocompatible, biodegradable, and possess mechanical integrity. In addition, the bone graft substitute should have an adequate shelf life, easily processed, and easily sterilized[22]. Multiple optional factors can enhance the performance of graft substitutes such as injectability, porosity, and incorporation of biologics such as growth factors. With all of these considerations in mind, several platforms have been used to obtain these properties.

Biodegradable Polymers

There are multiple natural and synthetic materials polymers that have been developed to treat bone defects. These materials are attractive as a biomaterial as they typically derive from natural resources with a reliable source of raw materials. Polymers are divided into two categories: natural and synthetic. Natural polymers such as type I collagen and hyaluronic acid have varying degradation times and are degraded through enzymatic mechanisms[23,24]. Type I collagen has mechanical properties in the range of trabecular bone, while hyaluronic acid has properties below it[23]. Polyesters such as poly(glycolide) (PGA), poly(lactide) (PLA), poly(glycolide) (PGA) and poly(ε-

caprolactone) (PCL) have been well studied as biodegradable orthopedic devices[22]. In clinical use, PLA and PGA have an established safe history with the FDA as several commercial products derived from these polymers have been approved[22]. Polyester polymers are synthesized from the ring opening reactions of their respective cyclic ester monomers[22]. These polymers undergo bulk hydrolytic degradation[22,23]. As these polymers have varying glass transition temperatures (Tg) and half-lives, they can be blended to produce polymers with different mechanical properties and degradation times. These mechanical properties can be in the range of trabecular bone[22,23]. These properties allow them to be suitable for applications such as bioresorbable screws, pins, and suture anchors. There are numerous other biodegradable polymers that are used as biomaterials[24] , but they mostly require external fixation if needed for load bearing applications. Furthermore, the bulk degradation that these polymers undergo can make it difficult to tune appropriate degradation rates. Rapidly degrading implants have been known to produce sinuses filled with fluid[25]. More slowly degrading amorphous polymeric implants can lead to crystallites that cause an inflammatory response[25] due to the small size of remnants[26].

Ceramics

As inorganic phase of bone provides the hardness of bone, ceramics are synthesized from inorganic, nonmetallic materials. Ceramics are attractive due to their high compressive strength. Calcium-based ceramics such as hydroxyapatite (HA) and tricalcium phosphate (TCP) are popular as it is possible to incorporate interconnected pores within the implant. Porous HA can created by several processes such as hydrothermal exchange of bone or naturally occurring coralline apatite [2728], while TCP is

made by homogenizing TCP powder with naphthalene[18,27]. HA is typically stronger than TCP; however, TCP is more soluble and readily to undergo biologic degradation[18]. HA and TCP have been shown to be effective in bridging long bone defect in animal models[27], but HA systems have been shown to slowly remodel in cancellous sites[18]. In contrast, TCP has exhibited rapid dissolution and resorption leading to poor structural properties[18]. The ions released from the dissolution of TCP can support osteoblastic bone formation, but can also cause systemic risk[27,29,30].

Calcium bone cements have been used for fracture augmentation in the hip, distal radius, and vertebral body [18,29]. Norian, one of several manufactured calcium phosphate cements, produces an injectable paste comprising of calcium phosphate cement which contains monocalcium phosphate, tricalcium phosphate, calcium carbonate, and a sodium phosphate solution [18,29]. Like HA and TCP, calcium phosphate cements can be brittle and have the potential to cause serious inflammatory reactions due to free ions in the mineral matrix[29]. Bioactive glass, which contains various oxides, has the ability to strongly bind with bone tissue[8]. Like calcium phosphates, bioactive glass can have strengths comparable to cortical bone[8]. However, bioactive glass is also reported to be brittle and often hard to machine for bone defects that are irregular in shape [4].

Composites

Integrating multiple biomaterials into one composite material utilizes the advantages of each constituent, while eliminating the potential disadvantages. Various fillers have been used in conjunction with polymeric technologies to form composites. Materials such as hydroxyapatite (HA) have been used as resorbable fillers. Composite intramedullary (IM) rods have been synthesized from HA and polylactide using

compression molding [31,32]. These IM rods ranged from 20-30% HA and exhibited bending strength and modulus up to 280 MPa and 7.8 GPa, respectively. Resorption and remodeling of new bone was observed after 5-7 years in a NZW rabbit femoral defect model. The results from this study indicate that polymer-based composites can meet both mechanical and biological targets. Bioactive glass/poly(ε-caprolactone-co-D,L-lactide) composites have been show to be injectable at a temperature range of 47-50 ˚C, which is not an ideal range. These injectable composites exhibit compressive strengths of 7.7 MPa and a Young's modulus of 153 MPa [33]. Young's modulus values as high as 13.6 GPa have been achieved using urethane dimethacrylate, 2-hydroxylethyl methacrylate, and a photosynthesizing agent [34].

Polyurethanes

Polyurethanes, a versatile material used for several applications, have been used for biomedical applications since 1960s and 1970s[35,36]. They are a versatile group of materials as it has a wide range of mechanical, physical, and biological properties. During the synthesis of polyurethanes, a nucleophilic reaction occurs between an isocyanate and polyol. In this reaction, the hydroxyl group of the polyol (nucleophile) reacts with the NCO group of the isocyanate (electrophile) to form a urethane bond. Isocyanates can react with alcohols, amines, and water. The reaction with water forms carbon dioxide gas, which forms pores throughout the material producing a porous foam.

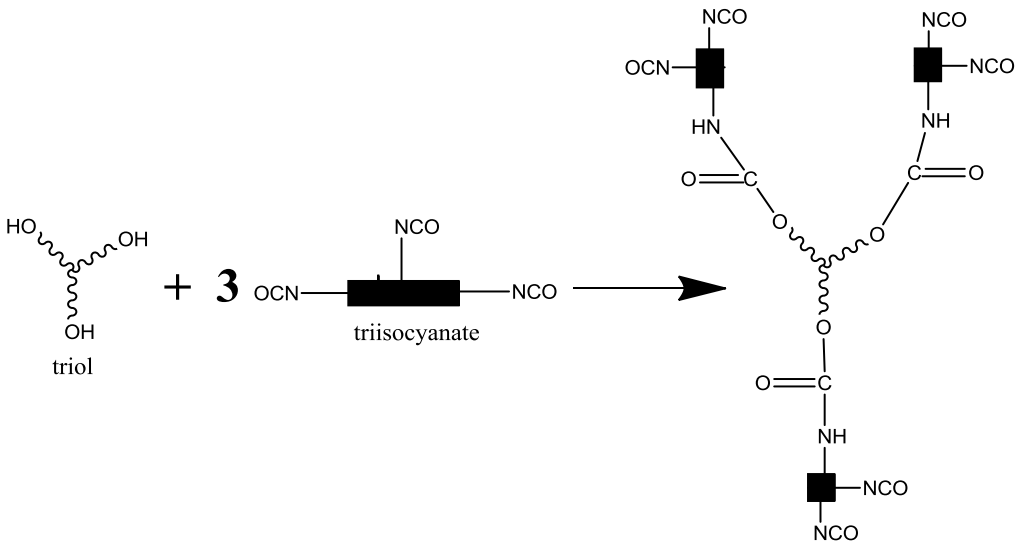

Figure I.3: Reaction between a polyester triol and triisocyanate that produces a polyurethane.

Isocyanates can be either aromatic or aliphatic. Although aromatic isocyanates are more active than allophatic isocyanates, aromatics are typically more toxic [36]. Normally, isocyanates are prepared as prepolymers or quasi-prepolymers prior to polyurethane synthesis. Prepolymers and quasi-prepolymers typically have a free NCO, unreacted isocyanate end groups, content of 1 to 15 wt% and 16 to 32 wt%, respectively [36]. These prepolymers are believed to enhance the mixing between the polyol and isocyanate phases[36]. Polyols, which can have a range of molecular weights, are synthesized using a starter molecule. The number of reactive hydroxyl groups on its ends is defined as its functionality. The ratio of monomer to starter controls the molecular weight of the polyol.

Polyurethane systems can be cast into various shapes using a reactive liquid molding process. In this process, the resin component (isocyanate or prepolymer) is mixed with the hardener component (polyol and catalyst). The hardener component can

also include fillers, water, and surfactants. The polyurethane index is the ratio of NCO equivalents to hydroxyl equivalents multiplied by 100. The equivalent weigh is the weight of the functional groups. Typically, the index for polyurethanes vary from 100 to 125[36].

The characterization of polyester-urethanes has been widely studied[35,36]. These polyurethanes degrade hydrolytically, but the presence of enzymes in the physiological environment can also contribute to degradation[35]. Microphase separation is common as the polyol component, which creates a soft segment with a typical has a melting point of less than 30 °C[35,36]. In contrast, the hard segment (isocyanate), has a melting point of greater than 100 °C. As soft segments have mobility, polyurethanes have the capacity to adapt to their environment with hard segments being polar and soft segments being non-polar[35].

Research Objective

In this research, a polyurethane composite system based from lysine-derived isocyanates, polyester polyols, and fillers was studied as a family of novel biomaterials for bone tissue engineering. As this is a versatile system, it is desirable that these materials span a wide range of mechanical properties and physical structures to support various bone tissue engineering applications. The PUR composite system should be both implantable and injectable. Furthermore, the PUR composite system should be both osteoconductive and osteoinductive.

To achieve these objectives the following approach was taken:

-Synthesis, characterization, and remodeling of calcium phosphate (CaP)/PUR implants (Chapter 2)

- Remodeling of AMBP/PUR implants in a rabbit distal femur model (Chapter 3)

-Synthesis, characterization, and remodeling of porous AMBP/PUR BVF in a rabbit calvarium model (Chapter 4)

-Remodeling of AMBP/PUR BVF with rhBMP-2 in a rabbit calvarium model (Chapter 5)

RERFENCES

1. United States Bone and Joint Decade: The Burden of Musculoskeletal Diseases in the United States. Rosemont, IL; 2008.

2. Yelin EH, Felts WR. A summary of the impact of musculoskeletal conditions in the united states. Arthritis & Rheumatism 1990;33(5):750-755.

3. Lubeck DP. The costs of musculoskeletal disease: health needs assessment and health economics. Best Practice & Research Clinical Rheumatology 2003;17(3):529-539.

4. Seeley RR. Anatomy & Physiology. Dubuque, IA: McGraw-Hill; 2008.

5. Copp DH, Shim SS. The homeostatic function of bone as a mineral reservoir. Oral Surgery, Oral Medicine, Oral Pathology 1963;16(6):738-744.

6. Buckwalter JA, Glimcher MJ, Cooper RR, Recker R. Bone biology. I: Structure, blood supply, cells, matrix, and mineralization. Instr Course Lect 1996;45:371-86.

7. Kalfas IH. Principles of bone healing. Neurosurg Focus 2001;10(4):E1.
8. Rezwan K, Chen QZ, Blaker JJ, Boccaccini AR. Biodegradable and bioactive porous polymer/inorganic composite scaffolds for bone tissue engineering. Biomaterials 2006;27(18):3413-3431.

9. Bonzani IC, Adhikari R, Houshyar S, Mayadunne R, Gunatillake P, Stevens MM. Synthesis of two-component injectable polyurethanes for bone tissue engineering. Biomaterials 2007;28(3):423-433.

10. Buckwalter JA, Cooper RR. Bone structure and function. Instr Course Lect 1987;36:27-48.

11. Wagner SWaHD. The Material Bone: Structure-Mechanical Function Relations. Annu. Rev. Mater. Sci. 1998(28):271-98.

12. JA Buckwalter MG, RR Cooper, R Recker. Bone Biology. J. Bone Joint Surg Am. 1995;77:1276-1289.

13. Frost HM. The Biology of Fracture Healing: An Overview for Clinicians. Part I: Clinical Orthopaedics & Related Research November 1989;248:283-293.

14. Rho JY, Kuhn-Spearing L, Zioupos P. Mechanical properties and the hierarchical structure of bone. Med Eng Phys 1998;20(2):92-102.

15. Stevenson S. Biology OF Bone Grafts. Orthopedic Clinics of North America 1999;30(4):543-552.

16. Marx RE. Bone and Bone Graft Healing. Oral and Maxillofacial Surgery Clinics of North America 2007;19(4):455-466.

17. Boyce T, Edwards J, Scarborough N. Allograft Bone: The Influence of Processing on Safety and Performance. Orthopedic Clinics of North America 1999;30(4):571-581.

18. Sammarco VJ, Chang L. Modern issues in bone graft substitutes and advances in bone tissue technology. Foot and Ankle Clinics of North America 2002;7(1):19-41.

19. Vouros I, Aristodimou E, Konstantinidis A. Guided tissue regeneration in intrabony periodontal defects following treatment with two bioabsorbable membranes in combination with bovine bone mineral graft. Journal of Clinical Periodontology 2004;31(10):908-917.

20. Su-Gwan K, Hak-Kyun K, Sung-Chul L. Combined implantation of particulate dentine, plaster of Paris, and a bone xenograft (Bio-Oss®) for bone regeneration in rats. Journal of Cranio-Maxillofacial Surgery 2001;29(5):282-288.

21. Hämmerle CHF, Chiantella GC, Karring T, Lang NP. The effect of a deproteinized bovine bone mineral on bone regeneration around titanium dental implants®. Clinical Oral Implants Research 1998;9(3):151-162.

22. Middleton JC, Tipton AJ. Synthetic biodegradable polymers as orthopedic devices. Biomaterials 2000;21(23):2335-2346.

23. Khan Y, Yaszemski MJ, Mikos AG, Laurencin CT. Tissue Engineering of Bone: Material and Matrix Considerations. J Bone Joint Surg Am 2008;90(Supplement_1):36-42.

24. Nair LS, Laurencin CT. Biodegradable polymers as biomaterials. Progress in Polymer Science;32(8-9):762-798.

25. An YH, Woolf SK, Friedman RJ. Pre-clinical in vivo evaluation of orthopaedic bioabsorbable devices. Biomaterials 2000;21(24):2635-2652.

26. Thomas C, Gupta V, Ahsan F. Particle Size Influences the Immune Response Produced by Hepatitis B Vaccine Formulated in Inhalable Particles. Pharmaceutical Research;27(5):905-919.

27. Rush SM. Bone Graft Substitutes: Osteobiologics. Clinics in Podiatric Medicine and Surgery 2005;22(4):619-630.

28. Ivankovic H, Gallego Ferrer G, Tkalcec E, Orlic S, Ivankovic M. Preparation of highly porous hydroxyapatite from cuttlefish bone. Journal of Materials Science: Materials in Medicine 2009;20(5):1039-1046.

29. Lieberman IH, Togawa D, Kayanja MM. Vertebroplasty and kyphoplasty: filler materials. Spine J 2005;5(6 Suppl):305S-316S.

30. Sauter D, Goldfrank L, Charash BD. Cardiopulmonary arrest following an infusion of calcium 2-amino ethanol phosphate. J Emerg Med 1990;8(6):717-20.

31. Hasegawa S, Ishii S, Tamura J, Furukawa T, Neo M, Matsusue Y, Shikinami Y, Okuno M, Nakamura T. A 5-7 year in vivo study of high-strength hydroxyapatite/poly(l-lactide) composite rods for the internal fixation of bone fractures. Biomaterials 2006;27(8):1327-1332.

32. K. Goto SS, S. Fujibayashi, J. Tamura, K. Kawanabe, S. Hasegawa, R. Kowalski, T. Nakamura. The biocompatibility and osteoconductivity of a cement containing beta-TCP for use in vertebroplasty. Journal of Biomedical Materials Research Part A 2006;78A(3):629-637.

33. Aho AJ, Tirri T, Kukkonen J, Strandberg N, Rich J, Seppälä J, Yli-Urpo A. Injectable bioactive glass/biodegradable polymer composite for bone and cartilage reconstruction: Concept and experimental outcome with thermoplastic composites of poly(ε-caprolactone-co-D,L-lactide) and bioactive glass S53P4. Journal of Materials Science: Materials in Medicine 2004;15(10):1165-1173.

34. Veronika A. Koleganova SMB, S. Jeffrey Dixon, Amin S. Rizkalla. Bioactive glass/polymer composite materials with mechanical properties matching those of cortical bone. Journal of Biomedical Materials Research Part A 2006;77A(3):572-579.

35. Santerre JP, Woodhouse K, Laroche G, Labow RS. Understanding the biodegradation of polyurethanes: From classical implants to tissue engineering materials. Biomaterials 2005;26(35):7457-7470.

36. Scott Guelcher JH. An Introduction to Biomaterials. Boca Raton: CRC Press; 2006. 553 p.

CHAPTER II.

Synthesis, characterization, and remodeling of calcium phosphate (CaP)/PUR implants

Introduction

Calcium phosphates (CaP) have been extensively investigated for treating osseous defects. Hydroxyapatite (HA) and tricalcium phosphate (TCP) have been shown to be osteoconductive [1]. Bone comprises approximately 70% mineral content, which is primarily HA [2]. Thus because of its natural presence in bone, synthetic HA is an attractive bone substitute. HA is prepared from the hydrothermal conversion of bone or naturally occurring coralline apatite, and it can be synthesized with variable porosity [3]. TCP is a biocompatible and bioactive ceramic that has been demonstrated to bond to bone directly [4,5]. While HA bone cements exhibit compressive strengths in the range of 4-50 MPa [6,7], TCP has a significantly lower strength than HA [3]. Despite their favorable biocompatibility and osteoconductivity, both HA and TCP are subject to brittle fracture and graft migration, potentially requiring additional surgeries for repair or removal [3,8,9].

CaP/polymer composites have been synthesized to reduce the brittleness of CaP as well as increase the bioactivity of the polymer [8]. Multiple polymeric systems have been used to prepare CaP composites with varying porosities and compositions [10]. HA/chitosan/PLA composites synthesized using *in situ* precipitation with 50-80 wt% HA exhibited compressive elastic modulus and strength values in the range of 416-857 MPa and 166-256 MPa, respectively [11]. HA/PLA composites synthesized using solvent

casting at lower HA contents (30-40 wt%) had a bending strength and modulus as high as 269 MPA and 7.6 GPa, respectively [12-15]. These composites remodeled almost completely when implanted in rabbit distal femurs after 5-7 years [12].

Two-component biodegradable polyurethanes (PUR) offer several advantages in the synthesis of CaP composites. PUR systems based on lysine polyisocyanates are biocompatible and degrade to non-toxic breakdown products [16-21]. Furthermore, they comprise a reactive system that is suitable for injectable applications [20,22]. TCP/PUR composites (10 wt% β-TCP) prepared from lysine ethyl ester diisocyanate (ELDI) exhibited compressive modulus and strength of 2.3 GPa and 139 MPa, respectively [21], and supported appositional bone growth and remodeling when injected into femoral cortical defects in sheep [22]. PUR chemistry also enables interfacial binding between the polymer and filler phases, as we have shown in composites prepared from lysine triisocyanate (LTI) and allograft bone particles [19]. While CaP/polymer composites incorporating relatively low volume fractions of CaP support cellular infiltration and new bone formation, remodeling of these materials proceeds slowly (e.g., 5 – 7 years for complete remodeling). In contrast, PUR composites utilizing mineralized allograft bone particles at concentrations above the random close packing (RCP) limit of 64 vol% supported rapid (e.g., 6 weeks) infiltration and remodeling by providing a pathway for cellular infiltration as osteoclasts resorb the filler phase [19]. In the present study, we fabricated CaP/PUR composites with the CaP filler content exceeding the RCP limit to promote cellular infiltration and remodeling. PUR composites were synthesized from both HA and β-TCP to investigate the mechanical properties, *in vitro* cellular response, and *in vivo* bioactivity when implanted in femoral defects in rats.

Materials and Methods

Materials

Lysine triisocyanate (LTI) was purchased from Kyowa Hakko (New York, NY). Tegoamin 33, a tertiary amine catalyst, was received from Goldschmidt (Hopewell, VA). Glycerol, stannous octoate, and ε-caprolactone were purchased from Sigma-Aldrich (St Louis, MO), and glycolide and DL-lactide were supplied by Polysciences (Warrington, PA). Hydroxyapatite (HA) (50-150 μm) and tri-calcium phosphate (TCP) (100-300 μm) were purchased from Berkley Biomaterials.

Fabrication of CaP/PUR Composites

A polyester polyol (600 MW) with a backbone of 60% caprolactone, 30% glycolide, and 10% lactide was synthesized using known methods. The components of the composite were mixed using a one-shot method, wherein the appropriate amounts of Tegoamin 33, polyester triol, CaP, and LTI were added to a 10 mL cup and mixed using a Hauschild SpeedMixer (FlackTek, Inc., Landrum, SC). The mixture speed was gradually ramped to 3300 rpm for one minute and mixing continued at 3300 rpm for 30s. The composites incorporated 79.0 wt% (66.2 vol%) CaP; composites incorporating 70.0 wt% (56.8 vol%) CaP were used in biomechanical testing for comparison. The reactive paste was transferred to a cylindrical mold, compressed to approximately 63,000 lbf for 50 minutes, de-molded to yield a green cylinder (6.1 mm diameter), and cured at 37˚C for twelve hours in a vacuum oven. The four formulations listed in Table 2.1 were synthesized to study mechanical properties, cellular infiltration, and remodeling in a rat femoral plug model.

Table II.1: CaP treatment groups.

Treatment	Filler	Filler wt%
HA70	hydroxyapatite	70
HA79	hydroxyapatite	79
TCP70	tricalcium phosphate	70
TCP79	tricalcium phosphate	79

Mechanical properties, Scanning electron microscopy, in vitro degradation

Cylindrical PUR/AMBP rods, approximately 6.3 x 12.6 mm (n = 3), were fabricated by compression molding. The rods were hydrated in PBS 24 hours prior to testing. The cylinders were placed between two fixed compression platens of an MTS 898 equipped with a 13 kN load cell, pre-loaded to approximately 12 N, and loaded at 24 mm min-1 until failure. Significant differences between treatement groups were determined by one-way ANOVA with bonferroni correction ($p<0.05$). Sample composites (approximately 5 mg) were mounted on a SEM pin stub mount and sputter-coated for 60 seconds using a Cressington Q108 sputter coater, which deposited gold at a 30 mA current. A Hitachi S-4200 scanning electron microscope was used to acquire images at a voltage of 10 kV.

The *in vitro* degradation rates of CaP/PUR composites were evaluated by measuring the mass loss at various time points up to 7 weeks of incubation of 10-mg samples (n=5) in 1 ml phosphate buffered saline (PBS; pH 7.4) at 37°C. At each time point, the samples were rinsed in deionized water, dried under vacuum for 48 h at room temperature, and weighed.

In vitro cell proliferation on CaP/PUR composites

Discs of approximately 250 μm in thickness were used for cell culture studies. The discs were cleaned and sterilized by sonicating in both deionized (DI) water and ethanol. Prior to seeding 2T3 cells (a clonal osteoblast cell line), the discs were washed with additional DI water and conditioned in incomplete alpha minimum essential media (α-MEM, Fisher Scientific). A cell number of 5×10^3 was seeded on each composite in 12-well tissue-culture polystyrene plates. Cells were cultured with α-MEM containing 10% fetal bovine serum (FBS, HyClone), and 1% penicillin/streptomycin (HyClone) at 37 ºC in a humidified incubator supplemented with 5% CO_2. The medium was changed every 2 days.

After 2 and 5 days, cell proliferation on CaP/PUR composites was evaluated. The cell-seeded scaffolds were washed with PBS, and 4 μM Calcein AM (Live/Dead Viability/Cytotoxicity Kit, Invitrogen-Molecular Probes) was added to the samples. Calcein AM dye is retained within live cells, imparting green fluorescence (excitation/emission: 495/515 nm). Cell proliferation was assessed qualitatively by fluorescent images acquired with an Olympus DP71 camera attached to a fluorescent microscope (Olympus CKX41, U-RFLT50). Osteoblastic cell proliferation on CaP/PUR composites was quantitatively evaluated using PicoGreen assays (n=4). After the cells were removed from the discs using 0.25% trypsin and 1 mM ethylenediaminetetraacetic acid (EDTA, Invitrogen), DNA content was measured using the Quant-iT PicoGreen dsDNA Assay kit (Invitrogen-Molecular Probes) according to the manufacturer's instructions. Fluorescence intensity was measured at excitation and emission wavelengths of 495 and 515 nm. Student's *t* test was performed for statistical comparison ($p<0.05$).

In vitro osteogenic differentiation on CaP/PUR composites

In vitro osteogenic differentiation of 2T3 cells cultured on CaP/PUR composites was evaluated (n=4). A cell number of 5 x 10^4 was seeded on CaP/PUR composites. After confluence, the cell-seeded scaffolds were cultured with osteogenic medium containing 2.5% FBS, 10 mM β-glycerophosphate (Sigma-Aldrich), and 100 μg/ml ascorbic acid phosphate (Wako, Osaka, Japan) for 7 days. The cells were removed from the CaP/PUR discs, washed with PBS and lysed with 0.1% Triton X-100. The cells were then subjected to three freeze/thaw cycles. The lysates (20μl) were added to 100μl of substrate buffer (2 mg/ml disodium p-nitrophenylphosphate hexahydrate and 0.75M 2-amino-2-methyl-1-propanol). After incubation of the mixtures at 37°C for 30 min, absorbance at 405 nm was measured. Alkaline phosphatase (ALP) activity was determined from a standard curve generated by employing the reaction of a p-nitrophenyl solution. The ALP activity was normalized by the total protein content determined using the BCA assay (Pierce). Student's *t* test was performed for statistical comparison ($p<0.05$).

In Vivo Rat Study

All surgical procedures were reviewed and approved by the Institutional Animal Care and Use Committee. Male Sprague–Dawley rats (Harlan Labs) aged 8 weeks (200–250 g) were used for this study. A monocortical plug bone defect with a diameter of 3mm was created in the distal region of the femur diaphysis, and a cylindrical CaP/PUR composite (3 x 5 mm) was implanted into the defect. After 4 weeks, the rats were sacrificed and the femurs removed and fixed in 10% phosphate-buffered formalin.

X-ray and μCT Analysis

Radiological analysis of the defect in the distal femur at week4 was performed using a Faxitron LX-60 x-ray system (Faxitron, 40kV at 8 s exposure time). Micro CT analysis was also performed using Scanco μCT40 (SCANCO Medical) at a voxel size of 24 μm. The X-ray source settings were 55 kVp and 145 mA with an integration time of 300 ms.

Histology

Rat bones were decalcified with 10% EDTA, dehydrated, embedded in paraffin, and sectioned at 5 μm thickness. The coronal slice sections were stained with hematoxylin and eosin (H&E). Specimens were examined under light microscopy. Tartrate resistant acid phosphastase (TRAP) staining was used to confirm the presence of osteoclasts.

Results

Mechanical properties, Particle size, In vitro degradation

Figure 2.1 summarizes the compressive modulus and strength values for the CaP/PUR composites, which ranged from 2.5-3.6 GPa and 59.6-87.0 MPa, respectively. HA/PUR composites exhibited significantly greater compressive modulus and strength than the TCP/PUR composites at both filler contents. However, the volume fraction of filler had no significant effect on compressive strength for either type of filler. Increasing the filler content for the β-TCP groups had no significant effect on the modulus unlike the effects seen for the HA group, where the modulus increased with filler content.

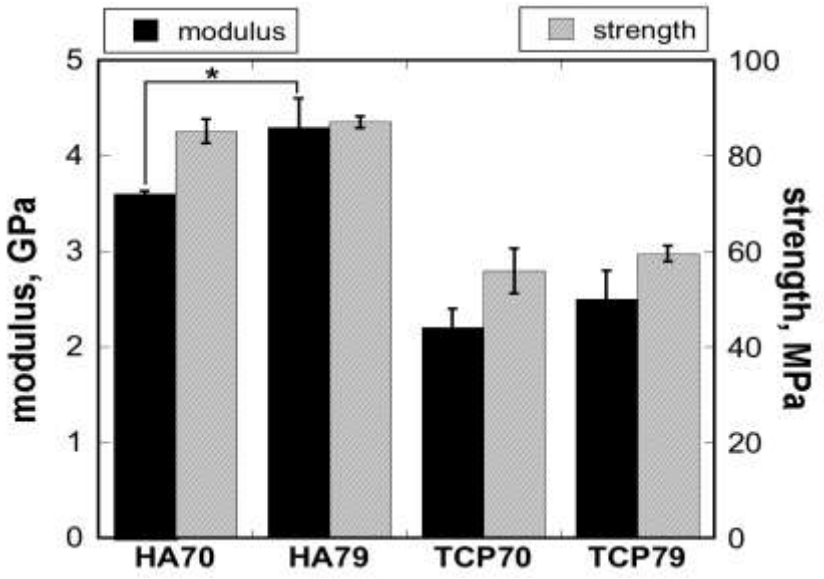

Figure II.1: Compressive properties of PUR/HA and PUR/TCP composites. HA70: 70 wt% HA, HA79: 79 wt% HA, TCP70: 70 wt% TCP, TCP79: 79 wt% TCP.

SEM images of the HA/PUR composites are shown in Figure 2.2. After compression molding, the particle size was reduced from 50 – 150 μm to <10 μm. Higher magnification views of the HAPUR (79 wt%) material reveal a large number of particles smaller than 1 μm (Figure 2.2B). These observations suggest that the process of compression molding resulted in attrition of the CaP particles and accompanied by a significant reduction in size .

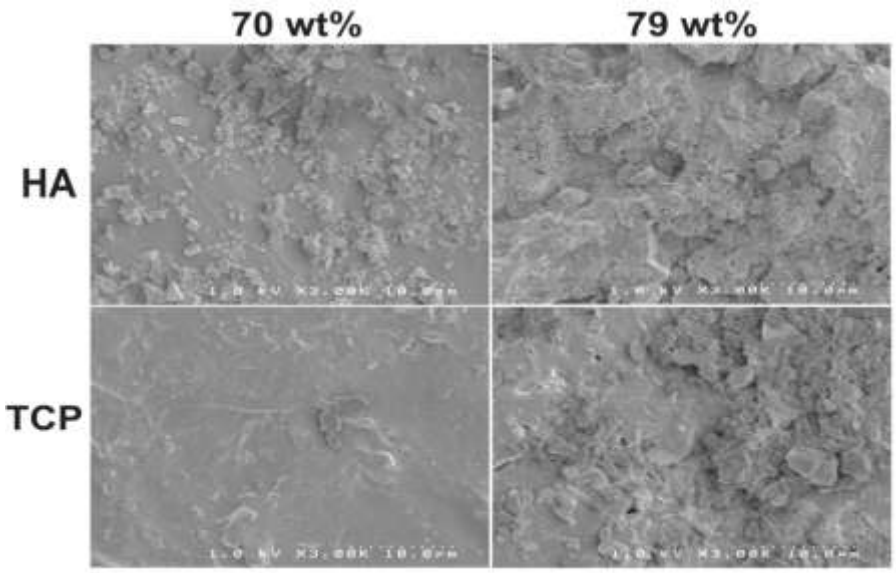

Figure II.2A: SEM images of HA70, HA79, TCP70, and TCP70 composites.

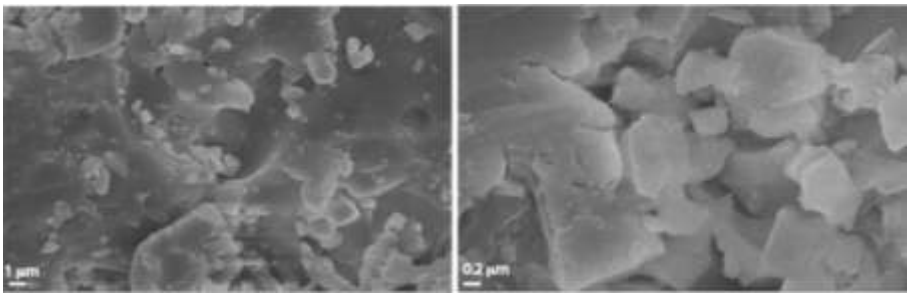

Figure 2.2B. Higher magnification images of the HA79 composites.

The degradation rates of the CaP/PUR composites are shown in Fig. 2.3. The composites showed a linear mass loss with time. *In vitro* degradation rates of the materials were relatively slow, as evidenced by the fact that both materials retained 85–95% of their original mass after 7 weeks.

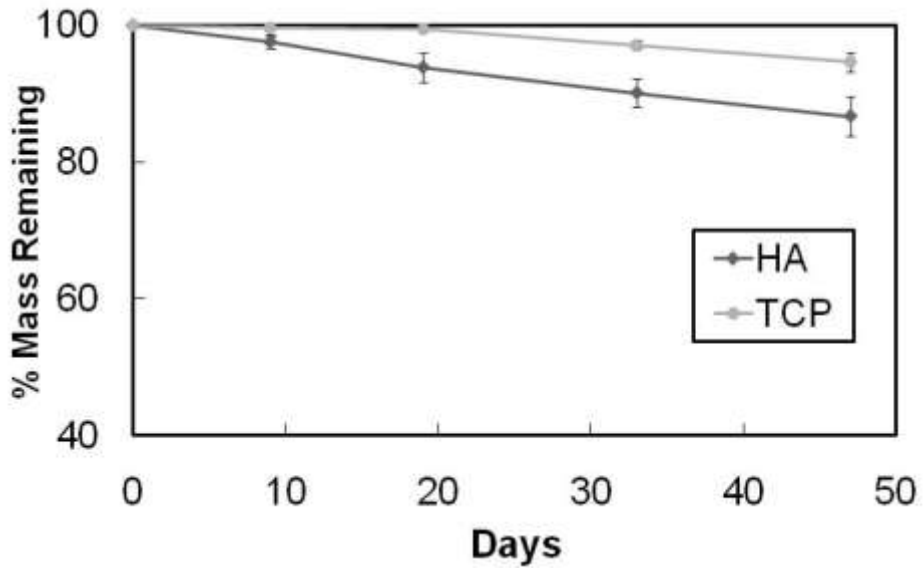

Figure II.3: In vitro degradation of PUR/HA and PUR/TCP composites.

In vitro cell proliferation on CaP/PUR composites

Calcein staining (Figure 2.4) showed favorable cell growth on the surface of CaP/PUR composites (79 wt%). The density of live cells at day 5 increase relative to day 2 on both HA/PUR and TCP/PUR composites. This finding suggests the biocompatibility of CaP/PUR composites. Quantitative analysis by PicoGreen assay also showed that DNA amount of the cells significantly increased at day 5 on both HA/PUR and TCP/PUR composites (Figure 2.5). The rate of proliferation on the TCP/PUR composites was greater than the rate of cell growth on HA/PUR composites.

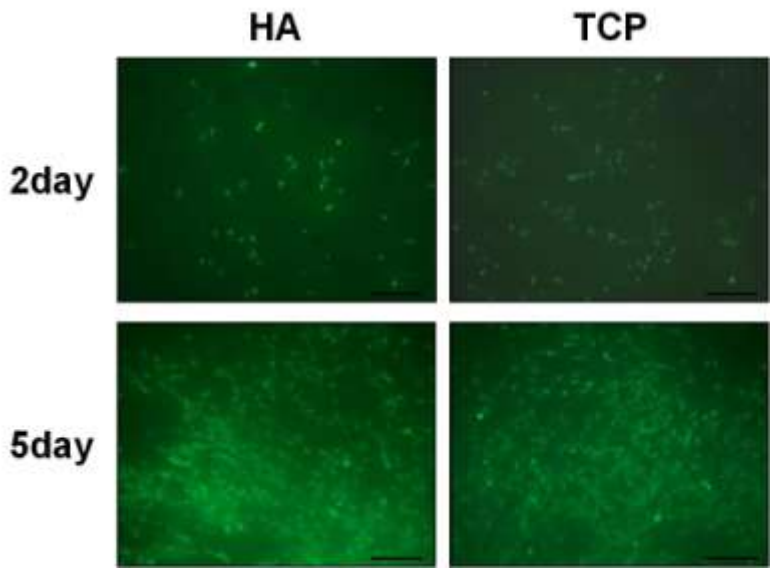

Figure II.4: Proliferation of 2T3 cells seeded on the surface of PUR/HA and PUR/TCP composites.
The cells were stained by calcein at day 2 and day 5. The bars: 250 μm.

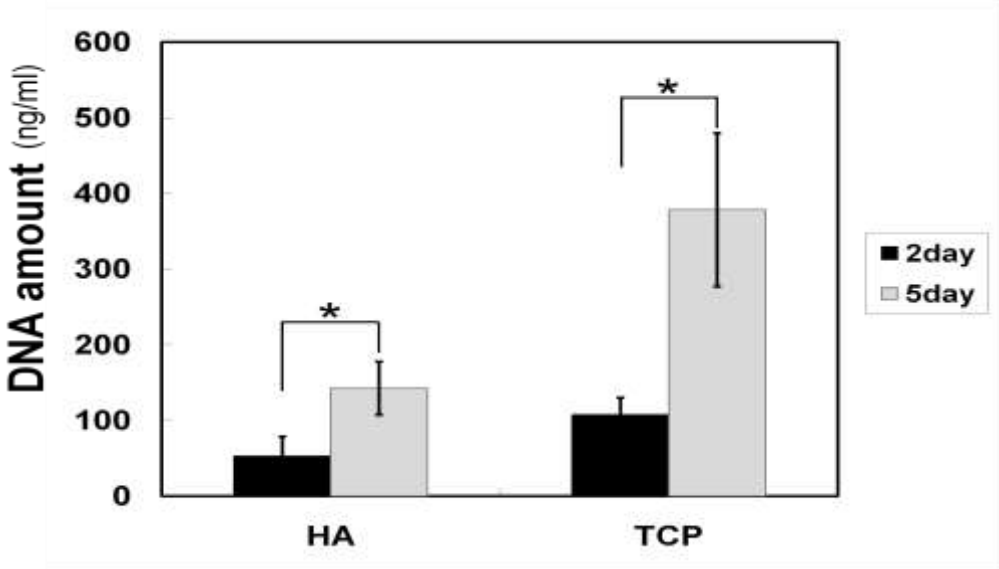

Figure II.5: DNA amount of 2T3 cells cultured on PUR/HA and PUR/TCP composites surfaces.
Time points: day 2 and day 5. *: $p<0.05$.

In vitro osteogenic differentiation on CaP/PUR composites

ALP activity of the cells seeded on CaP/PUR composites significantly increased when cultured with osteogenic medium (Figure 2.6), suggesting that the cells can differentiate on the surface of the composites. There was no significant difference in ALP activity between HA/PUR and TCP/PUR composites.

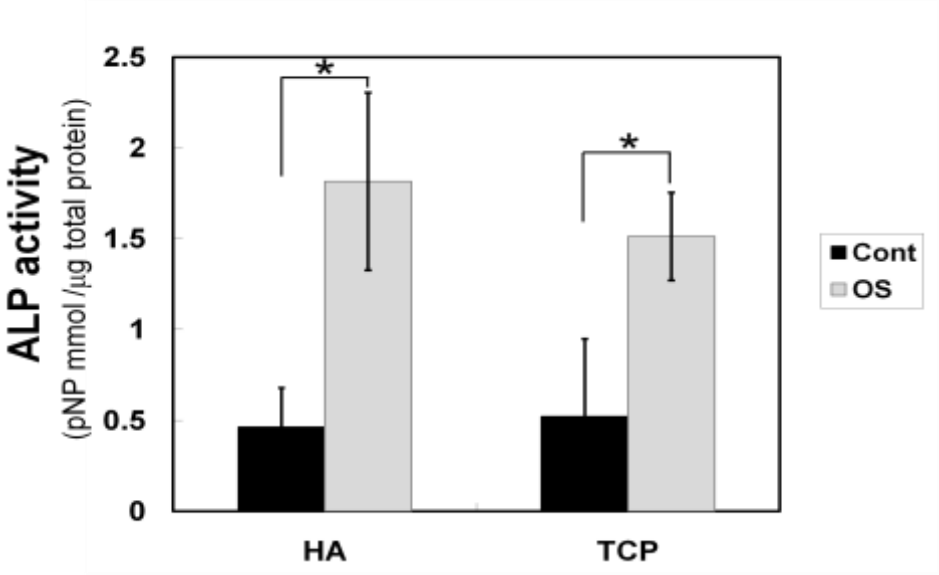

Figure II.6: Osteogenic differentiation of 2T3 cells seeded on PUR/HA and PUR/TCP composites.
ALP activity was measured at day7 after culture on the composites with osteogenic supplement (OS). Cont: culture without OS. *: $p<0.05$.

X-ray and μCT Analysis

X-rays from the extracted femurs at week4 (Figure 2.7) showed new bone formation around both HA/PUR and TCP/PUR composites. Similar observations were made from the μCT images (Figure 2.8). The material shape became irregular at the boundary between the implant and newly formed bone on μCT images. These findings show that the composites are osteoconductive and support appositional bone growth.

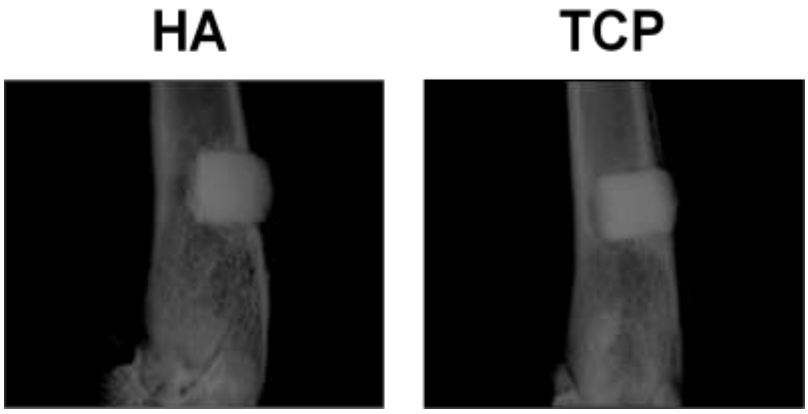

Figure II.7: X-rays of PUR/HA and PUR/TCP composites at week 4 after implantation in the distal femur of Sprague-Dawley rats.

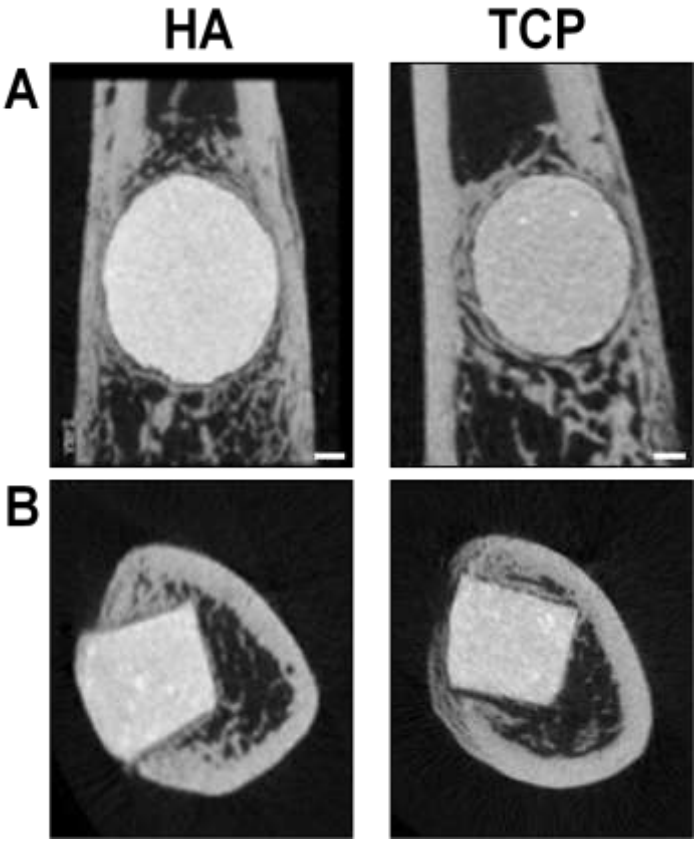

Figure II.8: Micro CT of PUR/HA and PUR/TCP composites at week4.
(A: Coronal view. B: Axial view. Scale bars: 500 μm.)

Histology

Histological sections of the implanted CaP/PUR composites (Figure 2.9) showed extensive bone matrix formation at the surface of both HA/PUR and TCP/PUR composites, which is consistent with the radiographs and μCT images. Higher magnification images revealed cellular infiltration into the materials. No inflammatory response was observed at week 4. As observed in Figure 2.9A, the HA/PUR composites showed evidence of limited remodeling near the base of the implant. However, there appeared to be a minimal change in the size of the original implants for both treatment groups, suggesting that the extent of cellular infiltration and remodeling in the composites was low. Histological sections stained for TRAP (Figure 2.10) showed osteoclast resorption at the boundary between the implants and newly formed bone.

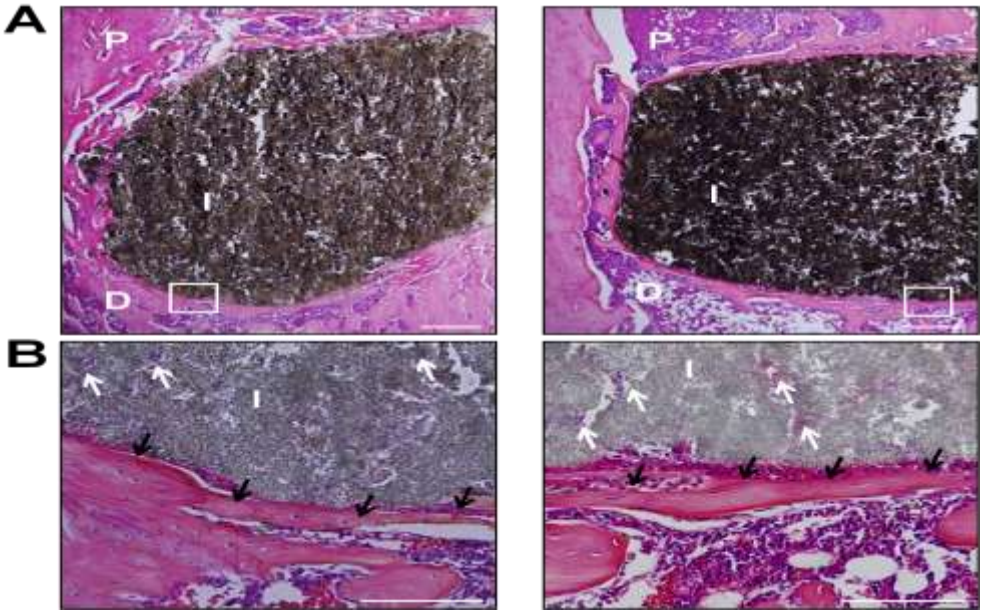

Figure II.9: Histological pictures (HE staining) of PUR/HA and PUR/TCP composites at week 4.
(A: P- proximal, D- distal, I- implants. The bars: 500 μm. B: High magnification. The white arrows: cell infiltration to the scaffolds. The black arrows: New bone formation. Scale bars: 100 μm.)

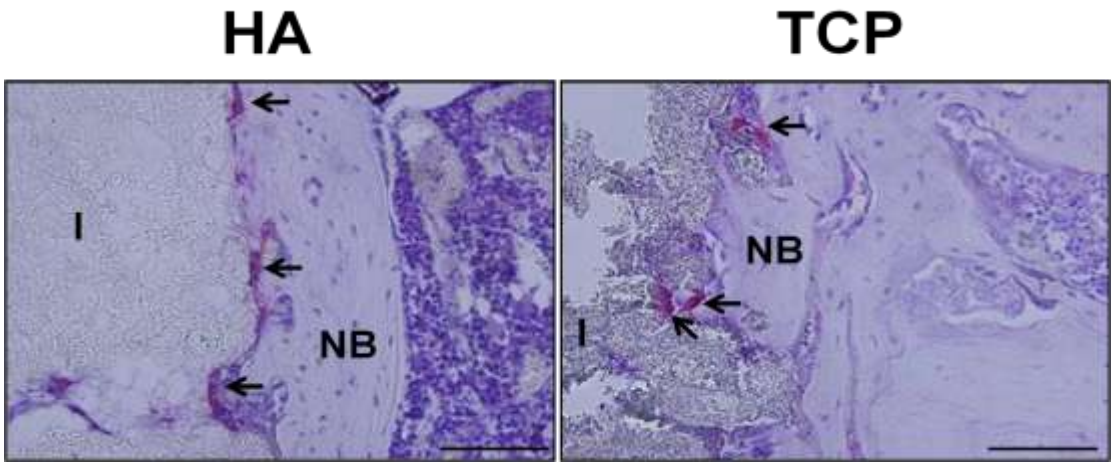

Figure II.10: Histological pictures (TRAP staining) of PUR/HA and PUR/TCP composites at week 4.
(I: implants, NB: New bone formation, The black arrows: TRAP positive multi-nucleated cells. Scale bars: 100 μm.)

Discussion

Multiple CaP/polymer composites with varying porosities and filler contents have been studied as biomaterials [10]. These systems typically incorporate filler contents far below the random closed packing limit (RCP) of spheres (~64 vol%) [23], and β–TCP/polymer composites have been reported to decrease in strength as the amount of β–TCP increases [10]. However, another study has shown that varying the filler content of HA/chitosan (CS) composites has a minimal effect on the strength of the overall composite at values under 80 wt% (~64 vol%) [11,23]. Similarly, varying the filler content from 70 to 79 wt% (56.8 to 66.2 vol%) for the CaP/PUR composites in this study had no significant effect on strength. As expected, HA/PUR composites exhibited superior compressive modulus and strengths compared with the β–TCP/PUR composites. At the 70 wt% filler content, there were no significant differences in the compressive modulus in the treatment groups. However, once the filler content was increased to 79 wt%, there was a significant difference suggesting a greater contribution of the filler composition at the higher loading. The strength of the HA/PUR composites (87.0 MPa) was lower than values reported for chitosan (CS)/HA composites, which were also prepared at 80 wt% HA (166 MPa) [11]. However, the compressive modulus of HA/PUR composite materials (4.3 GPa) was an order of magnitude higher than that of the CS/HA composites (416 MPa).

The *in vitro* degradation rate of CaP/polymer composites varies substantially depending on the polymers and ceramic components, as well as the manufacturing methods [24-26]. Generally, the composites degraded more slowly and maintained their shape longer than the pure polymer [27]. The CaP/PUR composites in this study also

degraded slowly *in vitro*, with degradation rates in PBS ranging from 0.8 – 2.0 wt%/week. While TCP is more water-soluble than HA [28,29], HA/PUR degraded relatively faster than TCP/PUR in this study. High HA content may influence the pH of the surrounding microenvironment [30], which can influence the polymer degradation rate [31].

Cellular proliferation was higher on the surface of the β–TCP composites. Previous studies have suggested that β-TCP can enhance osteoblast viability and proliferation, as calcium and phosphate ions stimulate osteoblastic activity [3,21,32]. In contrast, the dissolution of crystalline HA is slow and reduces the pH of the surrounding microenvironment, thereby slowing cell growth [30]. Similarly, in the present study the β-TCP/PUR composites supported significantly higher proliferation of osteoprogenitor cells compared to the HA/PUR composites, which is conjectured to result from the dissolution of β-TCP particles exposed on the surface of the composites. Interestingly, the filler type had no effect on ALP activity of the cells.

Remodeling of CaP/polymer composites *in vivo* has been observed in several studies. HA/PLLA composites implanted in rabbit femoral plug defects have taken up to 7 years to remodel [12]. In the present study, both radiographs and histological sections show appositional bone growth at the surface the CaP/PUR composites, which has also been observed for allograft/PUR composites implanted in the rabbit distal femur [19]. However, in the present study there was less resorption and cellular infiltration observed for the CaP/PUR composites compared to the allograft/PUR composites. Osteoclasts infiltrated and resorbed the CaP/PUR composites near the bone-implant interface, as confirmed by TRAP staining. While there is limited evidence of remodeling at the early time point (4 weeks) investigated, infiltration of osteoclasts near the implant-bone

interface suggests that at later time points the CaP/PUR composites may remodel via slow reverse creeping substitution [33-35], as reported previously for allograft/PUR composites. However, the rates of cellular infiltration and resorption were substantially less than those observed for allograft/PUR composites at similar filler loadings [19]. The SEM images (Figure 2.2) indicate that the CaP particles were fractured due to the compression molding process, which reduced the size of many of the particles to <10 μm. In contrast, these results were not observed for compression-molded allograft bone/polymer composites.[19] The size of allograft bone particles dramatically affects the potential of the particles to remodel, which is highest for particles ranging from 90-300 μm [36], and particles < 100 μm are only slowly resorbed. Thus the relatively slow osteoclast-mediated resorption of the CaP composites is likely due, at least in part, to the small size of the particles. Alternatively, previous studies have suggested that cortical allograft bone particles are more rapidly resorbed and replaced by living bone in the rabbit distal femur than HA particles due to the organic components in the allograft bone [37]. Allograft bone particles, which have been reported to undergo up to 70% resorption by osteoclasts after 14 days[38], resorb faster than HA particles (0.02 μm^3 μm^{-2} day^{-1})[39] *in vitro*. These observations suggest that the slower resorption rate of CaP composites could also be attributed to the differences in composition between CaP and allograft.

In this study, we examined the *in vivo* bioactivity of CaP/PUR composites using a rat femoral plug defect model with a short-term observation period. Large animal models with a long-term observation may be required in the future to further investigate the osteoconductive ability and full remodeling of the materials. However, the data from this

study suggest the potential of CaP/PUR composites for weight-bearing implants as a biocompatible, osteoconductive, and resorbable material.

Conclusions

CaP/PUR composites have been synthesized using a two-component polyurethane derived from LTI. The mechanical properties of the composites suggest that they could be useful for weight-bearing applications as the PUR increased the compressive strength of the CaP. Cell culture studies showed that CaP/PUR composites are biocompatible, with β-TCP further enhancing cell viability and proliferation. CaP/PUR composites also supported the differentiation of 2T3 cells into osteoblasts. When implanted in the distal femurs of rats, CaP/PUR composites were shown to be biocompatible and osteoconductive with no adverse responses observed. Histological sections revealed evidence of infiltration of osteoclasts and resorption of CaP near the bone-implant interface, as well as appositional remodeling via slow reverse creeping subsitution. The current study suggests that CaP/PUR composites could be a potentially useful option for weight-bearing implants.

REFERENCES

1. Giannoudis PV, Dinopoulos H, Tsiridis E. Bone substitutes: an update. Injury 2005;36 Suppl 3:S20-7.

2. Buckwalter JA, Glimcher MJ, Cooper RR, Recker R. Bone biology. I: Structure, blood supply, cells, matrix, and mineralization. Instr Course Lect 1996;45:371-86.

3. Sammarco VJ, Chang L. Modern issues in bone graft substitutes and advances in bone tissue technology. Foot and Ankle Clinics of North America 2002;7(1):19-41.

4. Kotani S, Fujita Y, Kitsugi T, Nakamura T, Yamamuro T, Ohtsuki C, Kokubo T. Bone bonding mechanism of beta-tricalcium phosphate. J Biomed Mater Res 1991;25(10):1303-15.

5. Neo M, Kotani S, Fujita Y, Nakamura T, Yamamuro T, Bando Y, Ohtsuki C, Kokubo T. Differences in ceramic-bone interface between surface-active ceramics and resorbable ceramics: a study by scanning and transmission electron microscopy. J Biomed Mater Res 1992;26(2):255-67.

6. Chim H, Gosain AK. Biomaterials in craniofacial surgery experimental studies and clinical application J Craniofac Surg 2009;20:29-33.

7. Moreira-Gonzalez A, Jackson IT, Miyawaki T, Barakat K, DiNick V. Clinical outcome in cranioplasty: critical review in long-term follow-up. J Craniofac Surg 2003;14:144-153.

8. Khan Y, Yaszemski MJ, Mikos AG, Laurencin CT. Tissue Engineering of Bone: Material and Matrix Considerations. J Bone Joint Surg Am 2008;90(Supplement_1):36-42.

9. Rezwan K, Chen QZ, Blaker JJ, Boccaccini AR. Biodegradable and bioactive porous polymer/inorganic composite scaffolds for bone tissue engineering. Biomaterials 2006;27(18):3413-3431.

10. Johnson AJ, Herschler BA. A review of the mechanical behavior of CaP and CaP/polymer composites for applications in bone replacement and repair. Acta Biomater.

11. Cai X, Tong H, Shen X, Chen W, Yan J, Hu J. Preparation and characterization of homogeneous chitosan-polylactic acid/hydroxyapatite nanocomposite for bone tissue engineering and evaluation of its mechanical properties. Acta Biomaterialia 2009;5(7):2693-2703.

12. Hasegawa S, Ishii S, Tamura J, Furukawa T, Neo M, Matsusue Y, Shikinami Y, Okuno M, Nakamura T. A 5-7 year in vivo study of high-strength hydroxyapatite/poly(l-lactide) composite rods for the internal fixation of bone fractures. Biomaterials 2006;27(8):1327-1332.

13. Shinsuke Ishii JT, Taizo Furukawa, Takashi Nakamura, Yoshitaka Matsusue, Yasuo Shikinami, Masaki Okuno. Long-term study of high-strength hydroxyapatite/poly(L-lactide) composite rods for the internal fixation of bone fractures: A 2-4-year follow-up study in rabbits. Journal of Biomedical Materials Research Part B: Applied Biomaterials 2003;66B(2):539-547.

14. Shikinami Y, Okuno M. Bioresorbable devices made of forged composites of hydroxyapatite (HA) particles and poly--lactide (PLLA): Part I. Basic characteristics. Biomaterials 1999;20(9):859-877.

15. Shikinami Y, Matsusue Y, Nakamura T. The complete process of bioresorption and bone replacement using devices made of forged composites of raw hydroxyapatite particles/poly l-lactide (F-u-HA/PLLA). Biomaterials 2005;26(27):5542-5551.

16. Zhang JY, Beckman EJ, Piesco NP, Agarwal S. A new peptide-based urethane polymer: synthesis, biodegradation, and potential to support cell growth in vitro. Biomaterials 2000;21(12):1247-1258.

17. Han J, Chen B, Ye L, Zhang A-y, Zhang J, Feng Z-g. Synthesis and characterization of biodegradable polyurethane based on poly(ε-caprolactone) and L-lysine ethyl ester diisocyanate. Frontiers of Materials Science in China 2009;3(1):25-32.

18. Guelcher SA, Srinivasan A, Dumas JE, Didier JE, McBride S, Hollinger JO. Synthesis, mechanical properties, biocompatibility, and biodegradation of polyurethane networks from lysine polyisocyanates. Biomaterials 2008;29(12):1762-75.

19. Dumas JE, Davis T, Holt GE, Yoshii T, Perrien DS, Nyman JS, Boyce T, Guelcher SA. Synthesis, characterization, and remodeling of weight-bearing allograft bone/polyurethane composites in the rabbit. Acta Biomater;6(7):2394-406.

20. Dumas JE, Zienkiewicz K, Tanner SA, Prieto EM, Bhattacharyya S, Guelcher SA. Synthesis and characterization of an injectable allograft bone/polymer composite bone void filler with tunable mechanical properties. Tissue Eng Part A;16(8):2505-18.

21. Bonzani IC, Adhikari R, Houshyar S, Mayadunne R, Gunatillake P, Stevens MM. Synthesis of two-component injectable polyurethanes for bone tissue engineering. Biomaterials 2007;28(3):423-433.

22. Adhikari R, Gunatillake PA, Griffiths I, Tatai L, Wickramaratna M, Houshyar S, Moore T, Mayadunne RTM, Field J, McGee M and others. Biodegradable injectable polyurethanes: Synthesis and evaluation for orthopaedic applications. Biomaterials 2008;29(28):3762-3770.

23. Radin C. Random Close Packing of Granular Matter. Journal of Statistical Physics 2008;131(4):567-573.

24. Ehrenfried LM, Farrar D, Cameron RE. The degradation properties of co-continuous calcium phosphate polyester composites: insights with synchrotron micro-computer tomography. J R Soc Interface;7 Suppl 5:S663-74.

25. Lin FH, Chen TM, Lin CP, Lee CJ. The merit of sintered PDLLA/TCP composites in management of bone fracture internal fixation. Artif Organs 1999;23(2):186-94.

26. Ang KC, Leong KF, Chua CK, Chandrasekaran M. Compressive properties and degradability of poly(epsilon-caprolatone)/hydroxyapatite composites under accelerated hydrolytic degradation. J Biomed Mater Res A 2007;80(3):655-60.

27. Heidemann W, Jeschkeit S, Ruffieux K, Fischer JH, Wagner M, Kruger G, Wintermantel E, Gerlach KL. Degradation of poly(D,L)lactide implants with or without addition of calciumphosphates in vivo. Biomaterials 2001;22(17):2371-81.

28. Ducheyne P, Radin S, King L. The effect of calcium phosphate ceramic composition and structure on in vitro behavior. I. Dissolution. J Biomed Mater Res 1993;27(1):25-34.

29. Koerten HK, van der Meulen J. Degradation of calcium phosphate ceramics. J Biomed Mater Res 1999;44(1):78-86.

30. Kenny SM, Buggy M. Bone cements and fillers: a review. J Mater Sci Mater Med 2003;14(11):923-38.

31. Leeuwenburgh SC, Wolke JG, Siebers MC, Schoonman J, Jansen JA. In vitro and in vivo reactivity of porous, electrosprayed calcium phosphate coatings. Biomaterials 2006;27(18):3368-78.

32. Rush SM. Bone Graft Substitutes: Osteobiologics. Clinics in Podiatric Medicine and Surgery 2005;22(4):619-630.

33. Eagan MJ, McAllister DR. Biology of Allograft Incorporation. Clinics in Sports Medicine 2009;28(2):203-214.

34. Newton CD, Nunamaker DB. Textbook of small animal orthopaedics. Philadelphia: Lippincott; 1985.

35. Yuan H, Li Y, de Bruijn JD, de Groot K, Zhang X. Tissue responses of calcium phosphate cement: a study in dogs. Biomaterials 2000;21(12):1283-1290.

36. Malinin TI, Carpenter EM, Temple HT. Particulate bone allograft incorporation in regeneration of osseous defects; importance of particle sizes. Open Orthop J 2007;1:19-24.

37. Voor MJ, Arts JJ, Klein SA, Walschot LH, Verdonschot N, Buma P. Is hydroxyapatite cement an alternative for allograft bone chips in bone grafting procedures? A mechanical and histological study in a rabbit cancellous bone defect model. J Biomed Mater Res B Appl Biomater 2004;71(2):398-407.

38. Muzylak M, Arnett TR, Price JS, Horton MA. The in vitro effect of pH on osteoclasts and bone resorption in the cat: implications for the pathogenesis of FORL. J Cell Physiol 2007;213(1):144-50.

39. Winkler T, Hoenig E, Gildenhaar R, Berger G, Fritsch D, Janssen R, Morlock MM, Schilling AF. Volumetric analysis of osteoclastic bioresorption of calcium phosphate ceramics with different solubilities. Acta Biomater;6(10):4127-35.

CHAPTER III.

Synthesis, characterization and remodeling of allograft mineralized bone particle/polyurethane implants in a rabbit distal femur model

Introduction

There are numerous biomaterials available to treat orthopaedic defects, however each of these platforms has limitations especially for weight-bearing applications. Several design parameters that must be considered during the development of weight-bearing biomaterials for bone tissue engineering such as porosity, mechanical strength, and degradation profile. Resorbable polymers have been extensively investigated for bone repair[1,2]. Ideally, scaffolds prepared from resorbable polymers should support cell attachment and ingrowth of new tissue, as well as biodegrade at a rate matching that of new tissue ingrowth. Fabrication of scaffolds with interconnected pores has long been considered a prerequisite for integration of bone within a polymer.[3,4] However, pores significantly diminish the initial mechanical properties[4] of the materials, thus rendering them largely unsuitable as load-bearing devices [5].

Biomedical devices based on poly(methyl methacrylate) (PMMA), such as hard-tissue replacement (HTR) implants[6], are used clinically to restore form and/or functionality. However, these biomaterials neither remodel nor integrate with host tissue and have a number of drawbacks, including toxicity of the monomer[7] and potential bone necrosis due to the exothermic reaction.[8,9] Furthermore, PMMA is not resorbable and can induce an inflammatory response.[10-13] Due to these undesirable properties, resorbable

alternatives to PMMA are have been developed, such as injectable calcium phosphate (CaP) bone cements. These materials cure endothermically at 37ºC[14] and are resorbable and osteoconductive[15-18], but in many cases, the degradation rate does not match that of new bone formation.[19,20] Furthermore, the rate of resorption is slow due to the small pore size.[21,22] Thus, despite substantial progress toward the design of therapeutics for healing bone, there remains a need for biomaterials that exhibit mechanical properties comparable to those of the host bone and that actively participate in the healing process, resulting in integration with recipient bone and remodeling with ultimate replacement by host tissue.

Ceramics, such as calcium phosphates, have been widely investigated as synthetic bone graft materials due to their bioactivity and biocompatibility. These biomaterials degrade *in vivo* by dissolution and osteoclastic resorption.[1] Resorbable polymer/ceramic composites have been investigated as weight-bearing implants that integrate with host bone.[23-26] Intramedullary (IM) rods fabricated from composites incorporating 30–40 wt% hydroxyapatite (HA) and 60–70 wt% poly(L-lactide) (PLLA) had bending strengths ranging from 260 – 280 MPa and moduli ranging from 7.6 – 9.8 GPa, which is a substantial improvement on the reportedly low bending and shear strengths of calcium phosphates.[27,28] When implanted in the distal femur of rabbits, the composites partially remodeled and integrated with host tissue after 4 years. The resorption and remodeling process was slow. After 4 years, the cross sectional area decreased 4 – 68%, and the extent of bony ingrowth varied from 18 – 30%.[26]

Both autograft and allograft bone have been extensively investigated in bone tissue engineering.[29-31] With the advent of new technologies for sterilization and viral

inactivation, mineralized human bone allografts have emerged as a preferred implant type for weight-bearing orthopaedic and spinal applications.[32] Autograft is highly effective, but requires a second surgical site with additional morbidity. Osteogenic cells present in the autologous bone are a major contributor to its effectiveness[33], so these materials must be implanted at the time of harvesting. Allografts have excellent biomechanical properties and they undergo extensive osseous integration. However, the anatomy of the donor bone limits the reproducibility and range of mineralized allograft shapes available for clinical use.[32] Furthermore, while the extent of integration is generally considered adequate, remodeling of the graft seldom exceeds 50%, which limits their use clinically.[34] Since remodeling proceeds from the external surface to the interior by the process of creeping substitution[18,33,35], the limited remodeling of allograft devices is likely due to their low specific surface area, which scales inversely with particle diameter. By processing the allograft cortical bone into small mineralized bone particles (AMBP, ~100 - 600 μm), the specific surface area is increased. The remodeling potential of materials incorporating particulated allograft was examined in a study wherein compression-molded composites comprising rabbit allograft mineralized bone particles (AMBP) (60-75 wt%) and poly(lactide-*co*-glycolide) (PLGA, 25-40 wt%) were implanted in bilateral unicortical plug defects in the distal femurs of adult NZW rabbits.[36] Histological sections as early as 4 weeks showed regions of cellular penetration, active bone-formation, and newly formed bone, which were most extensive at 75 wt% (~61 vol%) AMBP. The dramatically higher rate of remodeling of the AMBP composites (~4 – 6 weeks) relative to the HA/PLLA implants (~4 – 5 years) was attributed to either the greater bioactivity of AMBP or the higher volume fraction at which it was present in the composite.[36]

Although previous studies have shown that composites with poly(α-ester) binders (e.g., PLGA and PLLA) remodel in rabbit models of bone healing, thermoplastic polymers cannot be injected and strategies for improving interfacial bonding are limited. To address these limitations, in this study we have investigated reactive two-component biodegradable polyurethane (PUR) networks as the polymer binder. Biodegradable polyurethanes support new bone ingrowth *in vivo* and biodegrade to non-cytotoxic decomposition products[37-44], and the mechanical properties and degradation rate can be controlled through the choice of intermediates.[43,45,46] Furthermore, polyurethanes can be processed by two-component reactive liquid molding[43,46-50], thus making them suitable for injectable applications such as bone cements and void fillers. It was reasoned that the polymer would covalently bind to the allograft bone filler through the reaction of isocyanate (NCO) groups with the collagen present in the bone particles. In addition, it was hypothesized that surface-demineralization[51] ,the process of acid etching to expose collagen fibrils, of the AMBP would enhance surface binding through exposure of collagen fibrils. Strong bonding between the polymer and filler phases is known to increase the mechanical strength of the composite.[52-54] Also, several studies have suggested that the presence of a collagen layer, specifically the P-15 peptide, on the surface of substrates enhances the attachment of osteoblast-like cells[55-57], which may provide added benefits of surface demineralization. In this study, we have investigated the effects of surface-demineralization and polymer composition on mechanical properties, cellular infiltration, and new bone formation in a unicortical plug defect model in NZW rabbits.

Materials and Methods

Materials

Lysine triisocyanate (LTI) was purchased from Kyowa Hakko (New York, NY). Tegoamin 33, a tertiary amine catalyst, was received from Goldschmidt (Hopewell, VA). Glycerol, stannous octoate, and ε-caprolactone were purchased from Sigma-Aldrich (St Louis, MO), and glycolide and DL-lactide were supplied by Polysciences (Warrington, PA). Rabbit allograft mineralized bone particles (AMBP, 481 μm mean particle size) were received as a gift from Osteotech, Inc. (Eatontown, NJ).

Synthesis of polyester triols

Polyester triols were synthesized using published techniques.[46,58] Briefly, the appropriate amounts of glycerol starter and ε-caprolactone, glycolide, and DL-lactide monomers were mixed under argon at 140^{o}C for 30h. When the reaction was complete, the polyester triol was cooled, washed with hexane, and dried at 80^{o}C under vacuum. The backbone of the polyester triols comprised 60% ε-caprolactone, 30% glycolide, and 10% DL-lactide (6C3G1L). Molecular weights of 300 g/mol (6C3G1L300) and 600 g/mol (6C3G1L600) were synthesized for this study.

Preparation of surface-demineralized bone particles (SDBP)

Surface demineralized bone particles (SDBP) were prepared using published methods.[59] AMBP was sonicated in 0.1 M hydrochloric acid for 2.5 minutes followed by saturation in 2.5% trypsin at 37˚C overnight. Sonication in hydrochloric acid was repeated for the same time period followed by 48 hours of saturation in 2.5% trypsin. The resulting SDBP was rinsed thoroughly with DI water and lyophilized for 48 hours.

Characterization of reactivity of allograft bone particles by FITC labeling.

Approximately 10 mg of rabbit AMBP or SDBP was added to 2 mL centrifuge tubes along with 1 mL of borate buffer. A solution of FITC, in borate buffer, was prepared to yield a concentration of 7 mg/mL, and 0.1 mL of the resulting solution was added to each tube. As a control, only borate buffer was added to three of the AMBP samples. The tubes were placed on a hematology mixer for 1 hour. The tubes were centrifuged at 2500 rpm for 3 minutes to remove excess FITC from each tube, and the AMBP was washed thrice with borate buffer solution. The AMBP was transferred to a 96 well plate by suspending it in a solution of 0.1 mL of borate buffer. The fluorescence of each well was read using a FL600 microplate reader at an excitation of 495 nm and an emission at 525 nm. The fluorescence was read at a sensitivity of 75.

Scanning Electron Microscopy

Rabbit AMBP (approximately 5 mg) was mounted on a SEM pin stub mount and sputter-coated for 60 seconds using a Cressington Q108 sputter coater, which deposited gold at a 30 mA current. A Hitachi S-4200 scanning electron microscope was used to acquire images at a voltage of 1 kV.

Fabrication of AMBP/PUR composites

The components of the composite were mixed using a one-shot method, wherein the appropriate amounts of Tegoamin 33, polyester triol, AMBP, and LTI were added to a 10 mL cup and mixed using a Hauschild SpeedMixer (FlackTek, Inc., Landrum, SC). The target index, the ratio of NCO groups to hydroxyl groups multiplied by 100, was 125. The target catalyst concentration was 5000 ppm. The mixture speed was gradually ramped to 3300 rpm for one minute and mixing continued at 3300 rpm for 30s. All

composites incorporated 79.0 wt% (66.2 vol%) allograft bone. The reactive paste was transferred to a cylindrical mold, compressed to approximately 63,000 lbf for 50 minutes, de-molded to yield a green cylinder (6.1 mm diameter), and cured at 37˚C for twelve hours in a vacuum oven. The four formulations listed in Table 3.1 were designed to investigate the effects of surface demineralization and polyester triol molecular weight on mechanical properties and remodeling in a rabbit distal femoral plug model.

Infrared spectroscopy

Potassium bromide pellets of both composites and AMBP were produced using a pellet die assembly. A thin disc from the composite rods was cut using a Buehler diamond embedded circular saw, and approximately 8 mg of the composite and AMBP were ground using mortar and pestle followed by the addition of 200 mg of potassium bromide. The resulting mixture was then pressed into a pellet. A Bruker Tensor 27 FTIR was used to scan each sample.

Mechanical and swelling properties

Cylindrical PUR/AMBP rods, approximately 6.3 x 12.6 mm (n = 3), were fabricated by compression molding. The rods were hydrated in PBS 24 hours prior to testing. The cylinders were placed between two fixed compression platens of an MTS 898 equipped with a 13 kN load cell, pre-loaded to approximately 12 N, and subsequently loaded at 24 mm/min until failure. Swelling data were calculated from the dry and wet mass of the composites after 24h incubation time in PBS (a time-course study showed that the composites attained equilibrium by 24h swelling time). One-way ANOVA with bonferroni correction ($p<0.05$) was used for evaluation of statistical significance for both μCT imaging and histomorphometry analysis.

Animal study

Six New Zealand White (NZW) rabbits weighing between 3.8 and 4.1 kg were used in this study. All surgical and care procedures were carried out under aseptic conditions per the approved IACUC protocol. The AMBP/PUR composite plugs were gamma irradiated using a dose of approximately 25 kGY. Glycopyrrolate was administered at 0.01 mg/kg IM followed by ketamine at 40 mg/kg IM. Bilateral defects of approximately 6.1 mm diameter by 11 mm in depth were drilled in the metaphysis of the distal femurs of each rabbit. AMBP/PUR plugs from each treatment group (n = 3) were subsequently inserted into each defect. Treatment groups for each composite were dispersed randomly among the rabbits. The rabbits were euthanized after six weeks using Fatal-plus (2.2 mL/10 kg) intra-venously. After 6 weeks' implantation time, the femurs were extracted and placed in a 1 X phosphate buffer solution for 2 hours followed by dehydration in a series of ethanol and fixation in 10% formalin for 3 weeks.

Table III.1: AMBP/PUR composite formulations.

Composite	**AMBP300**	**SDBP300**	**AMBP600**	**SDBP600**
Polyol	6C3G1L300	6C3G1L300	6C3G1L600	6C3G1L600
Filler	MBP	SDBP	MBP	SDBP

Radiograph and Histological evaluation

A Faxitron LX-60 x-ray system was used to acquire micrographs of the extracted femurs after the PBS wash. Micrographs of each femur were taken at 40 kV with an exposure time 10 s. After fixation, the femurs were embedded in Technovit 7200 and 200-μm sections were cut from the resulting blocks using an Exakt band saw. The sections were then ground and polished using an Exakt grinding system to less than 100 μm and stained with Sanderson's rapid bone stain counterstained with van Gieson. Old allograft bone stained light brown, while new bone stained pink with dark blue osteocytes within the matrix. The polymer was stained dark blue, while cells were stained light blue.

Histomorphometry

A rectangular region approximately 9.5 mm from the plug insertion point across the composite was selected for histomorphometry of the AMBP300 and SDBP300 groups. To determine the AMBP distribution, a 1.8 x 3.9 mm rectangle in the unremodeled core was also examined. MetaMorph 7.1 was used to obtain

histomorphometry data from the histology micrographs. Differentiation between new bone and cellular infiltration was accomplished using the Smart Brush tool in the Photoshop Elements 7.0 software. The fractions of allograft, cellular infiltration, new bone, and residual polyurethane were measured in the regions of interest. Significant differences between the AMBP300 and SDBP300 groups were determined by a t-test ($p < 0.05$).

Results

AMBP and SDBP characterization

The density of dry AMBP was determined at Micromeritics Analytical Services by helium pyconmetry to be 2.30 g cm^{-3}. As evidenced by the low magnification SEM images (Figures 3.1A and 3.1B), there were insignificant changes in particle size and shape after surface demineralization. Laser light scattering was used to measure the particle size distribution, which was found to be log-normal with a mean value of 481± 7 μm (Figure 3.1F).

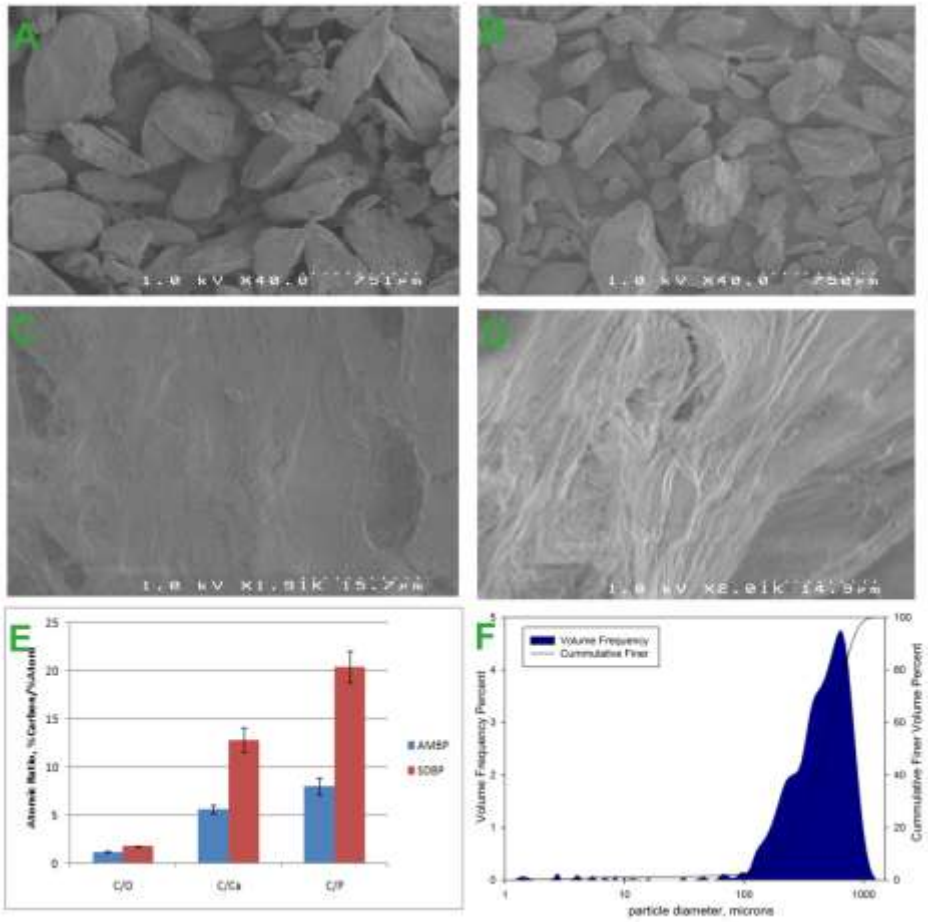

Figure III.1: Characterization of rabbit mineralized particles.
Low magnification SEM images of (A) AMBP and (B) SDBP showing negligible changes in size and shape after surface deminerilzation. High magnification SEM images of (C) MBP and (D) SDBP particles showing exposure of collagen fibrils on the surface after demineralization, (E) composition of the surface of MBP and SDBP measured by XPS, and (F) particle size distribution measured by laser diffraction (micrometrics).

Reactivity of AMBP and SDBP particles

The surfaces of the AMBP and SDBP particles were analyzed by XPS to characterize the composition. Surface-demineralization removed a substantial amount of the mineral content at the surface, as evidenced by the significant decrease in Ca and P atomic concentrations and significant increase in C atomic concentration inferred from

the XPS spectra (Figure 3.1E). The removal of the mineral content was anticipated to increase the reactivity of the surface by exposing a greater number of collagen fibrils at the surface, as shown by the high magnification SEM images in Figures 3.1C and 3.1D. The higher reactivity of the SDBP particles is demonstrated by the FITC assay (Figure 3.2), where active hydrogen (e.g., hydroxyl and amine) groups present in the proteins on the surface of the particles react with the nucleophilic isothiocyanate group (N=C=S) in the FITC molecule. As anticipated, surface demineralization significantly increased the FITC-related absorbance consistent with a significant increase in the number of FITC molecules bound to the surface of SDBP particles compared to AMBP. The higher reactivity suggests a higher concentration of active hydrogen molecules on the surface of SDBP, which is anticipated to enhance the mechanical properties of the composite due to the higher degree of interfacial bonding between the allograft filler and reactive two-component PUR binder. However, it is important to note that the fluorescence of the AMBP was also higher than that of the FITC-untreated control (AMBP in the absence of FITC) and FITC-treated control (tissue culture polystyrene well plate, which is anticipated to have a relatively low reactivity toward FITC).

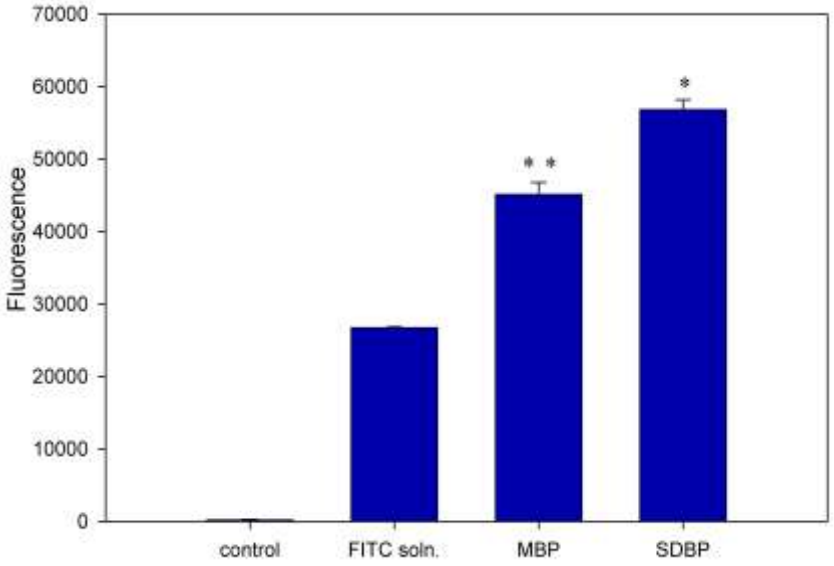

Figure III.2: Results from a fluorescein isothiocyanate (FITC) assay. Surface demineralization enhances the reactivity of rabbit allograft bone particles. Rabbit MBP and SDBP were incubated in a FITC solution (7 mg ml-1) in 1 ml borate buffer for 1 h. As a negative FITC-untreated control, only borate buffer was added to three of the MBP samples. After washing with borate buffer solution, the MBP and SDBP were suspended in 0.1 ml borate buffer and transferred to a 96-well plate. As a positive FITC-treated control, the tissue culture polystyrene well plate was also incubated in FITC solution. MBP in borate buffer was used as a control in this study. The fluorescence of each well was read using a FL600 microplate fluorescence reader at an absorption of 495 nm and an emission at 525 nm.

IR characterization

The IR spectrum (Figure 3.3) suggests that the PUR phase cured completely, as evidenced by the absence of an NCO peak in the range of 2285-2250 cm^{-1} [46,60]. Ester and urethane carbonyl stretching vibrations are observed near 1765 cm^{-1} [40,46]. The peaks near 560 and 1030 cm^{-1} correspond to the phosphate bands in hydoxyapatite that is part of the allograft bone matrix.[61] Thus the IR spectra confirm that the reactive AMBP/PUR mixture cured at high conversion to form the expected structure.

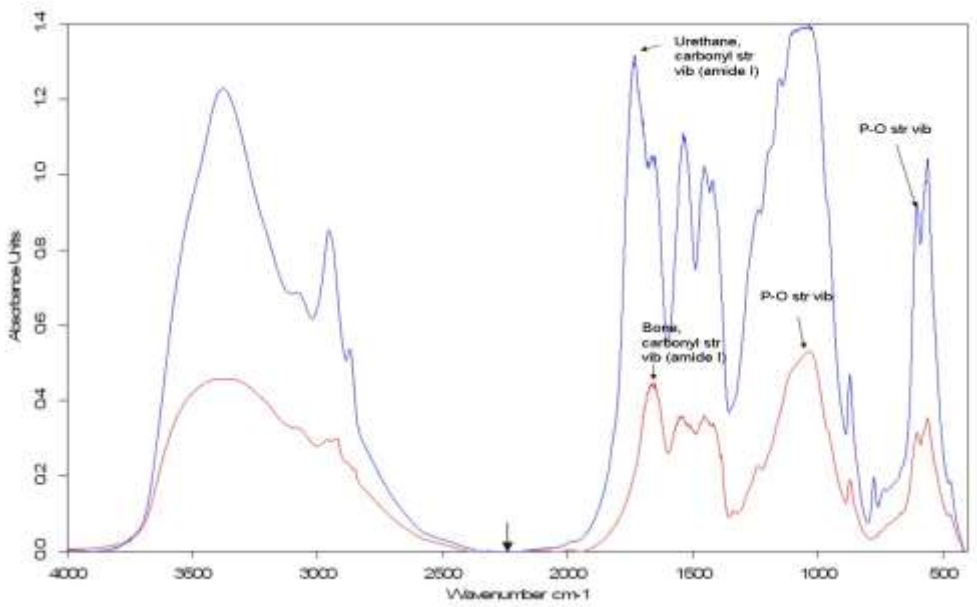

Figure III.3: IR spectra of 6C3G1L600-SDBP composite (blue) and mineralized bone particles (red).
The absence of a peak at 2285–2250 cm^{-1}, marked by the black arrow, indicates that there is a negligible amount of free NCO. Most peaks are overlapping between the MBP/PUR composite and the MBP with the exception of the ester and urethane carbonyl peaks.

Mechanical and swelling properties

The values for the compressive modulus, strength, yield strain, and swelling are listed in Table 3.2. The modulus and strength values of the composites ranged from 3.05 to 6.01 GPa and 107.8 to 172.4 MPa, respectively. The strain at yield varied from 4.56 to 5.52% while swelling ranged from 2.54 to 2.97%. Composites prepared from the 6C3G1L300 polyester triol exhibited higher strengths and lower strains at yield than the composites based on the 6C3G1L600 triol, presumably due to the higher strength and crosslink density of the polymer binder. Composites failed in a diagonal fracture during the compression testing. Surprisingly, surface-demineralization had no effect on the mechanical properties of the composite, as evidenced by the absence of statistically

significant differences in swelling or mechanical properties between treatment groups with the same molecular weight polyester triol.

Table III.2: Mechanical and swelling properties of bone/polymer composites.

Property	**MBP300**	**SDBP300**	**MBP600**	**SDBP600**
Compressive modulus, GPa	6.01 ± 0.34	5.52 ± 0.11	3.05 ± 0.64	3.66 ± 0.39
Compressive strength, MPa	172.4 ± 4.7	166.2 ± 3.8	107.8 ± 1.8	113.1 ± 3.9
Yield strain, %	4.56 ± 0.21	4.80 ± 0.15	5.52 ± 0.57	5.77 ± 0.25
Swelling, %	2.54 ± 0.28	2.97 ± 0.27	2.89 ± 0.35	3.33 ± 0.25

Volume fraction bone

Histological sections near the center of the implants where cells had not yet infiltrated are shown in Figures 3.4A and B. Histomorphometric analysis of the region of the implant shown in Figure 3.4C was performed to calculate the volume fractions of bone and polymer for each treatment group. As shown in Figure 3.4D, the polymer fraction near the core ranged from 26 – 32 vol%, while the bone fraction varied from 66 – 74 vol%. There was a significant difference in bone fraction observed between the 6C3G1L300-AMBP and 6C3G1L600-SDBP groups. From the mass balance data, the volume fraction polymer ranged from 32.1 – 32.4 vol%, while the volume fraction allograft varied from 68.6 – 68.9 vol%, respectively. Thus the histomorphometric and

mass balance data are in agreement that the bone content exceeded the random close-packed (RCP) limit of 64 vol%. Furthermore, the micrographs in Figure 3.4A and B exhibit multiple contacts between adjacent bone particles.

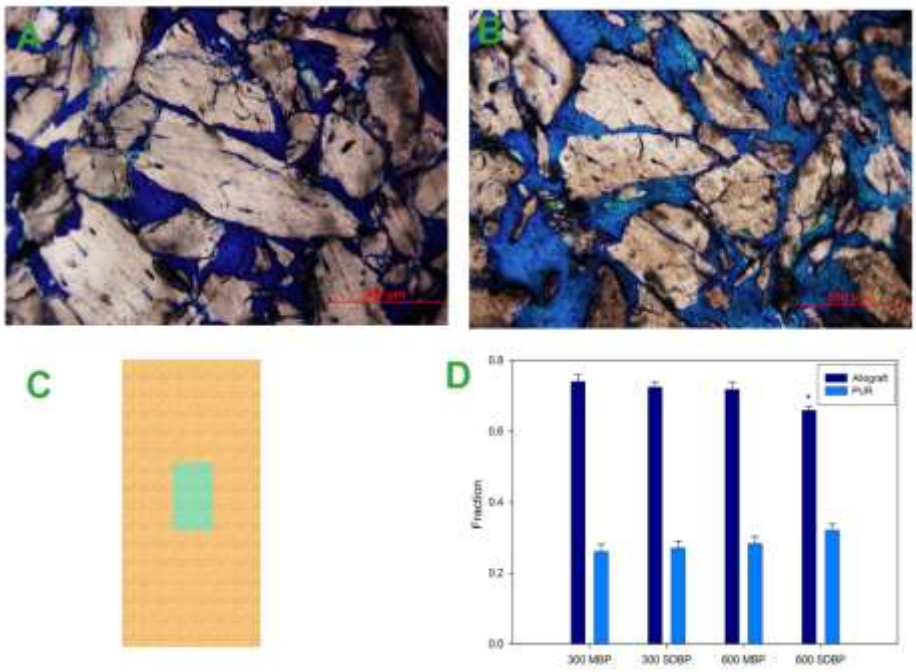

Figure III.4: Distribution of allograft bone composites.
Allograft particles are more uniformly distributed in 300 MW composites compared to 600 MW SDBP composites. A: 6C3G1L300-MBP, B: 6C3G1L600-SDBP, C: region of interest, D: Volume fractions of bone and polymer measured by histomorphometry (n = 6) show higher variability in the center region of the implant for 600 MW SDBP compared to the other treatment groups with a significant difference between the 6C3G1L300-MBP and 6C3G1L600-SDBP groups.

Radiograph analysis

At 6 weeks, the implants were more radiodense than the host trabecular bone allowing the general region of the remaining implant to be evident (Figure 3.5). However, regions of host bone immediately surrounding the implant appeared just as radiodense as the implant making the border between the implant and host bone indistinguishable in some areas. Resorption of AMBP was observed by the changes in radiodensity within the implant cavity. The radiographs suggest that the composites from the 6C3G1L600-SDBP treatment group resorbed faster than the other groups, as evidenced by the presence of radiolucent zones at the implant margins.

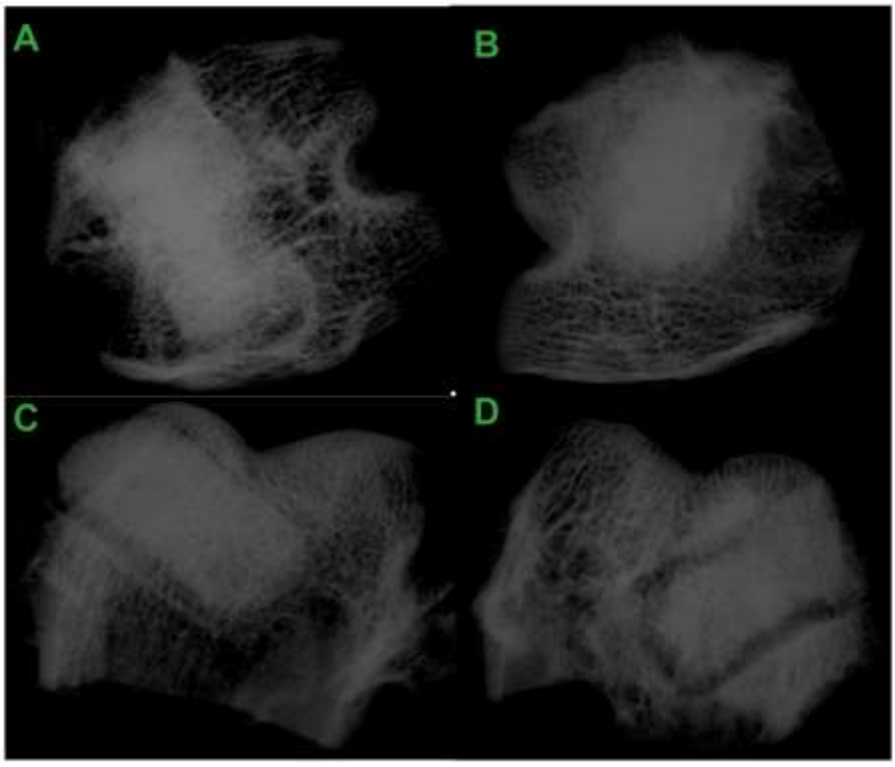

Figure III.5: Radiographs of extracted rabbit distal femurs.
(A: 6C3G1L300-MBP, B: 6C3G1L300-SDBP, C: 6C3G1L600-MBP, D: 6C3G1L600-SDBP. These radiographs suggests that the 6C3G1L600 group resorbed faster than the other groups.)

Histological evaluation

All of the histological micrographs suggest that the PUR/AMBP composite plugs were biocompatible, as evidenced by the absence of a significant inflammatory response. Furthermore, the composites did not disrupt the normal wound healing process, as evidenced by the presence of osteoid lining the host bone surrounding the implant. One rabbit that was treated from the 6C3G1L300-SDBP group died at 2 weeks due to causes unrelated to the surgery. As shown in Figure 3.6, histological sections processed at this 2 week time point suggest that the AMBP/PUR plugs remodeled by the mechanism of creeping substitution.[33,62] The boundary between the implant and the host bone is well-defined in the low magnification micrograph (Figure 3.6A). Growth of new bone in apposition to the surface of the implant followed by the onset of a wall of bone forming around the implant can also be seen (Figure 3.6A). The onset of cellular infiltration and resorption of AMBP, stained tan/pink, is illustrated in Figures 3.6B-C. Resorption is followed by new bone formation (Figure 3.6C). At this early time point, there is minimal degradation of the polymer (blue-green color). Osteoid, stained green, lines the edge of the newly formed bone around the implant in Figure 3.6D.

Low magnification micrographs at the 6 week time point (Figure 3.7) show differences between treatment groups. In all of the treatment groups, a majority of the resorption, cellular infiltration, and remodeling occurred in the peripheral regions of the implant with little activity occurring in the central core of the implant. The 6C3G1L300-AMBP treatment group showed the least cellular infiltration, while the 6C3G1L600-SDBP showed the greatest cellular activity (Figures 3.7A and 3.7D). There was a significant amount of polymer remaining in all of the treatment groups, especially at the

core of the implants. However, composites prepared with the 6C3G1L600 polyol appeared to degrade faster than the materials incorporating the 6C3G1L300 polyester triol (Figure 3.7D). The 6C3G1L600-SDBP material supported the most extensive cellular infiltration and polymer degradation. As shown in Figure 3.7D, at six weeks cells had infiltrated throughout the entire volume of one end of the implant. Higher magnification micrographs (Figure 3.8) show both the resorption of allograft bone particles and new bone formation on their surfaces within the implant cavity. Newly mineralized bone matrix formed on the surface of the allograft particles is evidenced by the more pronounced pink color and the dark blue osteocytes within the matrix. Figure 3.8A shows bridging of two allograft particles by new bone. On some allograft particles, both new formation and resorption by osteoclasts appeared to occur simultaneously (Figure 3.8C). New bone formation was not limited to the surface of the allograft bone particles, as Figure 3.8D shows ingrowth of new bone at the border of the implant. From the images in Figure 3.7, remnants of polymer that has not yet resorbed can also be seen. In particular, an island of polymer surrounded by new bone is evident in Figure 3.8D. While the continuing presence of the polymer is anticipated to delay new bone formation, especially for the case of bone particles completely embedded in polymer, modest amounts of new bone formed around the polymer remnants. Figure 3.8D also shows that the host bone is lined with osteoid, suggesting future ingrowth into the implant cavity.

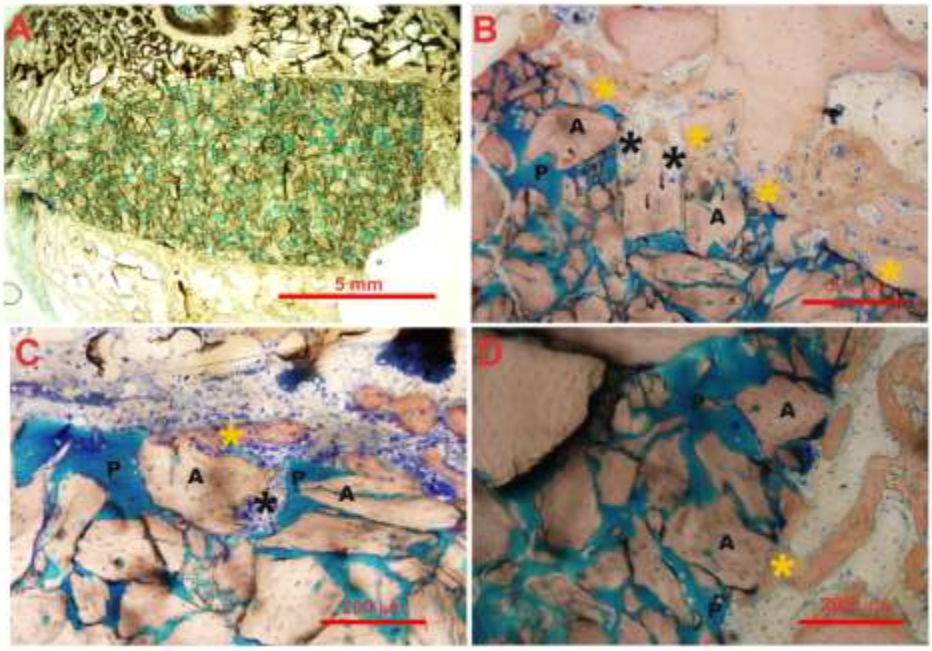

Figure III.6: Histology at 2 weeks for 6C3G1L300-SDBP treatment group. ((A) – (D) Histological sections of the 6C3G1L300-SDBP treatment group are stained with Sanderson's rapid bone stain. (A) At two weeks, there is evidence of bone apposition and the composite is encapsulated in a bony shell (1.25X). (B) – (D) Higher magnification images (20X) show bone apposition (orange asterisk), resorption (black asterisk) and remodeling of the allograft component via the process of creeping substitution (20X).)

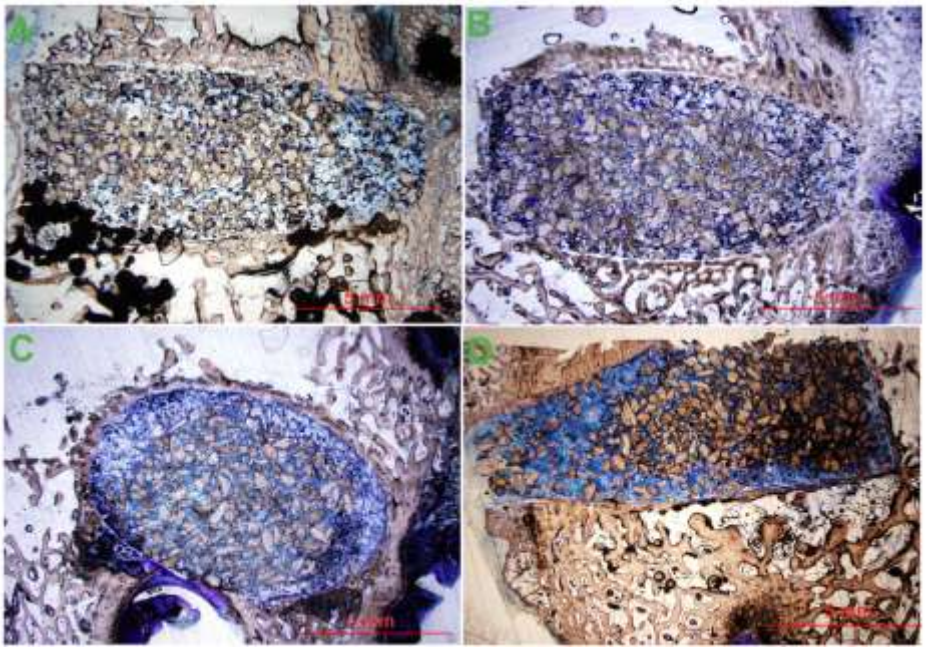

Figure III.7: Low magnification (1.25X) histological sections of all treatment groups at 6 weeks.
(A: 6C3G1L300-MBP, B: 6C3G1L300-SDBP, C: 6C3G1L600-MBP, D: 6C3G1L600-SDBP)

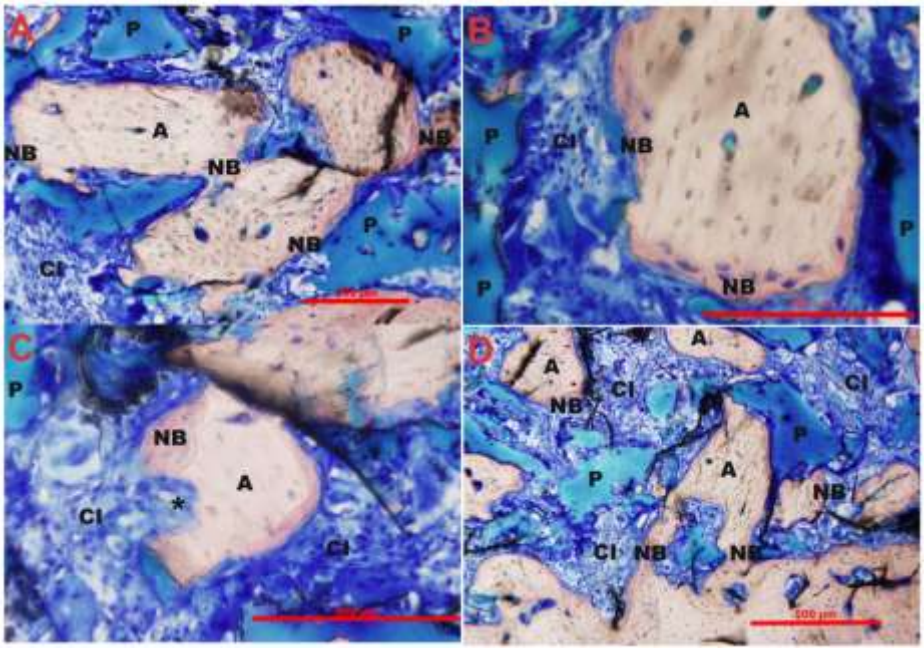

Figure III.8: Remodeling of allograft bone particles in 6C3G1L600-SDBP treatment group.
((A) – (B): New bone formation around the edge of SDBP. Osteocytes are stained blue within the new bone matrix. (20X), (C): Both new bone formation and resorption of SDBP (10X), (D): Islands of polymer surrounded by new bone formation (20X).)

Histomorphometry

Histomorphometric analysis of the 6C3G1L300-AMBP and 6C3G1L600-AMBP implants (Figure 3.9) was performed to quantify the effects of polyester triol molecular weight on allograft resorption, cellular infiltration, polymer degradation, and new bone formation. After 6 weeks implantation time, the AMBP300 implants exhibited 28.3 ± 3.5% residual polymer compared to 29 ± 0.9% for the AMBP600 implants, which is not a significant difference. Furthermore, the concentration of polymer at 6 weeks was close to the initial concentration (32.4 vol% from the mass balance), which suggests that the polymer underwent only a modest amount of degradation after 6 weeks. Despite the small differences in polymer resorption at 6 weeks, cellular infiltration and allograft resorption

were accelerated in the AMBP600 composites, although differences between the two treatment groups were only significant ($p \leq 0.06$) for allograft resorption. However, although bone resorption and cellular infiltration were higher for the AMBP600 composites, the amount of new bone formation was small for both treatment groups (<5%) and the difference between the treatment groups was not significant.

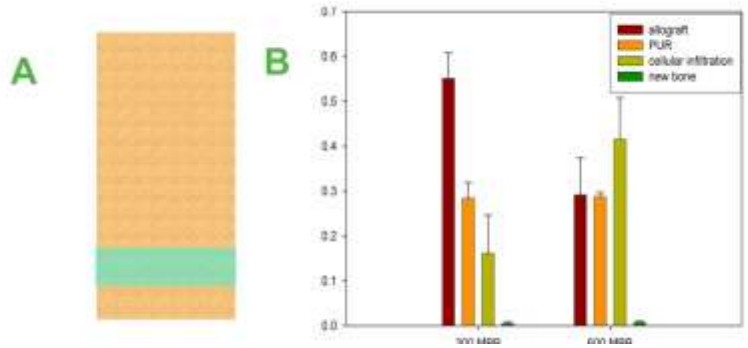

Figure III.9: Histomorphometry of AMBP/PUR composites implanted *in vivo*. Polymer degradation, cellular infiltration, and new bone formation are accelerated in MBP composites incorporating a polyurethane binder with a lower crosslink density. Histomorphometric analysis of an active region of remodeling shows that composites fabricated from the 600 g/mol polyol exhibit faster polymer degradation, cellular infiltration, and new bone formation relative to those prepared from the 300 g/mol polyol.

Discussion

A variety of polymers have been utilized to augment fracture fixation devices and bone replacement materials. While interconnected pores are generally considered necessary to promote bone ingrowth into a polymeric scaffold[3,4], pre-existing pores significantly reduce the initial load-bearing properties[4] of the device. In the present study, we have fabricated allograft bone/polyurethane composites that have tunable initial mechanical properties comparable to those of host bone. When implanted in plug defects in the femoral condyles of NZW rabbits, the allograft bone component of the composites

was resorbed by osteoclasts, thereby creating pores in the composite into which cells infiltrated. Modest polymer degradation and new bone formation were observed. For some of the implants, infiltration of cells deep into the interior was observed after 6 weeks *in vivo*, which is surprising for solid composites with minimal void space (e.g., <5% porosity).

Several studies have described the preparation of weight-bearing composites incorporating various fillers (such as bioactive glass or hydroxyapatite) for orthopaedic applications. Composites fabricated from synthetic polymers and bioactive glass, which was developed in the early 1970's, have been reported.[63] Young's modulus values as high as 13.6 GPa have been achieved for materials comprising bioglass, urethane dimethacrylate, 2-hydroxylethyl methacrylate, and a photosynthesizing agent.[64] While this value of Young's modulus is close to that of cortical bone, the acrylate polymer component of the bioglass composites was non-degradable. Furthermore, bioactive glass has a slow resorption time, typically greater than 1 year.[1,65] Thus the combination of a non-degradable polymer and slowly resorbing filler is anticipated to limit the extent of bone ingrowth and remodeling of the composite. Resorbable composite IM rods have been fabricated from hydroxyapatite (HA, 20-30 wt%) and poly(L-lactide) (PLLA) that exhibit bending strength and modulus up to 280 MPa and 7.8 GPa, respectively.[26] Resorption and new bone formation were observed after 5-7 years when HA/PLLA composites were implanted in NZW rabbit femoral plug defects. In a rabbit femoral intramedullary (IM) rod study, bone bridging between HA and host bone was dependent upon the degradation rate of PLLA to allow exposure of HA particles on the surface of the implant.[66] Slowly degrading PLLA implants can take up to 2 years to degrade,

leaving behind crystallites that have been reported to induce an inflammatory response.[67] In the metaphyseal region of the rabbit femur, the complete degradation of the PLLA occurred after 4.5 years, while the HA particles were replaced with new bone after 5.5 years.[66] In contrast, the AMBP/PUR composites supported rapid bone resorption and cellular infiltration after only 6 weeks *in vivo*. Since the cells infiltrated the implants through resorption of the nearly continuous AMBP phase (as discussed in greater detail below), degradation of the PUR binder was not necessary. The histomorphometry data (Figure 3.8) further support the observation that polymer degradation did not precede remodeling, considering that the allograft bone volume fraction decreased from 67.6 vol% to 30 – 55 vol%, a substantial reduction compared to that observed for the polymer.

Allograft bone has been a standard of care for the treatment of orthopedic defects because of its osteoconductive properties.[68,69] However, allograft devices remodel slowly due to the low specific surface area. By combining particulated allograft bone at volume fractions approaching the random close packing limit (64%[70]) with a polymer binder, we reasoned that it would be possible to fabricate composites that undergo more rapid remodeling due to the presence of a nearly continuous allograft bone surface throughout the implant. The extent of bone remodeling in particulated allograft bone/polymer composites has been reported to increase with increasing allograft bone content, with a dramatic increase in both cellular penetration into the implant and new bone formation at 75wt% (~61 vol%) bone particles.[36] In the present study, the particulated allograft content was increased to 79 wt% (67.6 – 67.9 vol% from the mass balance), which slightly exceeded the RCP limit for spheres and approached the limit for acceptable mechanical properties (83 wt%). At the RCP limit, bone particles were in close contact or

separated by a thin film, thus presenting a nearly continuous osteoconductive pathway for cells to penetrate the implant by resorbing allograft and migrating into the resulting newly formed pores (Figure 3.10A, B, and C). However, in some cases, non-ideal mixing of the reactive composite paste resulting in polymer-rich regions where the continuous bone phase was partially interrupted (Figure 3.10C). While cellular infiltration slowed in the polymer-rich region, cells further infiltrated the implant in an adjacent region where there was closer contact between bone particles (Figure 3.10B). Non-ideal mixing is not surprising due to the high viscosity of the reactive two-component PUR binder, especially in the case of the 600 MW groups.

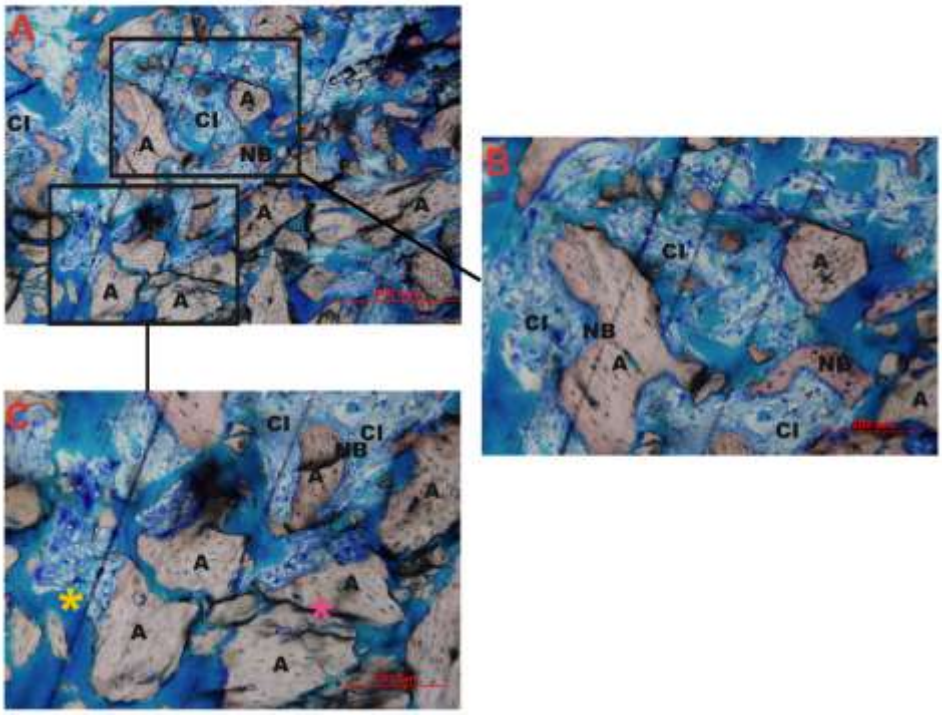

Figure III.10: The process of creeping substitution is accelerated by the presence of a continuous, percolated bone phase.
(Remodeling of MBP/PUR composite occurring around the un-remodeled core. (A) 10X micrograph near the boundary between an actively remodeling region and the un-remodeled core. (B) An area of active of active remodeling just outside the un-remodeled core (20X). (C) A region enriched in polymer where the residual polymer hinders the penetration of cells (20X). (D) A region where bone particle contacts provide a pathway for infiltration.)

A majority of the composite treatment groups showed increased remodeling activity at the ends of the implant (top and bottom), particularly when the implant was both in direct apposition to the host trabecular bone and exhibited regions enriched in allograft due to non-ideal mixing. Figure 3.11 shows the top of a composite from the AMBP300 group that underwent both extensive cellular infiltration as well as polymer degradation, and exhibited greater new bone formation. Cellular infiltration, allograft resorption, polymer degradation, and new bone formation were substantially higher in this particular implant compared to other samples in the AMBP300 treatment group,

presumably due to close contact between an allograft-rich region of the implant and host bone at the base of the implant. With the exception of the implant shown in Figure 3.11, composites prepared from the 600 MW groups exhibited faster polymer degradation, cellular infiltration, and allograft resorption due to the lower cross-link density of the PUR networks synthesized from 600 g/mol polyester triols. The dramatically faster rate of remodeling of bone/polymer composites (~6 wks) relative to the HA/PLLA implants (~4 yrs) is conjectured to result from either the greater bioactivity of AMBP, the presence of a particulated continuous osteoconductive phase, or both. In the AMBP/PUR composites, resorption of the bone particles is thus independent of polymer degradation because the particles are already exposed on the surface of the implant, unlike the HA/PLLA composites.

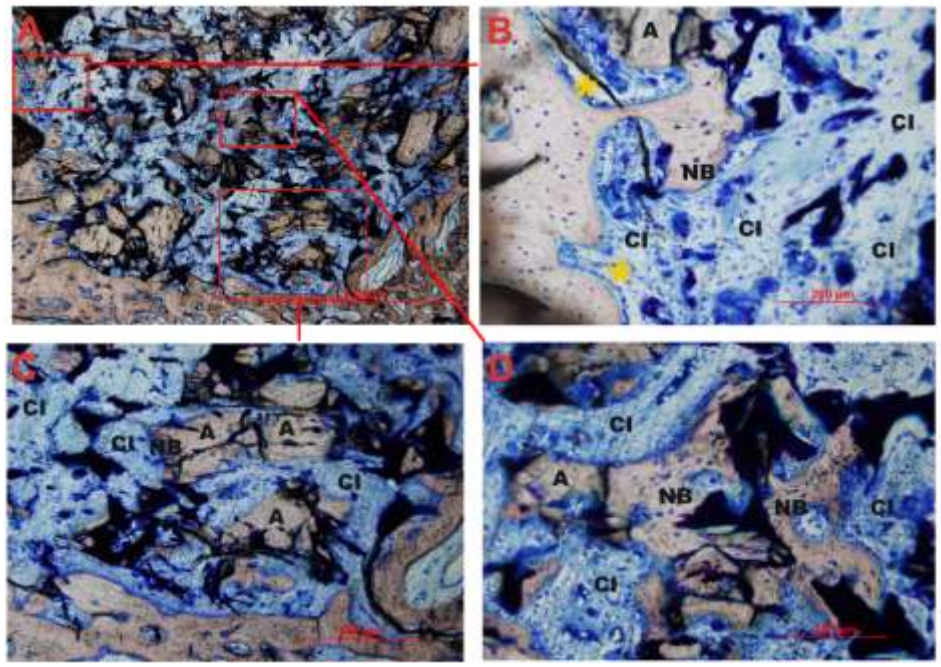

Figure III.11: Low magnification histology (2.5x).
(There is extensive cellular infiltration, polymer degradation, and new bone formation in a 6C3G1L300-MBP implant. (B) – (C) Higher magnification (20X). (D) – (E) high magnification (40X).)

The AMBP/PUR implants initially remodeled by creeping substitution, characterized by resorption of allograft followed by new bone formation.[62,71] However, the rate at which osteoclasts resorbed allograft and cells infiltrated the implant strongly depended on the formulation of the composite (Figure 3.7D). Cellular infiltration was highest for the 6C3G1L600-AMBP group, where cells had penetrated deep into the interior of the non-porous implant after only 6 weeks. As a result of these processes, an outer ring of demineralized tissue with a modest amount of new bone formation was created around the un-remodeled core. It is conjectured that as the resorption and remodeling proceeds, cells will penetrate further into the core of the implant and new bone will form behind the resorption front, resulting in re-mineralization of the entire

implant. Thus the allograft particles function as a biologically active "porogen", wherein pores are created as the allograft particles are resorbed, followed by cellular migration, matrix deposition, and new bone formation in the newly formed pores. At the short 6 week time point investigated in this study, the amount of new bone formation was modest. Considering that weight-bearing implants must maintain a threshold mechanical strength during the remodeling process, it is desirable that that the resorption front be as sharp as possible, since a broad resorption front would reduce the mechanical properties of the implant to levels substantially below its initial value. Considering the well-known effects of angio-osteogenic factors, such as rhFGF-2 and rhBMP-2, on enhanced mineralization of porous polymeric scaffolds, it is conjectured that addition of a suitable growth factor would accelerate new bone formation, thereby possibly preserving the weight-bearing mechanical properties of the implant throughout the remodeling process.

Interfacial bonding is well-known to enhance the mechanical properties of composites. The absorbance data in Figure 3.2 show that AMBP in contact with FITC exhibited a higher absorbance than the negative (AMBP + buffer with no FITC) and positive (FITC solution in a tissue culture plastic well plate with no AMBP) controls. The higher fluorescent absorbance observed for FITC-treated AMBP is conjectured to result from covalent binding of the isothiocyanate (N=C=S) groups in FITC with nucleophiles such as amine and hydroxyl groups present in the proteins in the allograft bone. SDBP treated with FITC exhibited significantly higher absorbance relative to FITC-treated AMBP, which is consistent with the XPS data showing that surface demineralization increased the concentration of protein on the surface. These data suggest that the amine and hydroxyl groups on the surface of the allograft particles react with the isocyanate

(N=C=O) groups in the LTI to form urea and urethane bonds, respectively, and that surface demineralization would increase the mechanical properties of the composites. Surprisingly, the data in Table 3.2 show that composites fabricated from SDBP exhibited comparable mechanical properties to those prepared from AMBP. Thus while surface-demineralization enhanced the reactivity of the allograft surface, it did not significantly increase the mechanical properties. Non ideal mixing is a contributor to the negligible effect of SDBP on mechanical properties as polyol can coat the surface of SDBP, preventing the reaction between the bone surface and isocyanate.

The Takayanagi models have been applied to model the mechanical properties of two-phase polymer blends and composites. Assuming the geometry of a circular cross section of the filler is isometric, the Takayanagi models yield the following equations for the compressive modulus E of the composite as a function of the volume fraction and compressive modulus for each phase[49]:

$$E = \left(\frac{\nu_1}{E_1} + \frac{\nu_2}{E_2} \right)^{-1} \tag{1}$$

$$E = \sqrt{\nu_1} \left[\frac{\sqrt{\nu_1}}{E_1} + \frac{1-\sqrt{\nu_1}}{E_2} \right]^{-1} + \left(1-\sqrt{\nu_1}\right) E_2 \tag{2}$$

$$E = \sqrt{\nu_2} \left[\frac{\sqrt{\nu_2}}{E_2} + \frac{1-\sqrt{\nu_2}}{E_1} \right]^{-1} + \left(1-\sqrt{\nu_2}\right) E_1 \tag{3}$$

$$E = \nu_1 E_1 + \nu_2 E_2 \tag{4}$$

where ν_1 is the volume fraction allograft bone, E_1 is the compressive modulus of the allograft bone particles, ν_2 is the volume fraction PUR, and E_2 is the compressive modulus of the PUR component. Eqs (1) – (4) were derived assuming different composite morphologies. Eq (1), which is equivalent to the well-known Reuss model[72], assumes that neither phase is continuous in space, and eq (4), which is equivalent to the well-known Voigt model[73], assumes that both the allograft particles and PUR binder are continuous in space. More physically relevant morphologies intermediate to these upper (Voigt model) and lower (Reuss model) bounds are described by eq (2), which assumes that the PUR binder is continuous, and eq (3), which assumes that the allograft particles are continuous. Values of the composite compressive modulus calculated from each of these conditions are listed in Table 3.3.

Table III.3: Takayanagi model calculations for compressive modulus of bone/polymer composites.

(All composites incorporated 79 wt% allograft bone particles. E_C denotes calculated compressive modulus calculated from the Takayanagi models.)

Property	**MBP300**	**SDBP300**	**MBP600**	**SDBP600**
Bone density, g cm^{-3}	2.3	2.3	2.3	2.3
PUR density, g cm^{-3}	1.274 ± 0.005[74]	1.274 ± 0.005[74]	1.290 ± 0.003	1.290 ± 0.003
Bone modulus, GPa[75]	18.6	18.6	18.6	18.6
PUR modulus, GPa	1.427 ± 0.039[74]	1.427 ± 0.039[74]	0.988 ± 0.055	0.988 ± 0.055
Volume fraction bone, %	67.60%	67.60%	67.90%	67.90%
Volume fraction polymer, %	32.40%	32.40%	32.10%	32.10%
E_C, both phases discont., GPa	3.79	3.79	2.76	2.76
E_C, PUR continuous, GPa	5.12	5.12	3.87	3.87
E_C, MBP continuous, GPa	9.36	9.36	9	9
E_C, PUR and MBP continuous, GPa	13	13	12.9	12.9
E_C, experimental, GPa	6.01 ± 0.34	5.52 ± 0.11	3.05 ± 0.64	3.66 ± 0.39

A value of 18.6 GPa was used for the modulus of allograft cortical bone.[74] The volume fraction of allograft calculated from the mass balance was ~68 vol%, which exceeds the

spherical random close packing (RCP) limit of 64 vol%. Histomorphometric analysis of the regions near the center of the implant (which were not penetrated by cells) yielded allograft volume fractions ranging from 66 – 74 vol% (Figure 3.4). Qualitative examination of the histological sections showed that the AMBP filler was nearly continuous throughout most of the implant, but there were some regions enriched in polymer and depleted in bone particle-particle contacts. Thus, the mass balance and histomorphometric data suggest that the AMBP filler was continuous and percolated throughout most of the implants, indicating that the compressive modulus of the composites is most accurately predicted by eq (3). Interestingly, the experimental values of the compressive modulus were within 1 GPa of the calculated values assuming a continuous PUR phase, but 3 – 6 GPa less than those calculated assuming a continuous AMBP phase. Considering that surface demineralization enhances allograft reactivity but not composite mechanical properties, insufficient interfacial bonding cannot explain the lower experimental values of the compressive modulus relative to the Takayanagi model predictions. Closer examination of the histological sections near the core (Figure 3.4) revealed that not all of the particle-particle interactions were point contacts, but rather extensive areas of contact where there was minimal polymeric binder present between the allograft particles, thereby creating defects along which cracks could propagate. However, it is conjectured that these defects also accelerated allograft resorption by increasing the area available for cellular infiltration. Thus biomechanics and remodeling are inter-related, such that the mechanical properties are reduced as the RCP limit is approached, but the processes of resorption and cellular infiltration are accelerated.

Conclusions

Non-porous AMBP/PUR composites are a high strength, osteoconductive biomaterial suitable with initial mechanical properties suitable for weight-bearing applications. The mechanical properties and cellular infiltration rate can be tuned for specific applications by manipulating the molecular weight of the polyester polyol used during synthesis. Cellular infiltration and new bone formation were observed in the interior of the implant at 6 weeks, which is surprising for composites with such low porosity (<5%). Osteoclast-mediated resorption of the allograft particles created pores into which cells migrated, followed by deposition of new collagen matrix and bone formation. Due to the time lag between resorption and re-mineralization, a resorption front was observed at 6 weeks, which is anticipated to reduce the mechanical properties as the implant remodels. Although further time points are needed to investigate the full resorption and the profile of new bone formation, the findings from this study suggest that AMBP/PUR composites may have potential application as biologically active weight-bearing devices for bone tissue engineering.

REFERENCES

1. Khan Y, Yaszemski MJ, Mikos AG, Laurencin CT. Tissue Engineering of Bone: Material and Matrix Considerations. J Bone Joint Surg Am 2008;90(Supplement_1):36-42.

2. Joseph J-G. Polymers for tissue engineering, medical devices, and regenerative medicine. Concise general review of recent studies. Polymers for Advanced Technologies 2006;17(6):395-418.

3. Murphy J, Pomrink G, Clineff T, Erbe E. Biocompatibility, mechanical and physical properties of a bone bonding ceramic reinforced polymer composite for orthopaedic implants. 2002; Reno, NV. p 395.

4. Burg KJ, Porter S, Kellam JF. Biomaterial developments for bone tissue engineering. Biomaterials 2000;21:2347-59.

5. Trends and Opportunities in U.S. Orthopaedic Markets for Implant, Reconstruction, and Trauma Products (Report A310). Newport Beach, CA: Medtech Insight; 2004. Report nr A310. 360 p.

6. Eppley BL. Craniofacial reconstruction with computer-generated HTR patient-matched implants: use in primary bony tumor excision. J Craniofacial Surgery 2002;13(5):650-657.

7. Ohlin A, Linder L. Biocompatibility of polyoxymethylene (delrin) in bone. Biomaterials 1993;14(4):285-289.

8. Belkoff SM, Molloy S. Temperature measurement during polymerization of polymethylmethacrylate cement used for vertebroplasty. Spine 2003;28(14):1555-9.

9. Deramond H, Wright NT, Belkoff SM. Temperature elevation caused by bone cement polymerization during vertebroplasty. Bone 1999;25(2 Suppl):17S-21S.

10. Diaz-Flores L, Gutierrez R, Lopez-Alonso A, Gonzalez R, Varela H. Pericytes as a supplementary source of osteoblasts in periosteal osteogenesis. Clin. Orthop. Rel. Res. 1992;275:280-286.

11. Mitchell W, Bridget Matthews J, Stone MH, Fisher J, Ingham E. Comparison of the response of human peripheral blood mononuclear cells to challenge with particles of three bone cements in vitro. Biomaterials 2003;24(5):737-48.

12. Tilyard MW, Spears GFS, Thomson J, Dovey S. Treatment of postmenopausal osteoporosis with calcitriol or calcium. N. Engl. J. Med. 1992;326:357-362.

13. Ishiguro N, Kojima T, Ito T, Saga S, Anma H, Kurokouchi K, Iwahori Y, Iwase T, Iwata H. Macrophage activation and migration in interface tissue around loosening total hip arthroplasty components. J Biomed Mater Res 1997;35(3):399-406.

14. Bai B, Jazrawi LM, Kummer FJ, Spivak JM. The use of an injectable, biodegradable calcium phosphate bone substitute for the prophylactic augmentation of osteoporotic vertebrae and the management of vertebral compression fractures. Spine 1999;24(15):1521-6.

15. Ohura K, Bohner M, Hardouin P, Lemaitre J, Pasquier G, Flautre B. Resorption of, and bone formation from, new beta-tricalcium phosphate-monocalcium phosphate cements: an in vivo study. J Biomed Mater Res 1996;30(2):193-200.

16. Knaack D, Goad ME, Aiolova M, Rey C, Tofighi A, Chakravarthy P, Lee DD. Resorbable calcium phosphate bone substitute. J Biomed Mater Res 1998;43(4):399-409.

17. Frankenburg EP, Goldstein SA, Bauer TW, Harris SA, Poser RD. Biomechanical and histological evaluation of a calcium phosphate cement. J Bone Joint Surg Am 1998;80(8):1112-24.

18. Yuan H, Li Y, de Bruijn JD, de Groot K, Zhang X. Tissue responses of calcium phosphate cement: a study in dogs. Biomaterials 2000;21(12):1283-1290.

19. Metsger DS, Driskell TD, Paulsrud JR. Tricalcium phosphate ceramic--a resorbable bone implant: review and current status. J Am Dent Assoc 1982;105(6):1035-8.

20. Hollinger JO, Battistone GC. Biodegradable bone repair materials. Synthetic polymers and ceramics. Clin Orthop Relat Res 1986(207):290-305.

21. Chim H, Gosain AK. Biomaterials in craniofacial surgery experimental studies and clinical application J Craniofac Surg 2009;20:29-33.

22. Hollier LH, Stal S. The use of hydroxyapatite cements in craniofacial surgery. Clin Plastic Surg 2004;31:423-428.

23. Pyhältö T, Lapinsuo M, Pätiälä H, Pelto M, Törmälä P, Rokkanen P. Fixation of distal femoral osteotomies with self-reinforced polymer/bioactive glass rods: an experimental study on rabbits. Biomaterials 2005;26(6):645-654.

24. Shinsuke I, Jiro T, Taizo F, Takashi N, Yoshitaka M, Yasuo S, Masaki O. Long-term study of high-strength hydroxyapatite/poly(L-lactide) composite rods for the internal fixation of bone fractures: A 2-4-year follow-up study in rabbits. Journal of Biomedical Materials Research Part B: Applied Biomaterials 2003;66B(2):539-547.

25. Stephane A, Denis C, Patrick F, Marie Francois H, Jean Charles Le H. Biological performance of a new beta-TCP/PLLA composite material for applications in spine surgery: <I>In vitro</I> and <I>in vivo</I> studies. Journal of Biomedical Materials Research Part A 2006;78A(2):416-422.

26. Hasegawa S, Ishii S, Tamura J, Furukawa T, Neo M, Matsusue Y, Shikinami Y, Okuno M, Nakamura T. A 5-7 year in vivo study of high-strength hydroxyapatite/poly(l-lactide) composite rods for the internal fixation of bone fractures. Biomaterials 2006;27(8):1327-1332.

27. Canul-Chuil A, Vargas-Coronado R, Cauich-Rodriguez JV, Martinez-Richa A, Fernandez E, Nazhat SN. Comparative study of bone cements prepared with either HA or alpha-TCP and functionalized methacrylates. J Biomed Mater Res B Appl Biomater 2003;64(1):27-37.

28. Hitchon PW, Goel V, Drake J, Taggard D, Brenton M, Rogge T, Torner JC. Comparison of the biomechanics of hydroxyapatite and polymethylmethacrylate vertebroplasty in a cadaveric spinal compression fracture model. J Neurosurg 2001;95(2 Suppl):215-20.

29. de Boer HH. The history of bone grafts. Clin Orthop Relat Res 1988(226):292-8.

30. Goldberg VM, Stevenson S. Natural history of autografts and allografts. Clin Orthop Relat Res 1987(225):7-16.

31. Yaszemski MJ, Payne RG, Hayes WC, Langer R, Mikos AG. Evolution of bone transplantation: molecular, cellular and tissue strategies to engineer human bone. Biomaterials 1996;17(2):175-85.

32. Boyce TM, Winterbottom JM, Kaes DR, Shimp LA, Knaack DA. Development of a bone-derived composite implant for skeletal applications. In: Hollinger JO, editor; 2003; Pittsburgh, PA. Proceedings from the Pittsburgh Bone Symposium, 2003.

33. Eagan MJ, McAllister DR. Biology of Allograft Incorporation. Clinics in Sports Medicine 2009;28(2):203-214.

34. Market Dynamics:Bone Substitutes and Growth Factors. New York: Datamonitor (DMHC1812); 2002. p 118-32.

35. Newton CD, Nunamaker DB. Textbook of small animal orthopaedics. Philadelphia: Lippincott; 1985.

36. Boyce TM WJ, Lee S, Kaes DR, Belaney RM, Shimp LA, Knaack D. Celluar Penetration and Bone Formation Depends upon Allograft Bone Fraction in a Loadbearing Composite Implant. Trans Soc. Biomaterials 2005(Society for Biomaterials Annual Meeting, 2005):p 133.

37. Zhang J, Doll BA, Beckman EJ, Hollinger JO. A biodegradable polyurethane-ascorbic acid scaffold for bone tissue engineering. J Biomed Mater Res A 2003;67(2):389-400.

38. Zhang JY, Doll BA, Beckman EJ, Hollinger JO. Three-dimensional biocompatible ascorbic acid-containing scaffold for bone tissue engineering. Tissue Eng 2003;9(6):1143-57.

39. Zhang JY, Beckman EJ, Piesco NP, Agarwal S. A new peptide-based urethane polymer: synthesis, biodegradation, and potential to support cell growth in vitro. Biomaterials 2000;21(12):1247-1258.

40. Zhang JY, Beckman EJ, Hu J, Yang GG, Agarwal S, Hollinger JO. Synthesis, biodegradability, and biocompatibility of lysine diisocyanate-glucose polymers. Tissue Eng 2002;8(5):771-85.

41. Katarzyna Gorna SG. Preparation, degradation, and calcification of biodegradable polyurethane foams for bone graft substitutes. Journal of Biomedical Materials Research Part A 2003;67A(3):813-827.

42. Guelcher SA, Patel V, Gallagher KM, Connolly S, Didier JE, Doctor JS, Hollinger JO. Synthesis and in vitro biocompatibility of injectable polyurethane foam scaffolds. Tissue Eng 2006;12(5):1247-59.

43. Guelcher S, Srinivasan A, Hafeman A, Gallagher K, Doctor J, Khetan S, McBride S, Hollinger J. Synthesis, in vitro degradation, and mechanical properties of two-component poly(ester urethane)urea scaffolds: effects of water and polyol composition. Tissue Eng 2007;13(9):2321-33.

44. Gogolewski S, Gorna K. Biodegradable polyurethane cancellous bone graft substitutes in the treatment of iliac crest defects. J Biomed Mater Res A 2007;80(1):94-101.

45. R. F. Storey JSWADP. Hydrolyzable poly(ester-urethane) networks from L-lysine diisocyanate and D,L-lactide/e-caprolactone homo- and copolyester triols. Journal of Polymer Science Part A: Polymer Chemistry 1994;32(12):2345-2363.

46. Guelcher SA, Srinivasan A, Dumas JE, Didier JE, McBride S, Hollinger JO. Synthesis, mechanical properties, biocompatibility, and biodegradation of polyurethane networks from lysine polyisocyanates. Biomaterials 2008;29(12):1762-1775.

47. Oertel G. Polyurethane Handbook. Berlin: Hanser Gardner Publications; 1994.

48. Guelcher SA. Biodegradable polyurethanes: synthesis and applications in regenerative medicine. Tissue Eng Part B Rev 2008;14(1):3-17.

49. Sperling LH. Polymeric Multicomponent Materials. New York: John Wiley & Sons; 1997.

50. Kumpf RJ, Wiggins JS, Pielartzik H. Reactive processing of engineering thermoplastics. Trends in Polymer Science 1995(3):132.

51. Kai-Uwe L, Vasan V, William WT, Kevin TS, Henry JM, Thomas FD. Kinetics of cortical bone demineralization: Controlled demineralization - a new method for modifying cortical bone allografts. Journal of Biomedical Materials Research 1996;31(3):365-372.

52. Hull D. An Introduction to Composite Materials. Cambridge: Cambridge University Press; 1981.

53. Tanoglu M, McKnight SH, Palmese GR, Gillespie JW. Use of silane coupling agents to enhance the performance of adhesively bonded alumina to resin hybrid composites. Int J Adhesion & Adhesives 1998;18:431-434.

54. Plueddemann EP. In: Kroschwitz JI, editor. Encyclopedia of Polymer Science and Engineering. New York: Wiley; 1985.

55. Nguyen H, Qian JJ, Bhatnagar RS, Li S. Enhanced cell attachment and osteoblastic activity by P-15 peptide-coated matrix in hydrogels. Biochem Biophys Res Commun 2003;311(1):179-86.

56. Thorwarth M, Schultze-Mosgau S, Wehrhan F, Srour S, Wiltfang J, Neukam FW, Schlegel KA. Enhanced bone regeneration with a synthetic cell-binding peptide--in vivo results. Biochem Biophys Res Commun 2005;329(2):789-95.

57. Jing Jing Q, Rajendra SB. Enhanced cell attachment to anorganic bone mineral in the presence of a synthetic peptide related to collagen. Journal of Biomedical Materials Research 1996;31(4):545-554.

58. Amarpreet S. Sawhney JAH. Rapidly degraded terpolymers of DL-lactide, glycolide, and &epsis;-caprolactone with increased hydrophilicity by copolymerization with polyethers. Journal of Biomedical Materials Research 1990;24(10):1397-1411.

59. Marotti G MM. A scanning Electron Microscope Study of Human Bony Lamellae. Proposal for a new model of collagen lamellar organization. Archivio italiano di anatomia e di embriologia. 1988;93(3):163-175.

60. H. Kothandaraman ASNRKL. Synthesis and thermal dissociation of phenol- and naphthol-blocked diisocyanates. Journal of Applied Polymer Science 1994;53(1):31-38.

61. Lozano LF, Peña-Rico MA, Heredia A, Ocotlán-Flores J, Gómez-Cortés A, Velázquez R, Belío IA, Bucio L. Thermal analysis study of human bone. Journal of Materials Science 2003;38(23):4777-4782.

62. Burchardt H. The biology of bone graft repair. Clin Orthop Relat Res 1983(174):28-42.

63. Kenny SM, Buggy M. Bone cements and fillers: a review. J Mater Sci Mater Med 2003;14(11):923-38.

64. Veronika A. Koleganova SMBSJDASR. Bioactive glass/polymer composite materials with mechanical properties matching those of cortical bone. Journal of Biomedical Materials Research Part A 2006;77A(3):572-579.

65. Hak DJ. The use of osteoconductive bone graft substitutes in orthopaedic trauma. J Am Acad Orthop Surg 2007;15(9):525-36.

66. Shikinami Y, Matsusue Y, Nakamura T. The complete process of bioresorption and bone replacement using devices made of forged composites of raw hydroxyapatite particles/poly l-lactide (F-u-HA/PLLA). Biomaterials 2005;26(27):5542-5551.

67. An YH, Woolf SK, Friedman RJ. Pre-clinical in vivo evaluation of orthopaedic bioabsorbable devices. Biomaterials 2000;21(24):2635-2652.

68. Sammarco VJ, Chang L. Modern issues in bone graft substitutes and advances in bone tissue technology. Foot and Ankle Clinics of North America 2002;7(1):19-41.

69. Stevenson S. Biology of Bone Grafts. Orthopedic Clinics of North America 1999;30(4):543-552.

70. Radin C. Random Close Packing of Granular Matter. Journal of Statistical Physics 2008;131(4):567-573.

71. Chacha PB. Vascularised pedicular bone grafts. International Orthopaedics 1984;8(2):117-138.

72. Watt JP, Davies GF, O'Connell RJ. The Elastic Properties of Composite Materials. Reviews of Geophysics and Space Physics 1976;14(4):541.

73. Dainiak N, Davies G, Kalmanti M, Lawler J, Kulkarni V. Platelet-derived growth factor promotes proliferation of erythropoietic progenitor cells in vitro. J Clin Invest 1983;71:1206-1214.

74. Cuppone M, Seedhom BB, Berry E, Ostell AE. The longitudinal Young's modulus of cortical bone in the midshaft of human femur and its correlation with CT scanning data. Calcif Tissue Int 2004;74(3):302-9.

CHAPTER IV.

Synthesis, characterization, and remodeling of porous allograft mineralized bone particle/polyurethane bone void filler in a rat model

Introduction

There is a well-recognized need for improved biomaterials for the treatment of bone defects. Although autologous bone grafts are considered to be the standard of care due to their osteoconductive and osteoinductive properties, there is a limited supply of autograft and the harvesting procedure introduces potential donor site morbidity. Due to these limitations, considerable effort has been expended toward the development of synthetic bone graft materials. Alternative biomaterials must be biocompatible, resorbable, support cellular attachment and proliferation, and support the ingrowth of new bone tissue.

Injectable biomaterials offer several advantages relative to implantable biomaterials due to their ability to cure *in situ*, thus conforming to irregularly-shaped defects. Some commercially available injectable materials marketed as bone void fillers include calcium phosphate-based bone cements.[1-4] These biomaterials are osteoconductive, have compressive strengths comparable to trabecular bone (e.g., 5 – 40 MPa), and have fast setting times (~10 – 15 minutes).[2,4] Although calcium phosphate bone cements are porous, the pore size is in the range of 1 μm.[5] This renders the material relatively impermeable to cellular infiltration leading to a slower rate of resorption and new bone formation.[2,6] Additionally, calcium phosphate cements are subject to brittle fracture and

graft migration, potentially leading to infections and requiring additional surgeries for repair or removal.[4,7,8] For craniofacial applications, mechanical failure of bone cements has been attributed to pulsatile forces from the blood supply of the dura.[6,8,9]

With the advent of technologies for sterilization and viral inactivation, mineralized human bone allografts have emerged as a preferred implant type for weight-bearing orthopaedic and spinal applications.[10] While concerns have been raised regarding the risk of disease transmission, it is significant that Osteotech has produced >3.5M grafts from >40,000 donors since 1991 with no confirmed report of disease transmission.[11] Allografts have excellent weight-bearing biomechanical properties and they undergo extensive osseous integration by osteoclasts and osteoblasts. Furthermore, these materials contain all the physiologically relevant elements and salts, such as silicon, boron, and strontium, in the exact proportions at which they are most effective.[12] However, the anatomy of the donor bone limits the reproducibility and range of mineralized allograft shapes available for clinical use.[10] Furthermore, while the extent of integration is generally considered adequate, remodeling of the graft seldom exceeds 50%, which limits its use in the clinic.[13] Since remodeling proceeds from the external surface to the interior through the process of creeping substitution[14], the limited remodeling of allograft devices is conjectured to be due in part to their low specific surface area, which scales inversely with particle diameter. By processing the allograft cortical bone into small particles < 1 mm, the specific surface area is increased, which can lead to incomplete remodeling.[15]

Two-component polyurethanes (PUR) are a potentially useful class of biomaterials due to their potential injectability. By mixing a polyisocyanate with a hardener

comprising a polyol, water, and tertiary amine catalyst, a reactive liquid mixture is formed that subsequently cures to form a solid porous elastomeric scaffold within 10 – 15 minutes *in situ*.[16] Use of isocyanate-functional prepolymers mitigates the toxicity hazards associated with injection of monomeric polyisocyanates. Biodegradable PUR scaffolds synthesized from lysine-derived and aliphatic polyisocyanates have been shown to degrade to non-toxic compounds[17] and support cell attachment and proliferation *in vitro*. These materials also have tunable degradation rates, which are shown to be highly dependent on the choice of polyol and isocyanate components.[18] Polyurethanes have tunable mechanical properties, which can also be enhanced with the addition of fillers,[19] and exhibit elastomeric rather than brittle mechanical properties. While many synthetic polymers (such as poly(α-ester)s and polyurethanes) support modest bone ingrowth, the addition of osteoconductive fillers such as α-TCP has been reported to increase not only the mechanical properties, but also the extent of bone ingrowth and new bone formation.[20]

In previous studies, the osteoconductive filler content ranged from 10 – 40 wt% (~4 – 18 vol%). Due to its relatively low volume fraction, the filler was completely embedded in polymer; thus the rate of remodeling scaled with the rate of polymer degradation.[21] Furthermore, the particle size of the mineralized filler was generally < 20 μm, which is below the preferred size range for remodeling by creeping substitution.[21] In the present study, we aimed to accelerate the rate of remodeling of bone/polymer composites by incorporating >100 μm allograft bone particles and a modest (e.g., 30 - 60%) amount of porosity. We reasoned that increasing the allograft content while maintaining porosity would accelerate cellular infiltration into the composites through

both migration of cells into open pores, as well as remodeling of allograft particles by creeping substitution. Thus we investigated the effects of porosity on the mechanical and processing properties of bone/polyurethane composites comprising 45 – 50wt% (31 – 36 vol%) allograft bone particles, which was the highest allograft loading achieved for an injectable system. To evaluate the *in vivo* biocompatibility and remodeling of the bone/polymer composites, the composition representing an optimum balance of porosity and initial mechanical properties was injected into bilateral femoral condyle plug defects in athymic rats.

Methods and Materials

Materials

ε-Caprolactone, the blowing catalyst bis (2-dimethylaminoethyl) ether (DMAEE), the gelling catalyst triethylene diamine (TEDA), dipropylene glycol (DPG), and poly(ethylene glycol) (PEG, MW 200-Da) were all obtained from Sigma-Aldrich (St. Louis, MO). Glycolide and D,L-lactide were purchased from Polysciences, Inc. (Warrington, PA). The tertiary amine gelling catalyst TEGOAMIN33 was received from Goldschimidt (Hopewell, VA). Lysine Triisocyanate (LTI) was obtained from Kyowa Hakko USA. Bovine (B-MBP) and human (H-MBP) mineralized bone particles (MBP) were obtained from Osteotech, Inc. (Eatontown, NJ). With the exception of ε-caprolactone, PEG, DMAEE, and glycerol, all materials were used as received. Prior to use, PEG and glycerol were dried at 10 mm Hg for at least 4 hours at 80°C, and ε-caprolactone was dried over anhydrous magnesium sulfate. DMAEE was blended with DPG at a 70:30 mass ratio.

Polyester macrotriol synthesis and characterization

Polyester triols of 900-Da molecular weight, T6C3G1L900, were prepared with a trifunctional glycerol starter and 60 wt% e-caprolactone, 30% glycolide, 10% D,L-lactide, and stannous octoate catalyst (0.1%), as previously described.[22] These components were mixed with mechanical stirring in a three-neck flask for 36 hours under argon at 140°C. The product was then dried under vacuum for at least 24 hours at 80°C, followed by the preparation ofa concentrated solution in dichloromethane and washing 3x with hexane.[22] The hydroxyl (OH) number was measured by titration according to ASTM D4274-99 Method C[22], and the molecular weight was measured by GPC (Waters Breeze) using two MesoPore 300x7.5mm columns (Polymer Laboratories, Amherst, MA) in series and a stabilized tetrahydrofuran (THF) mobile phase. The polyol hardener was produced by mixing the appropriate amounts of T6C3G1L900, deionized (DI) water, DMAEE, and TEGOAMIN33 in a Hauschild SpeedMixer™ DAC 150 FVZ-K vortex mixer (FlackTek, Inc., Landrum, SC). In an alternative method, a high NCO quasi-prepolymer was synthesized by adding the polyester to hexamethylene diisocyanate (HDI). The %NCO of the prepolymer was measured by titration using ASTM D2572-97[23], and the hydroxyl number calculated from the mass balance and measured %NCO.

Prepolymer synthesis and characterization

The LTI-PEG prepolymer was synthesized by adding poly(ethylene glycol) (200 g/mol, PEG200) dropwise over the course of 1 hour to LTI in a three-neck flask while stirring under argon. The mixture was then stirred for 24 hours at 45°C, and the subsequently dried under vacuum for at least 24 hours at 80°C. The NCO:OH equivalent ratio of the prepolymer was 3.0:1.0. The %NCO was measured by titration according to

ASTM D2572-97[24], the molecular weight distribution was measured by GPC as described previously, and the viscosity was determined using a Brookfield viscometer. The prepolymer was stored under argon at 4°C.

Preparation and characterization of surface-demineralized and defatted allograft bone particles

Mineralized bovine bone particles (B-MBP) were sonicated in 0.1M HCl for 90 seconds. An equal volume of DI water was subsequently added, and the particles subsequently filtered and rinsed with DI water. This entire process was repeated for a total of two times, and the particles were subsequently rinsed with 70% ethanol and dried. The resulting surface-demineralized bone particles (SDMBP) were then lyophilized for a minimum of 14 hours at 0.10 mbar. To prepare defatted mineralized bovine bone particles (DFMBP), mineralized bone particles were stirred with a 50/50% volume solution of acetone/chloroform in a volumetric ratio of 1:10 for at least 48 h. Mineralized human bone particles (H-MBP) were used as received from Osteotech. H-MBP was prepared by comminuting debrided and cleaned cortical bone in a mill. Ground particles were sieved between 106-500 μm diameter and defatted in 70% denatured alcohol for at least an hour. Particles were washed with sterile deionized water, lyophilized for a minimum of 6 hrs at -35 ºC, and by vacuum-dried for a minimum of 12 hrs at 35 ºC and 500 mtorr. Lyophilized bone particles were treated with supercritical carbon-dioxide at 105^0C for at least 25 minutes. The bone was packaged under dry argon and gamma irradiated at 25-35 KGy.

B-MBP, SDMBP, DFMBP, and H-MBP were imaged by scanning electron microscopy (Hitachi S-4200 SEM, Finchampstead, UK). The skeletal density, which

accounts for both the volume of the solid as well as the blind (e.g., inaccessible) pores, was measured by gas pycnometry using nitrogen as the penetrating gas (Micromeritics, Norcross, GA). The skeletal density (ρ_{MBP}, see Eq (1) below) was used to calculate the porosity of the composites because it was assumed that the PUR binder would wet the external pores but not the internal (blind) pores. The particle size distribution was measured using a Saturn DigiSizer 5200 V1.12 (Micromeritics, Norcross, GA).

The surfaces of B-MBP, SDMBP, DFMBP, and H-MBP were characterized by XPS using a PHI 5000 VersaProbe XPS with a 25W monochromatic Al K-α X-ray source and a 100-µm spot size. Survey and high resolution spectra were collected using 187.85 and 23.5 eV pass energies respectively. All the measurements were done using a 45^{o} take-off angle and charge neutralization under ultrahigh vacuum. Analysis of the data was performed using the software CasaXPS Version 2.3.14 (© 1999-2008 Neal Fairley).

Synthesis and characterization of the injectable MBP/PUR composite void filler

The complete process for preparation of injectable MBP/PUR composites is summarized in Figure 4.1. To prepare the void filler, the hardener, LTI-PEG prepolymer, and allograft bone were charged to a mixing cup and hand-mixed for 1 minute. Composites incorporating bovine bone were prepared with 50 wt% (36 vol%) allograft particles, the maximum that could be successfully injected using the 5-ml syringe (for H-MBP it was 45 wt% (30 vol%)). The relative amounts of the prepolymer and hardener components were calculated assuming an index of 115 (the index is defined as 100 x (no. of NCO equivalents/no. of OH equivalents)).[25] The OH titration, NCO titration, and GPC measurement yielded different values of the OH number that bracketed the theoretical OH number; therefore, the theoretical OH number was used to formulate the

composites. This approach has been reported to yield PUR networks with minimal sol fraction when indexed at 115.[19] The resulting reactive paste was subsequently transferred into a 5-ml syringe and injected into a mold. The composites were cured overnight at ambient temperature prior to the density measurements. The density of the scaffolds was determined from mass and volume measurements of triplicate cylindrical samples with 12 mm diameters and lengths varying from 15–25 mm. The porosity, defined as the volume fraction pores, was calculated from the composite foam density[16], which was measured gravimetrically:

$$\varepsilon = 1 - \frac{\bar{\rho}}{\rho_c} \qquad (1)$$

where $\bar{\rho}$ is the average measured composite foam density (cored) and ρ_c is the density of the composite assuming there are no pores:

$$\rho_c = \frac{1}{\frac{x_B}{\rho_B} + \frac{1 - x_B}{\rho_P}} \qquad (2)$$

In eq (2), ε is the porosity, ρ_F is scaffold density, ρ_{MBP} = 2100 kg-m^{-3} is the density of MBP (measured by pycnometry), ρ_{PUR} = 1200 kg-m^{-3} is the density of PUR (measured gravimetrically), and x_B is the weight fraction of MBP. Data are presented as mean ± standard deviation of triplicate samples. Scanning electron microscope (SEM) micrographs were obtained using a Hitachi S-4200 (Finchampstead, UK), and pore size was measured using MetaMorph 7.1 Image Analysis software (MDS Analytical Technologies, Mississauga, Canada).

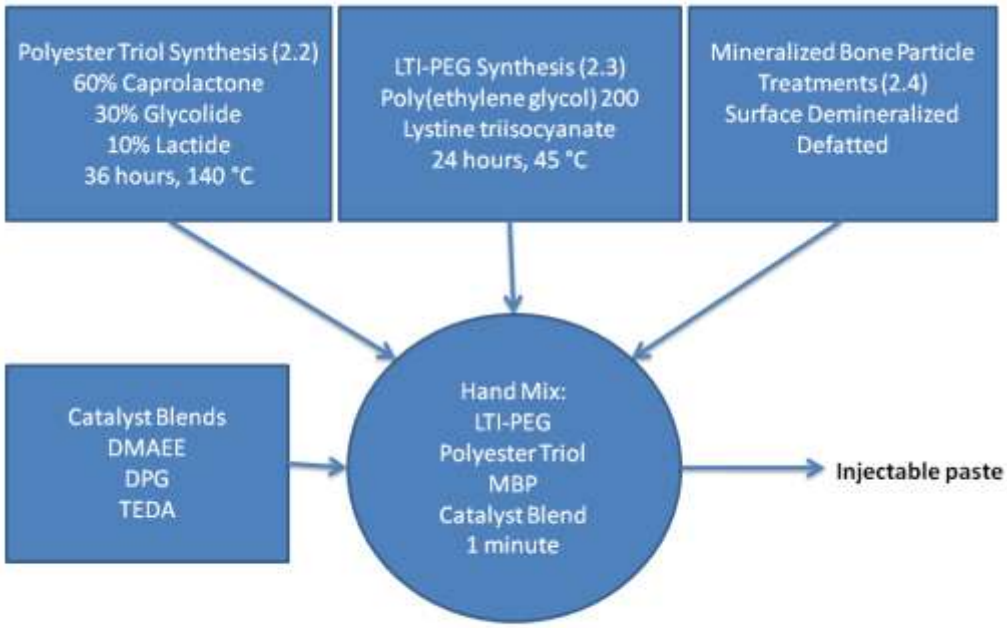

Figure IV.1: A schematic of the synthesis of injectable MBP/PUR composites. MBP, mineralized bone particle; PUR, polyurethane; LTI, lysine triisocyanate; PEG, poly(ethylene glycol); DMAEE, bis-(2-dimethylaminoethyl) ether; DPG, dipropylene glycol; TEDA, triethylene diamine.

Working and tack-free times

The working time is defined in the ISO9917 standard as "the period of time, measured from the start of mixing, during which it is possible to manipulate a dental material without an adverse effect on its properties."[25] For a two-component polyurethane, the working time is determined by the gel point, the time at which the crosslink density of the polymer network is sufficiently high that the material gels and no longer flows.[25] The working time was measured by loading the syringe with the reactive composite and injecting <0.25ml every 30s. The working time was noted as the time at

which the material was more difficult to inject, indicating a significant change in viscosity. For polymeric materials, the tack-free time (TFT) is an effective measure of the time required for the material to cure to form a solid elastomer. Thus the TFT approximates the setting time reported for bone cements, and is defined as the time at which the material could be touched with a spatula with no adhesion of the spatula to the foam. At the TFT, the wound could be closed without altering the properties of the material.

Mechanical Testing

Cylindrical samples with 12mm diameters and lengths ranging from 10–30mm were prepared. Samples designated "wet" were submerged in phosphate-buffered saline (PBS) for 24 hours prior to testing. Samples were tested in compression mode using the MTS Bionix system (Eden Prairie, MN USA) with 1 kN load cell. The displacement rate was adjusted on a lot-by-lot basis maintain a relatively constant strain rate for all test samples. The displacement rate varied between 2 mm/min and 6 mm/min; this corresponds to a strain rate of approximately 20-25%/min for each test sample. Data are presented as mean ± standard deviation of triplicate samples.

Viscosity Measurements

A TA Instruments AR-G2 rheometer with a Peltier Plate Temperature Control Unit was used to determine the initial viscosity of the MBP/PUR composite without the catalyst mix to prevent the material from curing and adhering to the Peltier plate. The composite was prepared by mixing the prepolymer, polyol, and allograft components and mixing for 60s. The test fixture was a set of 40mm parallel plates and the test was carried

at 20°C. The viscosity was measured dynamically with a frequency sweep from 0.1 rad/s to 100 rad/s and controlled strain amplitude of 0.02%.

In Vitro *Degradation*

Samples (6mm diameter × 1mm long) were individually placed in small vials, immersed in PBS, and stored at 37°C under mechanical agitation. At each time point samples were immersed in DI water for at least 1 hour for a total of 2 water changes at room temperature. The samples were then lyophilized for 16 hours, and weighed to determine mass lost. Data are presented as mean ± standard deviation of quadruplicate samples.

In vivo *study*

An athymic rat study was conducted at the Osteotech rodent facility, which is fully compliant with the American Association for Laboratory Animal Sciences guidelines. Two technicians certified by the American Association for Laboratory Animal Sciences (AALAS) performed the surgery. The polyol hardener, LTI-PEG prepolymer, and human MBP (H-MBP) were sterilized by gamma irradiation at a dosage of 25 – 35 kGy. The components were hand-mixed by charging the polyol, allograft bone particles, and prepolymer to a 20-ml cup and mixing for 1 minute. The catalyst solution comprising 5% TEDA and 1.2 pphp water in DPG was subsequently added and the reactive paste mixed for another 30 s. The mixture was transferred to a syringe and injected into 4-mm unicortical femoral plug defects in athymic rats. Two approaches were pursued to investigate the effects of wound closure time on material properties. In one treatment group, the material was injected into the defect and the wound immediately closed. In the second treatment group, the material was injected into the defect and allowed to expand

for 15 minutes before the wound was closed. Bleeding occurred primarily when the defects in the bone were drilled. The defects were immediately packed with gauze to dry the wound site, and the sample subsequently injected. For the samples where wound closure was delayed for 15 minutes, no additional bleeding was observed between the time of injection and the time of wound closure. After 3 weeks, the femurs were extracted, fixed in neutral buffered formalin, and imaged by μCT. The bones were then decalcified with 10% formic acid solution followed by dehydration in increasing concentration of alcohol followed by a clearing agent. Finally, samples were soaked in in glycidyl methacrylate (GMA) and embedded in GMA. Post curing, 4-6 μm thin sections were cut, mounted on slides, and stained with toluidene blue/basic fuchsin mixture. Slides were washed in water followed by dehydration in increasing concentration of alcohol followed by a clearing agent. Dehydrated slides were cover-slipped and prepared for micrographs.

Results

Maximum loading of bone in the composites

One objective of the present study was to synthesize MBP/PUR composite scaffolds at the highest bone fraction that could be injected through a 12-ga syringe needle. While for formulation purposes it is easier to express the bone content in terms of the weight fraction (or wt%), the volume fraction ϕ_{MBP} controls the viscosity of the suspension and is calculated from the weight fraction x_{MBP} as follows:

$$\phi_{MBP} = \frac{\frac{x_{MBP}}{\rho_{MBP}}}{\frac{x_{MBP}}{\rho_{MBP}} + \frac{x_{PUR}}{\rho_{PUR}}} \qquad (3)$$

The highest weight fraction of bone particles that could be ejected from a standard laboratory 3-ml syringe was found to be 50 wt% (36.0 vol%) for B-MBP and 45 wt% (31.1 vol%) for H-MBP. Therefore, all subsequent experiments were performed at these conditions.

Characterization of reactive PUR intermediates

The %NCO of the prepolymer was measured to be 22.8%, which is in good agreement with the theoretical value of 23%. The viscosity was measured to be 21,000 cP using a Brookfield viscometer. As shown in Table 4.1, the molecular weight of the prepolymer is broadly distributed, ranging from monomeric LTI to the LTI-PEG-LTI-PEG-LTI-PEG-LTI-PEG-LTI adduct comprising 5molecules of LTI and 4 molecules of PEG. This observation is consistent with previously reported data for polyurethane prepolymers, which are typically characterized by a broad molecular weight distribution.[16]

The molecular weight and OH number of the polyester macrotriol are listed in Table 4.2. The number-average molecular weight was measured to be 1405 g/mol, compared to the theoretical value of 900 g/mol. However, GPC is a relative measure of molecular weight, and is therefore not as useful for formulating two-component polyurethanes, which requires the absolute molecular weight. The OH number is a more reliable value for formulating the PUR composition.[16] While the theoretical OH number was 187 mg KOH/g, the measured value was 153 mg KOH/g, and the calculated value

from the prepolymer %NCO titration was 212 mg KOH/g. Considering that the theoretical value of the OH number was between the two measured values, the theoretical value was used to formulate the polyurethanes, as reported previously.[2,6]

Table IV.1: Molecular Weight Distribution of Lysine Triisocyanate-Poly(Ethylene Glycol) Prepolymer.

Component	*Theoretical M_n (g/mol)*	*Measured M_n (g/mol)*	*Calculated M_n (g/mol)*	*Area (%)*
LTI	269	309	309	16.8
PEG	200	424	424	<0.5
LTI-PEG	469	708	733	<0.5
LTI-PEG-LTI	738	1071	1042	22.5
LTI-PEG-LTI-PEG-LTI	1207	1788	1775	17.0
LTI-PEG-LTI-PEG-LTI-PEG-LTI	1676	2470	2508	11.9
LTI-PEG-LTI-PEG-LTI-PEG-LTI-PEG-LTI	2145	3122	3241	31.7

Table IV.2: Characterization of Polyester Macrotriol.

Theoretical OH number (mg KOH/g)	187
Measured OH number (mg KOH/g)	153
OH number calculated from high %NCO prepolymer (mg KOH/g)	212
Theoretical molecular weight (g/mol)	900
Measured molecular weight (g/mol)	$M_n = 1405$ $M_w = 2048$ $M_p = 2036$ PD = 1.46

NCO, isocyanate; PD, polydispersity.

Characterization of the allograft bone particles

SEM images of B-MBP, SDMBP, DFMBP, and H-MBP are shown in Figure 4.2. The B-MBP particles had a mean size (measured by SEM) of 175 ± 91 μm (Table 4.3), and the H-MBP particles had a mean size of 98 ± 48 μm. Considering that defatting and surface-demineralization only affected the external surfaces of the particles, these processes had negligible effects on the skeletal density and mean size of the particles. The variation in skeletal densities (measured by helium pycnometry) was minimal, ranging from 2.13 – 2.20 g cm^{-3} for all four particle treatment groups (Table 4.3). The compositions of the surfaces of the bone particles, as measured by XPS, are also presented in Table 4.3. B-MBP was extensively covered with a layer of fat, as evidenced by the high carbon content and low oxygen, calcium, and phosphorous concentration. Defatting the bone successfully removed the layer of fat on the surface, as shown by the reduction in carbon and increase in oxygen, calcium, and phosphorous concentrations. Similarly, surface-demineralization effectively removed the mineral content from the surface of the allograft particles. The surface of B-SDMBP is depleted in calcium and phosphorous but enriched in carbon and nitrogen, indicating that the surface of the allograft has been partially demineralized.

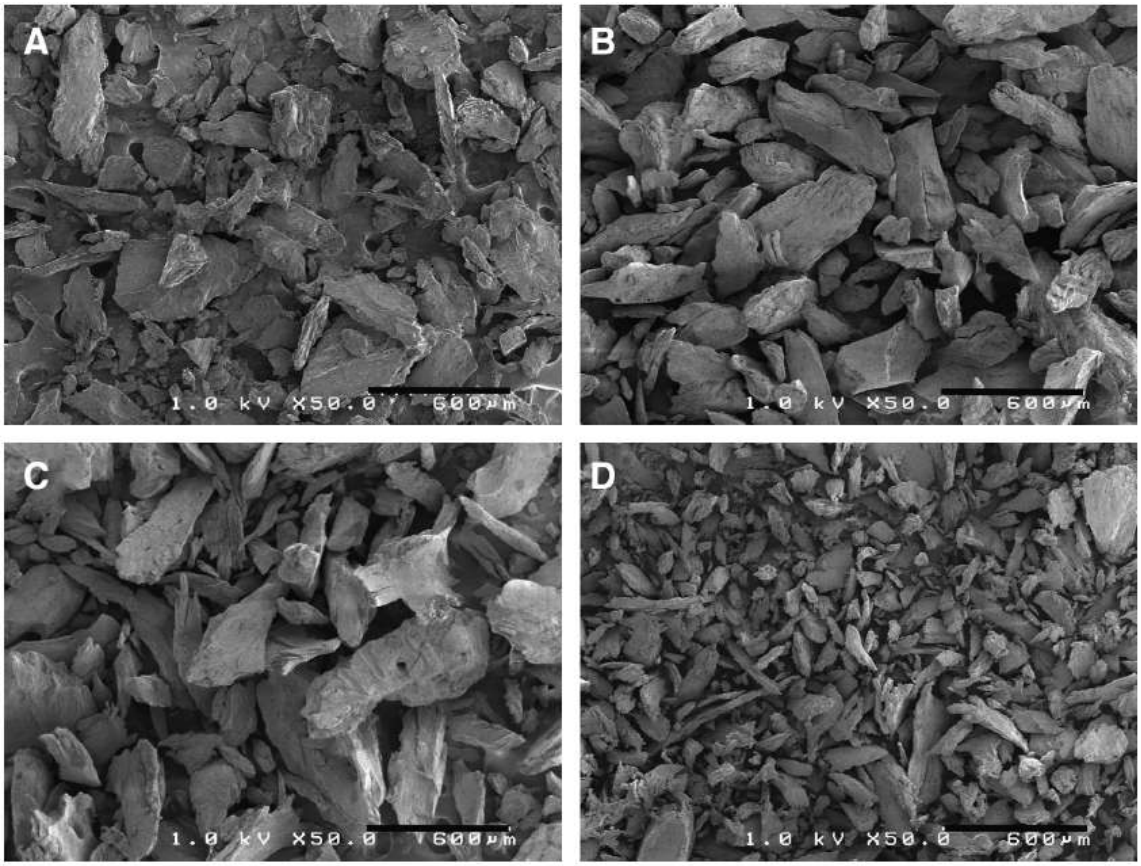

Figure IV.2: Scanning electron microscopy images of allograft bone particles. (A: Bovine MBP, B: SDMBP, C: DFMBP, and D: human MBP. SDMBP, surface-demineralized bone particle; DFMBP, defatted mineralized bovine bone particle.)

Table IV.3: Characterization of Bovine and Human Allograft Bone Particles.

Material	*Mean size (µm)*	*Density (g/cm^3)*	*XPS %C*	*XPS %O*	*XPS %Ca*	*XPS %P*	*XPS %N*
B-MBP	175 ± 91	2.13	86.1 ± 2.16	11.8 ± 1.49	1.04 ± 0.50	0.48 ± 0.20	0.97 ± 0.25
DFMBP	Not measured	2.20	51.6 ± 0.35	31.1 ± 0.57	6.75 ± 0.49	4.5 ± 0.42	6.05 ± 0.07
SDMBP	Not measured	2.13	57.4 ± 2.62	25.1 ± 1.98	3.15 ± 0.78	1.85 ± 0.64	12.6 ± 0.78
H-MBP	98 ± 48	2.18	45.9 ± 4.2	33.4 ± 3.3	7.03 ± 1.15	4.57 ± 0.35	9.07 ± 0.50

Density and porosity of the injectable composites

The density of the injectable composites was adjusted by varying the concentrations of the catalysts and water, as well as the processing technique. In initial experiments with SDMBP, allograft composite foams were prepared using published techniques, wherein a hardener was first prepared by combining the polyester triol, catalyst, and water to form a hardener component.[4,7,8] While previous studies required the use of a fatty acid-derived stabilizer and pore opener to generate small (e.g., <1 mm) pores, scaffolds synthesized from LTI-PEG prepolymer did not require these components to achieve the targeted porosity and pore size distribution. The SDMBP component was added to the hardener and mixed by hand for 30s, followed by addition of the prepolymer and mixing for 60s. The material was then charged to a 3ml syringe and injected into a mold. As shown in Figure 4.3a, in the presence of the tertiary amine catalyst triethylene diamine (TEDA, added at a concentration of 0.8 parts per hundred parts polyol (pphp) as a 33% solution in dipropylene glycol), the porosity of SDMBP/PUR composites varied over the range of 2 – 48%. Even at higher water concentrations it was not possible to increase the porosity beyond 50%. TEDA is a potent gelling catalyst that preferentially catalyzes the isocyanate-polyol reaction, but it also has some activity toward the isocyanate-water blowing reaction.[26] In the presence of DMAEE, the maximum achievable porosity was increased to 70%, which is consistent with the fact that DMAEE is a tertiary amine catalyst that preferentially catalyzes the isocyanate-water blowing reaction relative to the isocyanate-polyol gelling reaction.[27] To investigate the effects of surface chemistry of the bovine bone particles on the density of the materials, composite foams were also prepared using bovine DFMBP in the hardener process with no

DMAEE. As shown in Figure 4.3, the composition of the bone surface had a dramatic effect on the porosity. The lower porosities achieved with SDMBP in the absence of DMAEE are conjectured to result from adsorption of water in the hardener to the hygroscopic demineralized layer on the surface of the bone.

An important limitation of the two-component hardener process was the storage stability of the hardener component. When the hardener component comprising polyol, water, and catalyst was stored for >3 days at 37^{o}C and subsequently used to prepare composite foams, the resulting materials exhibited dramatic (e.g., >10 – 20%) changes in porosity. In order to prepare an injectable composite with acceptable storage stability, the two (liquid) component process was modified to an alternative three (liquid)-component process wherein the TEDA catalyst (0.8 pphp) and water were dissolved in a dipropylene glycol (DPG) solution. Another advantage of the three-component process is that the volume of DPG could be increased to yield a sufficiently large solution volume that can be reproducibly filled in a syringe (e.g., ~200 μl for a clinically relevant batch size of 5g). Allograft/PUR composite foams were synthesized by first mixing the polyol and DPG+catalyst+water solution for 60s, followed by addition of allograft particles, and finally addition of the LTI-PEG prepolymer. The resulting reactive paste was mixed for 30s, charged to a 3-ml syringe, and injected into a 3-ml polypropylene mold. There were no significant differences in the porosity of the composite foams between the two- and three-component processes.

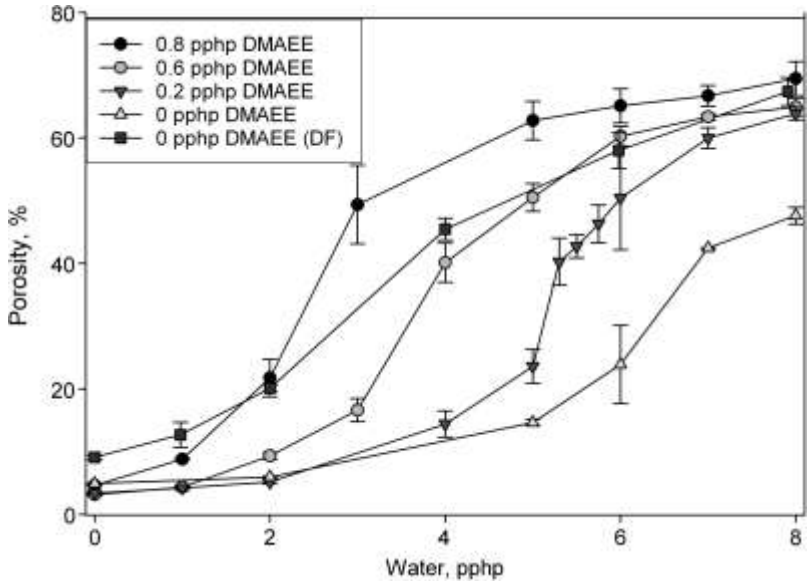

Figure IV.3: SDMBP/PUR scaffold porosity as a function of water concentration at varying concentrations of DMAEE.
The TEGOAMIN concentration was 1.8 pphp (0.6 pphp TEDA) for all samples. Data are presented as mean standard deviation of triplicate samples. pphp, parts per hundred parts polyol.

Mechanical properties

As anticipated, the mechanical properties of the scaffolds are highly dependent on the porosity. Figure 4.4 shows the compressive stress-strain curves of the SDMBP/PUR scaffolds with porosities ranging from 38 – 60%. Figure 4.5 shows that the compressive strength of the SDMBP/PUR dry scaffolds varied from 4.38 – 9.47 MPa as the porosity was reduced from 50 to 30%. The compressive modulus of the scaffolds ranged from 173.4 – 444.1 MPa in the same porosity range, as shown in Figure 4.6. For the wet samples, the compressive strength of the scaffolds varied from 4.06 – 12.88 MPa, while the compressive modulus varied from 53.2 – 331.5 MPa as the porosity decreased from 47 to 30%. However, the wet 60% porosity scaffolds exhibited substantially lower mechanical properties, with compressive strength 0.167 MPa and modulus 3.11 MPa.

These compressive properties are in the range previously reported for unfilled PUR scaffolds.[28] For composites with the same porosity, there were no significant differences in modulus or strength between materials prepared from SDMBP or DFMBP. Considering that the reinforcement of mechanical properties resulting from the allograft component was retained at porosities ≤50%, the targeted porosity was selected as 40% for *in vivo* experiments.

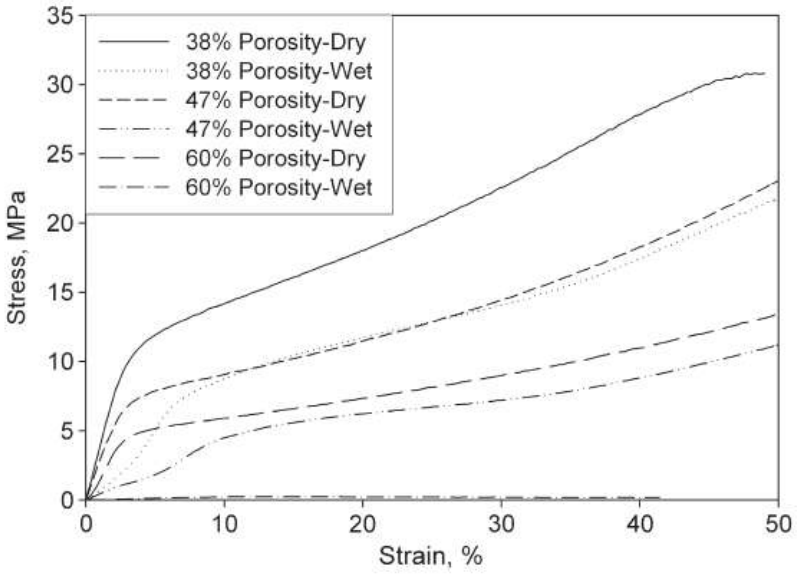

Figure IV.4: Compressive stress–strain curves for the 38%, 47%, and 60% porosity scaffolds fabricated from SDMBP.

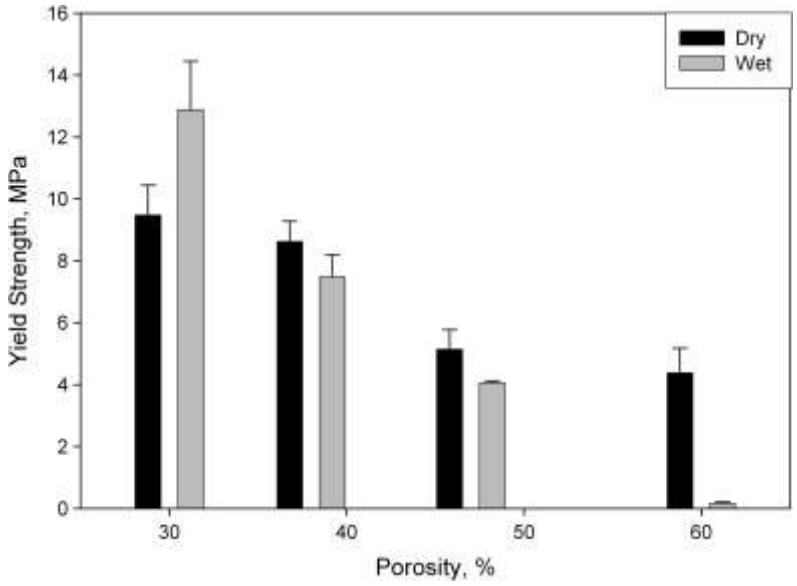

Figure IV.5: Compressive strengths of dry and wet 50 wt% (36 vol%) SDMBP/PUR scaffolds at porosities ranging from 30% to 60%.

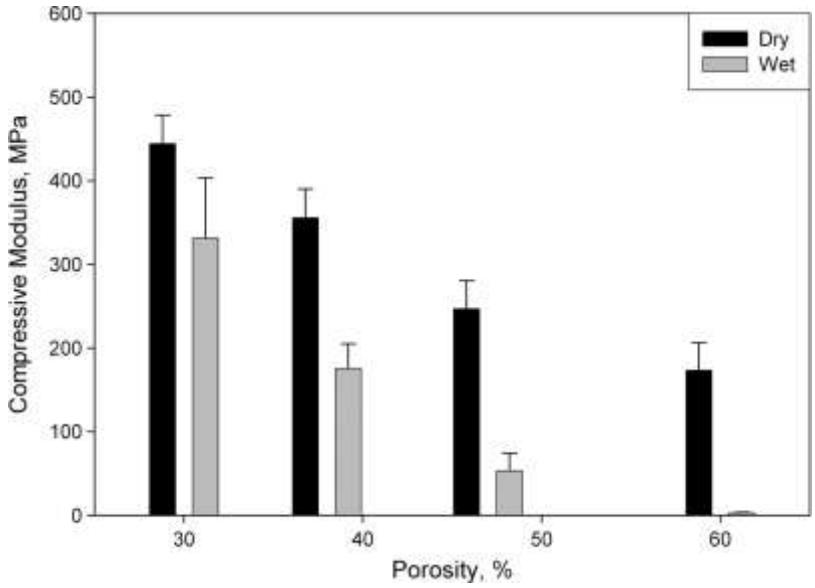

Figure IV.6: Compressive moduli of dry and wet 50 wt% (36 vol%) SDMBP/PUR foam scaffolds at varying porosities.

Porosity and pore size

SEM images of the allograft/polymer composites are shown in Figure 4.7 for composites with porosities of 35, 47, and 65%. Allograft bone particles (outlined in black) are dispersed throughout the scaffold, and are generally separated from one another by a polymer film. The pore size distribution in the interior of the composite was measured by image analysis of the SEM micrographs. While the pore size distribution at the surface of the composite is anticipated to strongly influence cellular infiltration, characterization of the pore size distribution at the surface of the material is very challenging due to differences in curing between hydrophobic (e.g., air) and hydrophilic (e.g., aqueous) environments. When the materials are cured in the laboratory, a thin skin forms at the material/air interface, but this skin is not present when the materials are cured in a moist environment. Thus it is difficult to reproduce the *in vivo* pore size distribution at the surface of the composite under *in vitro* conditions. At 35% and 47% porosities, the pores in the interior of the composite are comparable in size (183 ± 90 μm for the 35% porosity scaffold and 177 ± 90 μm for the 47% porosity scaffold), and do not appear to be inter-connected. At 65% porosity, the pores are larger (701 ± 317 μm) and appear to be inter-connected, which is consistent with previous studies investigating non-filled scaffolds.[29]

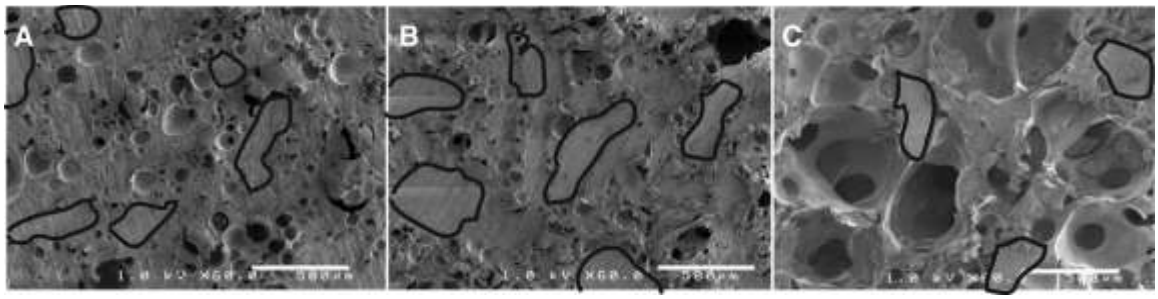

Figure IV.7: Scanning electron microscopy images of SDMBP/PUR scaffolds. (50wt% SDMBP/PUR foam scaffolds at (A) 35%, (B) 47%, and (C) 65% porosity. Allograft bone particles are traced in black. Scale bar represents 500 mm.)

Working and tack-free times

The working and tack-free times were adjusted by varying the concentration of TEDA catalyst using the two-component process. At elapsed times shorter than the working time, the mixed components of the scaffold can be injected from the syringe and manipulated without disrupting the pore structure. As defined in Section 2.6, the tack-free time is the period of time required for the scaffold to sufficiently cure such that the surface can be touched with a probe that is subsequently removed without adhering to the surface. As shown in Figure 4.8, the tack-free time of the SDMBP/PUR scaffolds (porosity 40%) varied between 10 – 20 minutes by reducing the TEDA concentration from 0.8 to 0.4 parts per 100 parts polyol (pphp). The working time varied from 4 – 8 minutes over the same TEDA concentration range. Working and tack-free times were not strongly influenced by water concentration, allograft surface chemistry, or the type of allograft.

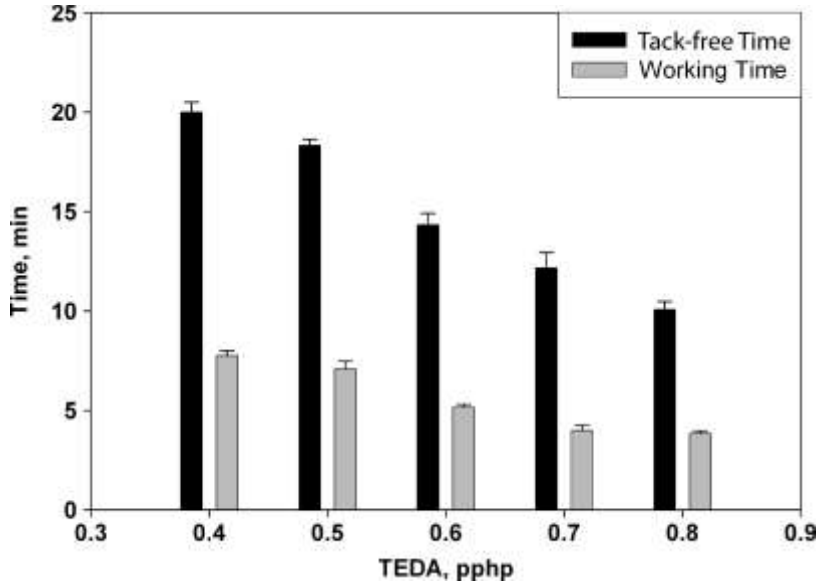

Figure IV.8: The tack-free and working times of 50wt% SDMBP/PUR scaffolds with varying TEDA concentrations.
(DMAEE and water concentrations were 0.6 and 4.0 pphp, respectively.)

Viscosity Measurements

Figure 4.9 shows the initial dynamic viscosity of the MBP/PUR composite mixture, which ranged from 180-1200 Pa*s. As expected, the MBP/PUR composite mixture exhibited the behavior of a shear thinning paste.

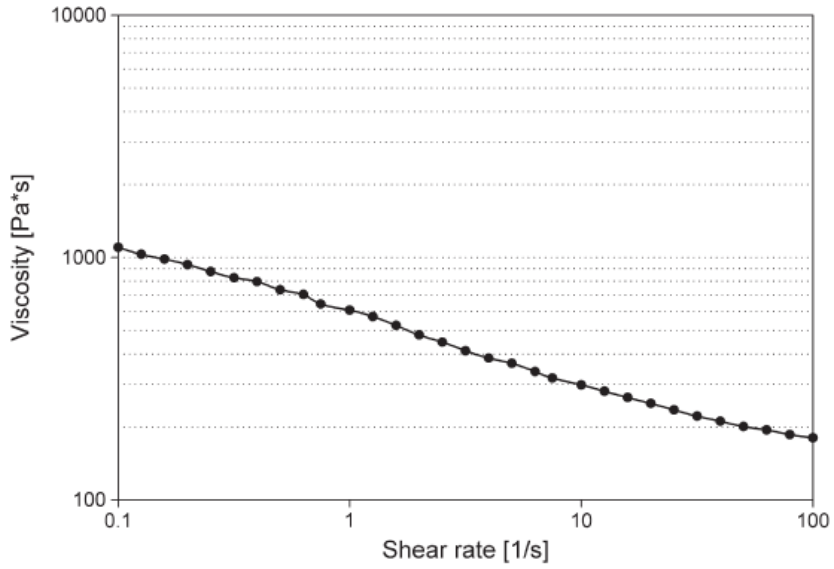

Figure IV.9: Initial dynamic viscosity of injectable MBP/PUR composites measured using an AR-G2 (TA Instruments) rheometer.
The viscosity was measured dynamically with a frequency sweep from 0.1 to 100 rad/s and controlled strain amplitude of 0.02%.

In vitro *degradation*

In vitro degradation data are presented in Figure 4.10. At 30 weeks degradation time, the remaining mass of the scaffolds varied from 75 – 88 wt%. While there were no significant differences between the 30%, 40%, and 60% treatment groups, the 70% porosity material exhibited slower degradation after 20 weeks. No significant changes in the surface morphology of the composites were observed during this time period.

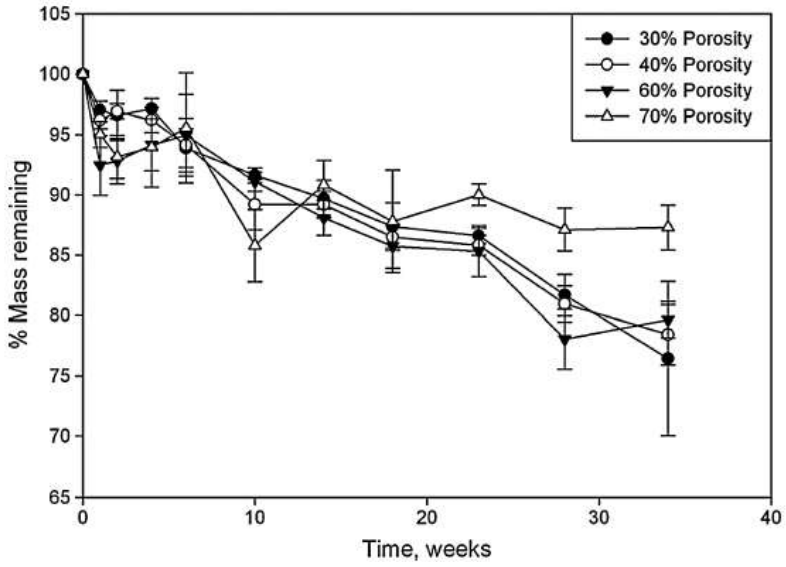

Figure IV.10: In vitro degradation of SDMBP/PUR scaffolds as a function of porosity. Samples were incubated in phosphate buffered saline at 378C and mixed end over end, and removed and weighed at each time point.

In vivo *osteoconductivity*

A pilot study was performed in an athymic rat model to demonstrate injectability of the material and investigate its potential to support new bone formation. The 40% porosity formulation was selected due to its suitable mechanical properties for weight-bearing applications. Considering that the manufacture of surface-demineralized allograft bone particles is challenging, as well as the observation that the differences in mechanical properties between SDBMP and DFMBP composites were minimal, H-MBP composites were selected for the animal study. The allograft concentration was 45 wt% (31.1 vol%), which was the highest concentration which could be easily injected using a standard-bore syringe. μCT images of the H-MBP/PUR void filler injected into the femoral plug defects are shown in Figure 4.11. For the images shown in Figures 4.11A-B, the wound was immediately closed after injection, while for the images in Figures

4.11C-D, the wound was closed 15 minutes after injection. Allograft within the composite, as well as evidence of new bone formation, can be seen in the materials.

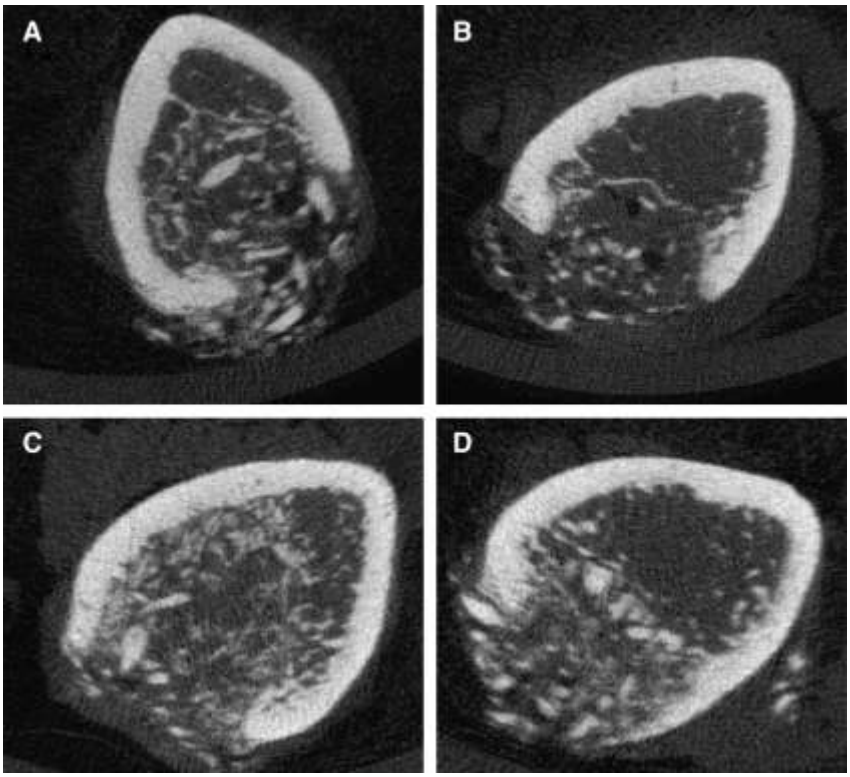

Figure IV.11: Microcomputed tomography images of human-SDMBP/PUR bone void filler injected into plug defects in the distal femurs of athymic rats
Images were acquired after 3 weeks of implantation. (A, B) Wound closed immediately after injection. (C, D) Wound closed 15 min after injection.

Thin (e.g., 4 – 6 μm) decalcified sections stained with fuchsin red/toluidene blue mixture are shown in Figures 4.12-14. Figure 4.12A corresponds to the case where the material was injected and the wound immediately closed, while Figure 4.12 B and Figure 4.13A correspond to the case where the wound was closed 15 minutes after injection. Figures 4.13s B, C, and D are higher magnification views of the material shown in Figure 4.13A C. Polymer is stained red, unresorbed allograft and cortical bone are stained light

pink, nuclei are stained purple, and collagen and connective tissue are stained blue. Direct apposition of the polymer (labeled "P) against the host bone (labeled "HB") surface is evident in the histological sections, suggesting that the injected composite established close contact with the host tissue. There is evidence of new bone growth adjacent to the material, as well as regions of new bone formation (labeled "RM") near the host bone/composite interface and also deep into the interior of the composite. These regions of new bone formation exhibit evidence of allograft resorption, osteoid (O) formation, collagen deposition, and new bone formation. While there is extensive remodeling of allograft particles throughout the composites, some of the allograft particles (labeled "A") were embedded in the polymer and thus did not remodel.

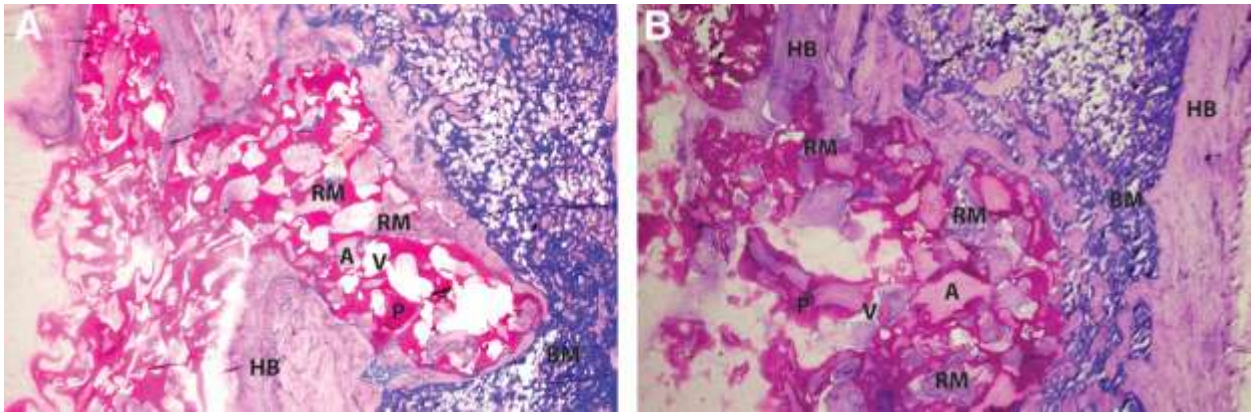

Figure IV.12: Thin (e.g., 4–6 mm) decalcified sections of the composite bone void filler injected in bilateral femoral plug defects in rats
Histology after 3 weeks of implantation stained with fuchsin red- toluidene blue. (A, B) Low magnification images showing host bone (labeled ''HB,'' pink), voids (labeled ''V''), residual polymer (labeled ''P,'' red), allograft particles embedded in polymer that have not been resorbed (labeled ''A,'' pink), regions of new bone formation (labeled ''RM,'' purple) into the interior of the composite, osteoid, and bone marrow (labeled ''BM,'' blue/purple) around the surface of the material. Panel (A) corresponds to the case where the wound was closed immediately after injection of the material, while panel (B) corresponds to the case where the wound was closed 15 min after injection.

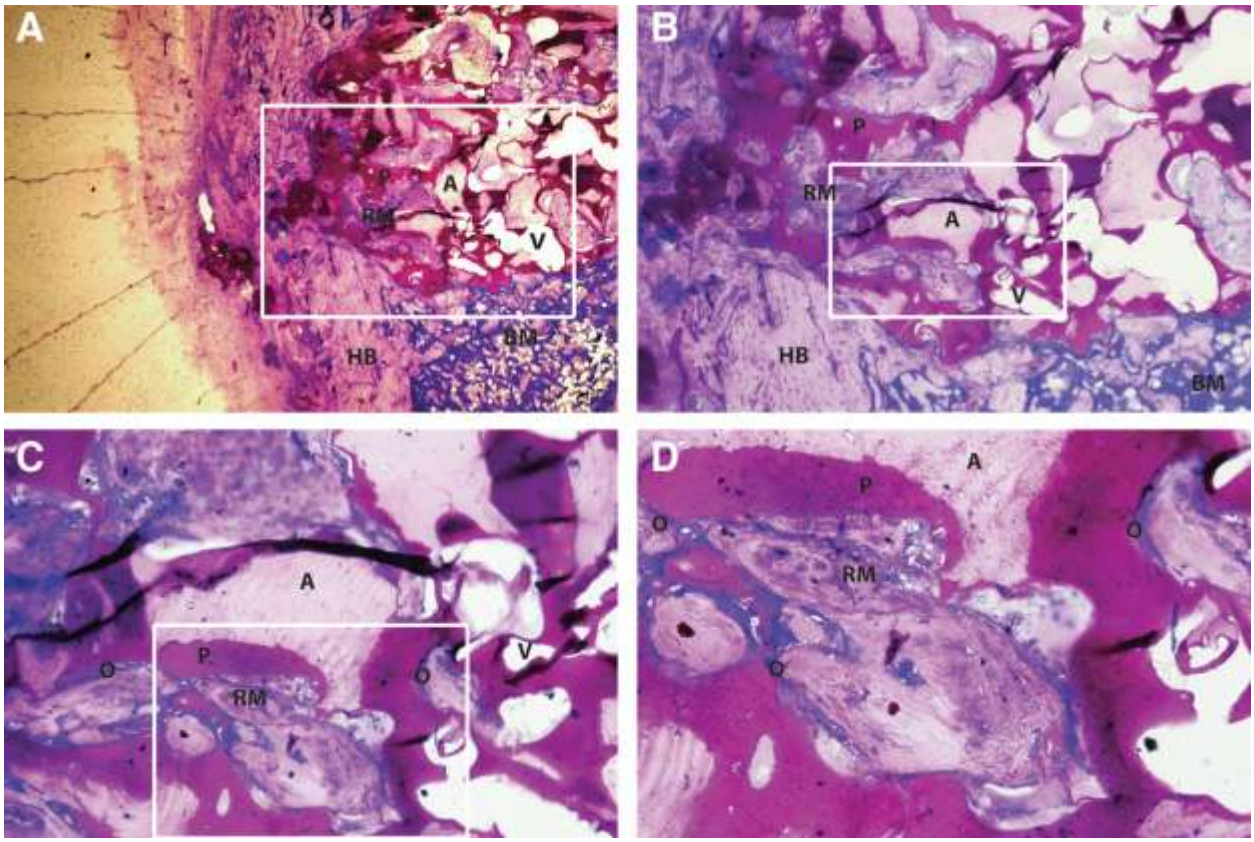

Figure IV.13: Histology of implant of wounds closed after 15 minutes.
(A: Low magnification of image showing host bone where the wound was closed 15 min after injection. (B–D) Higher magnification views of the implant shown in panel A. The labels ‘‘P’’, ‘‘A’’, ‘‘RM’’, ‘‘V’’, and ‘‘HB’’ are defined as shown in Figure 4.12.)

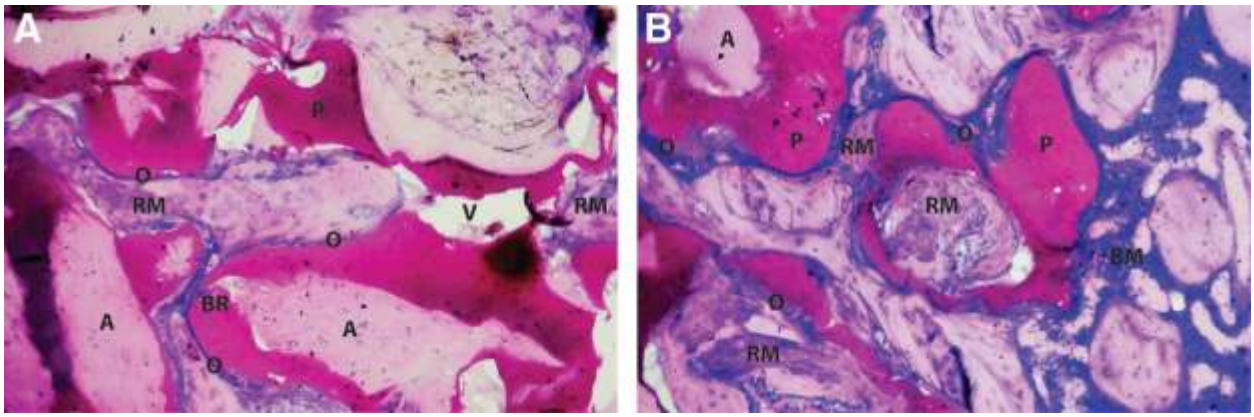

Figure IV.14: Histology of areas of new bone formation.
((A, B) Higher magnification of regions of new bone formation characterized by allograft (pink) resorption, cells (purple), and collagen deposition (blue). Panel (A) shows the cellular pathway in an interior region of the composite, while panel (B) shows the infiltration of cells into the composite from the bone marrow. In the center of panel (B) there is an allograftparticle undergoing active remodeling that appears to be embedded in polymer except for a small breach (labeled ‘‘BR’’) where cells infiltrated along the allograft/polymer interface. The labels ‘‘P’’, ‘‘A’’, ‘‘RM’’, ‘‘V’’, and ‘‘HB’’ are defined as shown in Figure 4.12.)

Cells appeared to infiltrate the material both by entering open pores (labeled “V”), as well as via resorption of allograft particles, as shown in Figures 4.14s A and B. Figure 4.14A shows the cellular pathway in an interior region of the composite, while Figure 4.14B shows the infiltration of cells near the composite/host bone interface, where cells from the marrow (labeled “BM”) are observed to migrate into the composite. In the center of Figure 4.14B there is an allograft particle undergoing active remodeling that appears to be embedded in polymer except for a small breach (labeled “BR”) where cells infiltrated along the allograft/polymer interface. Similarly, Figures 4.13s C and D show a large allograft particle that appears to be embedded in polymer except for two breaches where cells have begun to infiltrate along the allograft/polymer interface. These observations suggest that resorption of the allograft creates pores into which cells

subsequently migrate, thereby presenting an alternative pathway (in addition to migration through open pores) by which cells can infiltrate the composite.

Discussion

Injectable biomaterials enable the filling of irregularly-shaped defects using minimally-invasive procedures. Injectable calcium phosphate bone cements, such as Norian SRS® (Synthes), have received FDA approval as a bone void filler for orthopaedic applications. In contrast to poly(methyl methacrylate) (PMMA), calcium phosphate cements are osteoconductive and biodegradable and have been shown to support bone ingrowth *in vivo*. However, due to the small pore size (e.g., on the order of 1 μm), the rate of cellular infiltration is slow with the material resorption and replacement rates inadequately matching the biology of the site.[24] Furthermore, the materials are prone to brittle fracture which can lead to infectious complications.[23,30] In this study, we have developed an injectable bone void filler comprising allograft bone particles and a reactive, two-component biodegradable polyurethane binder. By varying the amount of water added, the porosity of the composites ranged from <5 to 70%. The working and tack-free times were adjusted by varying the concentrations of the tertiary amine catalysts, and varied from 4 – 8 min for the working time and from 10 – 20 min for the tack-free time (similar to the setting time of a calcium phosphate cement). This tack-free time corresponds with the time in which the material can be injected and sutured without sticking to the tissue of the wound. The dynamic viscosity of MBP/PUR injectable composites (180-1200 Pa*s) is comparable to that of injectable bone cements used in vertebroplasty (50-2900 Pa*s).[16] General strategies to improve the injectability of pastes include the utilization of a broad particle size distribution and an increased viscosity of

the mixing fluid.[31] MBP/PUR composites utilize both of these key attributes to facilitate a smooth injection. As shown in the SEM micrographs (Figure 4.2), the mineralized bone particles range in size from 100 – 1000 μm.[32] The viscosity of the LTI-PEG prepolymer is sufficiently high such that the allograft particles remain evenly distributed during the injection process, which is critical during the remodeling process as the particles create additional cellular pathways once resorbed.

As shown in Figure 4.3, the composition of the surface of the allograft particles has a dramatic effect on the porosity. For SDMBP, the porosity approaches 50% even at very high water contents (8 pphp) in the absence of DMAEE, while for DFMBP, 50% porosity is attained at modest (4 pphp) water content. Furthermore, addition of the DMAEE blowing catalyst is required to increase the porosity of SDMBP composites above 50%. Demineralized bone matrix (DBM) is well-known to be significantly more hygroscopic than allograft bone. Therefore, the process of surface demineralization is conjectured to present a hygroscopic surface that serves as a water sink, which could account for the lower porosity observed for SDMBP composites.

The compressive stress-strain curves show that the 50 wt% SDMBP/PUR scaffolds, with the exception of the wet 60% porosity material, exhibited elastomeric properties up to 50% strain. The mechanical properties of the composites generally decreased after immersion in saline for 24 hours. In particular, the 60% porosity scaffolds were substantially weaker and failed under mechanical loading at strains less than 50%. This is in agreement with a previous study reporting that the organic/inorganic interfacial bonding strength for composites comprising biodegradable polymers and hydroxyapatite could be reduced by 80–90% after 30 hours in a humid environment.[28,33] Swelling of the

allograft component is also conjectured to contribute to the reduction in mechanical properties at >50 vol% allograft.

The tack-free (e.g., setting) times of the injectable composites were tunable in the range of 10 – 20 minutes by reducing the TEDA concentration from 0.8 to 0.4 pphp (Figure 4.8). A short setting time is clinically desirable, since in many cases the wound cannot be closed until the material has sufficiently cured to preserve its shape and morphology. The TEDA catalyst concentration also controlled the working time of the composites, which ranged from 4 – 8 minutes. Clinically, it is desirable to maximize the working time and minimize the setting time to facilitate handling in the operating room. As shown in Figure 4.8, the working and setting times were related and decreased with increasing TEDA concentration, and the difference between these times also decreased with increasing TEDA concentration. The allograft surface composition had a negligible effect on working and setting times, which is not surprising due to the fact that the onset of the gel point in the polymer network depends primarily on the polymerization reaction.[34] Thus the cure properties of the allograft/PUR composites were comparable to the working (6 – 10 min) and setting (10 – 15 min) time requirements reported for injectable bone cements and void fillers.[35] Furthermore, the effects of wound closure time did not appear to significantly affect new bone growth and cellular infiltration, which suggests that the waiting period after injecting the material could potentially be shortened by closing the wound prior to the setting time.

After 18 weeks (98 days) incubation time in saline, the SDMBP/PUR composites (ranging from 30 – 70% porosity) retained 86 – 92% of their initial weight. The degradation time of the composites was slower than that measured for the pure polymer

scaffold (~50% of initial weight remaining after 14 weeks *in vitro*[28]) due to both lower porosity as well as the allograft component, which does not degrade in saline. Interestingly, the allograft composites degraded faster than porous PUR/TCP composites reported previously, where >95% of the material remained after 18 weeks incubation time in saline despite the lower TCP content (<10 vol%).[31] The slower degradation time of the TCP composites is conjectured to result from the slower degradation rate of the polymer component.[18]

In a recent study, porous PUR scaffolds (without allograft) implanted in plug defects in rat femora exhibited rapid cellular infiltration and modest new bone formation, primarily around the perimeter of the scaffold in contact with host bone, at 4 weeks. However, PUR scaffolds without the allograft component are not suitable for injection, considering that it is not possible to control the pore size or expansion without adding a filler such as mineralized bone particles as there is reactivity with the filler and isocyanate groups. Furthermore, the absence of mineralized filler substantially reduces the mechanical properties of the cured composite. Other studies have shown that allograft/polymer composites support cellular infiltration through osteoclast-mediated resorption of the allograft phase. Non-porous allograft/polymer composites exhibited extensive cellular infiltration into the interior, as well as modest new bone formation, when implanted in femoral condyle plugs in rabbits. Cellular infiltration was dramatically accelerated when the bone volume fraction approached the random close-packing (RCP) limit (64 vol%), resulting in multiple allograft particle-particle contacts which presented a continuous osteoconductive surface through the implant. In contrast, for PLLA/HA composites where the HA component was <40 wt% (~18 vol%), the rate

of cellular infiltration and new bone formation was very slow (e.g., 5 – 7 years) and dependent on the rate of polymer degradation. The slower rate of cellular infiltration could be explained in part by both the relatively low HA volume fraction, as well as the small size of the HA particles (0.3 – 20 μm with a mean of 3 μm), which is below the optimal size range for remodeling by creeping substitution. Histological sections of allograft/polymer composites suggested that the allograft particles functioned as a porogen, wherein osteoclast-mediated resorption of the allograft created pores in the implant into which osteoblasts migrated and deposited new bone. Osteotech has utilized cortical allograft bone fibers to achieve this effect in the commercially available Plexur platform, which are moldable, porous implants. The Plexur platform has had substantial clinical success as it is widely accepted by surgeons with hundreds of surgical cases to date. The two-component PUR system is moldable without a heating process. Furthermore, pores are naturally produced from the water reaction with isocyanate end groups. We therefore reasoned that a combination of allograft particles and pores would facilitate rapid cellular infiltration and remodeling of the implant, while providing sufficiently high initial mechanical properties comparable to those of calcium phosphate-based bone cements as well as trabecular bone.

Two-component PUR/TCP porous and non-porous composites have been reported to exhibit polymer degradation and new bone formation when implanted or injected into 6 × 12 mm bilateral diaphyseal cortical defects in the femurs of sketally mature Merino wether sheep. The yield strength varied from 6 – 13 MPa and the modulus from 270 – 580 MPa; these mechanical properties are comparable to the PUR/allograft composites of the present study. The materials implanted or injected in the sheep femoral plug defects

exhibited either 42 or 55% porosity, and in one case incorporated 20 wt% (8.8 vol%) 5 μm TCP. New bone formation and osteogenic tissue were observed within the initial pores, as well as in the voids resulting from polymer degradation. New bone formation progressively advanced towards the center of the materials with increasing implantation time (e.g., from 6 to 24 weeks), and cellular infiltration and new bone formation were more evident in faster degrading materials relative to slower degrading materials. Additionally, while the 5 μm TCP particles effectively reinforced the mechanical properties of the composites, their small size precluded remodeling by creeping substitution. Taken together, these observations suggest that the rates of cellular infiltration and new bone formation were controlled by the rate of polymer degradation. In contrast, the PUR/allograft composites of the present study exhibited allograft resorption, cellular infiltration, collagen deposition, and new bone formation in the interior of the implant as early as 3 weeks. This observation suggests that the combination of porosity and allograft bone particles provides connected pathways for cellular infiltration that are critical for remodeling. Considering the large amount of polymer remaining throughout the composite, it is unlikely that the rapid remodeling could be attributed to polymer degradation. Furthermore, while the pores in the interior of the composite were sufficiently large (177 ± 90 μm) to support cellular infiltration, the SEM images suggest that the pores were not interconnected. Thus assuming that the pore size distribution at the surface of the composite is similar to that in the interior, it is unlikely that the rapid cellular infiltration and remodeling could be attributed to pre-existing pores. The histological sections (Figures 4.12-4.14) suggest that allograft remodeling by creeping substitution presented an alternative pathway for cells to

infiltrate the composite by migrating along the allograft/polymer interface. These observations suggest that a continuous path for cellular migration into the interior of the implant may be achieved by a combination of pre-existing pores and allograft particles that are in the desirable size range (e.g., >100 μm) for remodeling by creeping substitution.

Conclusions

Injectable, biodegradable allograft bone/polyurethane composite scaffolds have been synthesized with tunable porosities, mechanical properties, degradation rates, and setting and working times that are comparable to those of calcium phosphate bone cements. When injected into femoral plug defects in athymic rats, the composites supported extensive cellular infiltration, allograft resorption, collagen deposition, and new bone formation at three weeks. The combination of both initial mechanical properties suitable for weight-bearing applications, as well as the ability of the materials to undergo rapid cellular infiltration and remodeling, may present potentially compelling opportunities for injectable allograft/polyurethane composites as biomedical devices for bone regeneration.

REFERENCES

1. Friedman CD, Constantino PD, Takagi S, Chow LC. BoneSource™ hydroxyapatite cement: a novel biomaterial for craniofacial skeletal yissue engineering and reconstruction. J Biomed Mater Res 1998;43(4):428-32.

2. Chim H, Gosain AK. Biomaterials in craniofacial surgery experimental studies and clinical application J Craniofac Surg 2009;20:29-33.

3. Gasparini G, Boniello R, Moro A, Tamburrini G, Di Rocco C, Pelo S. Cranial reshaping using methyl methacrylate:technical note. J Craniofac Surg 2009;20:184-190.

4. Moreira-Gonzalez A, Jackson IT, Miyawaki T, Barakat K, DiNick V. Clinical outcome in cranioplasty: critical review in long-term follow-up. J Craniofac Surg 2003;14:144-153.

5. Bohner M. Calcium orthophosphates in medicine: from ceramics to calcium phosphate cements. Injury 2000;31(Supplement 4):S-D37-47.

6. Hollier LH, Stal S. The use of hydroxyapatite cements in craniofacial surgery. Clin Plastic Surg 2004;31:423-428.

7. Kalfas IH. Principles of bone healing. Neurosurg Focus 2001;10(4):E1.

8. Baker SB, Weinzweig J, Kirschner RE, Bartlett SP. Applications of a new carbonated calcium phosphate bone cement: early experience in pediatric and adult craniofacial reconstruction. Plast Reconstr Surg 2002;109:1789-1796.

9. Goldberg CS, Antonyshyn O, Midha R, et al. Measuring pulsatile forces on the human cranium. J Craniofac Surg 2005;16(1):134-9.

10. Boyce TM, Winterbottom JM, Kaes DR, Shimp LA, Knaack DA. Development of a bone-derived composite implant for skeletal applications. In: Hollinger JO, editor; 2003; Pittsburgh, PA.

11. Osteotech I. Concerned about the safety of your autograft? ; 2006.

12. Bilezikian JP, Raisz LG, Rodan GA, editors. Principles of Bone Biology. Volume One. New York: Academic Press; 1996. 1-1398 p.

13. Market Dynamics:Bone Substitutes and Growth Factors. New York: Datamonitor (DMHC1812); 2002. p 118-32.

14. Newton CD, Nunamaker DB. Textbook of small animal orthopaedics. Philadelphia: Lippincott; 1985.

15. Eagan MJ, McAllister DR. Biology of Allograft Incorporation. Clinics in Sports Medicine 2009;28(2):203-214.

16. Hafeman A, Li B, Yoshii T, Zienkiewicz K, Davidson J, Guelcher S. Injectable biodegradable polyurethane scaffolds with release of platelet-derived growth factor for tissue repair and regeneration. Pharm Res 2008;25(10):2387-99.

17. Guelcher S. Biodegradable polyurethanes: synthesis and applications in regenerative medicine. Tissue Eng B 2008;14(1):3-17.

18. Malinin TI, Carpenter EM, Temple HT. Particulate bone allograft incorporation in regeneration of osseous defects; importance of particle sizes. Open Orthop J 2007;1:19-24.

19. Storey RF, Wiggins JS, Puckett AD. Hydrolyzable poly(ester-urethane) networks from L-lysine diisocyanate and D,L-lactide/e-caprolactone homo- and copolyester triols. Journal of Polymer Science, Part A: Polymer Chemistry 1994;32(12):2345-2363.

20. ASTM-International. ASTM D4274-99: Standard Test Method for Testing Polyurethane Raw Materials: Determination of Hydroxyl Numbers of Polyols. Section 8 - Plastics: ASTM International; 1999.

21. ASTM-International. ASTM D2572-97: Standard Test Method for Isocyanate Groups in Urethane Materials or Prepolymers. Section 8 - Plastics. West Conshohocken, PA: ASTM International; 2000.

22. Guelcher SA, Patel V, Gallagher KM, Connolly S, Didier JE, Doctor JS, Hollinger JO. Synthesis and in vitro biocompatibility of injectable polyurethane foam scaffolds. Tissue Engineering 2006;12(5):1247-1259.

23. Clarkin OM, Boyd D, Madigan S, Towler MR. Comparison of an experimental bone cement with a commercial control, Hydroset^{TM}. J Mater Sci: Mater Med 2009;20:1563 - 1570.

24. Sperling LH. Introduction to Physical Polymer Science. New York: Wiley-Interscience; 2001.

25. Oertel G. Polyurethane Handbook. Berlin: Hanser Gardner Publications; 1994.

26. Baroud G, Bohner M, Heini P, Steffen T. Injection biomechanics of bone cements used in vertebroplasty. Biomed Mater Eng 2004;14(4):487-504.

27. Bohner M, Baroud G. Injectability of calcium phosphate pastes. Biomaterials 2005;26(13):1553-1563.

28. Dumas JE, Davis T, Holt GE, Yoshii T, Perrien DS, Nyman JS, Boyce T, Guelcher SA. Synthesis, characterization, and remodeling of weight-bearing allograft bone/polyurethane composites in the rabbit. Acta Biomater;6(7):2394-406.

29. Neuendorf RE, Saiz E, Tomsia AP, Ritchie RO. Adhesion between biodegradable polymers and hydroxyapatite: Relevance to synthetic bone-like materials and tissue engineering scaffolds. Acta Biomater 2008;4:1288-1296.

30. Lewis G. Percutaneous Vertebroplasty and Kyphoplasty for the Stand-Alone Augmentation of Osteoporosis-Induced Vertebral Compression Fractures: Present Status and Future Directions. J Biomed Mater Res Part B : Appl Biomater 2007;81B:371-386.

31. Adhikari R, Gunatillake PA, Griffiths I, Tatai L, Wickramaratna M, Houshyar S, Moore T, Mayadunne RT, Field J, McGee M and others. Biodegradable injectable polyurethanes: synthesis and evaluation for orthopaedic applications. Biomaterials 2008;29(28):3762-70.

32. Li B, Yoshii T, Hafeman AE, Nyman JS, Wenke JC, Guelcher SA. The effects of rhBMP-2 released from biodegradable polyurethane/microsphere composite scaffolds on new bone formation in rat femora. Biomaterials 2009;30(35):6768-79.

33. Boyce TM, Winterbottom JM, Lee S, Kaes DR, Belaney RM, Shimp LA, Knaack D. Cellular Penetration And Bone Formation Depends Upon Allograft Bone Fraction In A Loadbearing Composite Implant. 2005. p 133.

34. Hasegawa S, Ishii S, Tamura J, Furukawa T, Neo M, Matsusue M, Shikinami Y, Okuno M, Nakamura T. A 5-7 year in vivo study of high-strength hydroxyapatite/poly(L-lactide) composite rods for the internal fixation of bone fractures. Biomaterials 2006;27:1327-1332.

35. Shikinami Y, Okuno M. Bioresorbable devices made of forged composites of hydroxyapatite (HA) particles and poly-L-lactide (PLLA): Part I. Basic characteristics. Biomaterials 1999;20:859-877.

CHAPTER V.

Remodeling of allograft mineralized bone particle/polyurethane bone void filler composite with recombinant human bone morphogenetic protein (rhBMP-2) in a rabbit calvarium model

Introduction

The treatment of craniofacial defects is a challenge as reconstruction must provide protection to the brain without while preventing infection and maintaining adequate cosmesis.[1] Therefore, the restoration of form and function is a critical goal. Craniofacial bones, which are generally flat bones, typically consist of two cortical plates with a core of trabecular bone that provides a minimum supply of osteoblastic precursor cells within the bone. Furthermore, the curvature of craniofacial bones poses a challenge to restore form. Several alloplastic materials such as titanium meshes, polymethylmethacrylate, and hydroxyapatite ceramics have been used in the past to treat craniofacial defects.[2] However, issues such as slow resorption rates and postoperative infections can arise with the used of these treatments.[2]

Craniofacial defects can arise from several causes, including trauma, tumor ablation, developmental anomalies, and infections due to needed surgical revisions. As with all bone injuries, autograft bone is the gold standard as it is both osteogenic and osteoconductive. However, limited supply and donor site morbidity are two significant disadvantages that hinder its use.[3] Treatment of congenital defects in children between the ages of 2 and 10 are particularly challenging as defects have lost the ability to

spontaneously heal, and split calvarial grafts[4] are not adequate due to the underdeveloped diploic space[5-7]. On the battlefield, craniomaxillofacial injuries caused by explosive devices are characterized by open wounds and comminuted fractures, and in severe cases, complicated by avulsion of soft tissue and burns[8,9]. Currently, several treatments are being developed to address the need to treat craniofacial defects.

Several calcium phosphate cements such as Norian, Biopex, and BoneSource have been used clinically to treat craniofacial defects. Calcium phosphates are useful since they provide strength and chemically bond to bone[10]. Norian is an injectable paste that comprises monocalcium phosphate, tricalcium phosphate, calcium carbonate and sodium phosphate and hardens within the defect[11,12]. The New Zealand white (NZW) rabbit critical sized defect (CSD) model has been used in several studies to investigate bone regeneration with Norian[11-13]. A modest amount of new bone formation was observed in these studies. New bone formation at 6 and 12 weeks was observed to be 1.36% and 11.66 %, respectively[11,13]. However, Norian calcium phosphate showed negligible penetration of cells into the material after 12 weeks and only appositional bone formation was observed [11-13]. Adverse effects on the soft tissue on the dura were observed in some cases due to fragmentation of the Norian material[11].

Demineralized bone matrix (DBM) contains bone morphogenetic protein (BMP), which accelerates the differentiation of mesenchymal stem cells into osteoblasts. It has been shown that DBM supports new bone growth in rabbit calvaria CSD[14]. However, a carrier such as glycerol is needed to enhance the handling properties of granular DBM. DBM in conjunction with a delivery system has also been studied as a potential treatment. A study with Grafton®, a DBM putty from Osteotech, has shown 52.4%

mineral density in the rabbit calvaria CSD model after 12 weeks[1]. In a similar study, DBM powder (47%) mixed with a poloxamer gel carrier (poloxamer 407) achieved 44.3% new bone formation in the CSD defect[11]. However, in contrast to calcium phosphates, DBM putties have weak mechanical properties and do not provide immediate protection to the brain[13].

Recombinant human bone morphogenetic protein 2 (rhBMP-2) is a potent growth factor that has been widely studied for the treatment of CSDs. Like DBM, it requires a carrier for delivery, which has been a challenge as the ideal carrier must maintain a sustained release of rhBMP-2 over a period of time due to its short half-life of 1-4 hours [15-18]. Since rhBMP-2 is an expensive protein, effective release strategies alleviate the cost to the patient by reducing required doses[16,19]. Medtronic has obtained FDA approval for the use of rhBMP-2 for single-level anterior lumbar interbody fusion, marketed as INFUSE® bone graft kits[16,20]. The rhBMP-2 is adsorbed on the surface of sterile absorbable collagen sponges during soaking and released from the sponge once implanted in the defect. However, *in vitro* studies have shown that collagen sponge can releases greater than 50% of rhBMP-2 within 24 hours[21]. Calcium phosphates have also been investigated as potential delivery vehicles of rhBMP-2; however, brittleness and the lack of suitable porosity negate its effectiveness[18]. A gel-based delivery system has been reported to effectively enhance spinal fusion in a rat model[22], but gel systems typically lack initial strength.

To address the challenges of craniofacial repair, an ideal material should have the ability to fit complex defects (i.e., be moldable), provide temporary protection until tissue remodels, and enhance tissue regeneration with the delivery of biologics.[23]

Polyurethanes based on lysine-derived isocyanates are an attractive biomaterial as they are biocompatible[24,25]. Allograft mineralized bone particle (AMBP)/polyurethane (PUR) composites, a two-component injectable system, have been investigated in both rabbit and rat distal femur models and have been shown to be biocompatible and support remodeling[26,27]. In these studies, the AMBP phase provided a pathway for cellular infiltration by osteoclast-mediated resorption. Cellular infiltration was accelerated by pores resulting from the blowing reaction that occurs when the isocyanate groups react with water, which allowed for migration of cells into pores. In this study, the potential of injectable AMBP/PUR composites to enhance bone healing in the NZW rabbit calvarial CSD model was studied. The composites incorporated 47% AMBP and 50% porosity. Delivery of INFUSE® rhBMP-2 from the AMBP/PUR composites to accelerate bone formation was also studied.

Materials and Methods

Materials

LTI-PEG prepolymer and polyester polyol were obtained from Ricerca Biosciences (Concord, OH), and Tegoamin 33 was received from Goldschimidt (Hopewell, VA). The gelling catalyst triethylene diamine (TEDA) and dipropylene glycol (DPG) were purchased from Sigma-Aldrich (St. Louis, MO). Ultrafoam collagen sponges were purchases from Davol (Warwick, RI). An Infuse Bone graft kit was acquired from Medtronic (Minneapolis, MN). Rabbit allograft mineralized bone particles (100-500 microns) were received as a gift from Osteotech, Inc. (Eatontown, NJ).

Preparation of rhBMP-2

A solution of rhBMP-2 (1.5 μg/mL) was prepared by reconstituting rhBMP-2 powder per mixing instructions provided with the Infuse kit. The solution was aliquoted into vials to achieve 80 μg/mL of active rhBMP-2 dose in each vial. The vials were frozen at -80 C and lyophilized to achieve a powder.

Synthesis of BVF

The polyester polyol background comprised 60% caprolactone, 30% glycolide, and 10% lactide and had a molecular weight of 900 g mol^{-1} (6C3G1L900). An index of 130 was targeted to produce a BVF composite with a porosity of approximately 50% upon injection. The TEDA catalyst was blended with DPG to yield a 10% solution of TEDA. The appropriate amounts of polyol, AMBP (47 wt%), and LTI-PEG prepolymer were added to a mixing cup and mixed for 90 seconds. The resulting paste was then added to the rhBMP-2 vial, followed by the addition of TEDA and mixed for 60 seconds. The resulting reactive paste had a working time of approximately 5 minutes and a cure time of 10 minutes.

In vitro rhBMP-2 release study

A 2.5 g cylindrical BVF was prepared using with a dose of 50 μg of rhBMP-2. Using previously published methods[27], an appropriate amount of water was added to the foam to produce a porosity of 50%. Discs of approximately 500 microns in thickness were cut from the BVF and placed in αMEM media with 1% BSA. Media was collected periodically over a 25 day period and analyzed using a BMP-2 Enzyme-linked immunosorbent assay (ELISA) to determine rhBMP-2 concentration.

Animal Study

As shown in Table 5.1, four treatment groups were investigated in this animal study using skeletally mature New Zealand white rabbits. Following standard practices for aseptic surgery, a full-thickness calvarial defect was prepared in the parietal bones using a 15-mm surgical trephine for rabbits as described previously. The defects were treated according to the pre-determined randomization scheme. An anteroposterior (anterior to the palpated occipital bone and posterior to the transverse line bisecting the ears) midline skin and periosteal incision was created along the palpated cranial vault (or external saggittal crest). The length of the incision was 3 – 4 cm. Periosteum was elevated with an elevator and retracted to expose the parietal bones and the transverse suture between the parietal and frontal bones. A MicroAire surgical drill with a brass trephine was used to create the critical size defect (CSD) of 15mm during copious saline irrigation. The location of the CSD is 1 – 2 mm distal to the transverse suture centered over the midline of the parietal bones. The cranial cap was carefully removed posterior to anterior while using an elevator to separate the attached dura from the underside of the cap. Pressure with sterile gauze was applied to stop excessive bleeding. Photos were taken and either no treatment (for the negative control rabbits) or treatment (a material was added to fill the defect) was completed. Collagen sponges were cut to fit the defect and soaked in the appropriate solution of rhBMP-2 for 10 minutes prior to application for a dose of 80 μg per sponge. Soft tissues were closed in layers using resorbable 3-0 Dexon sutures to create 2 sets of continuous sutures.

Table V.1: Treatment groups for in vivo rabbit calvaria study.

	6 weeks	**12 weeks**
negative control	n = 10	n=10
Norian	n = 10	n=10
BVF	n = 10	n=10
BVF with rhBMP-2	n = 10	---

X-ray Analysis

X-rays were acquired for each calvarium after extraction. CTAn software was used to analyze the volume and density of bone for each treatment group. A region identical to the size of the defect created during the original study was outlined on each x-ray. The percent of the defect filled by ossified tissue was measured to the pixels of gray to the total number of pixels in the defect area. The bone density was determined by the ratio of the mean gray histogram (distribution of gray) to the defect to the mean histogram of the surrounding host bone.

Histology and histomorphometry

The calvaria were placed in a solution of 10% formalin followed by a series of ethanol dehydration. The specimens were then embedded in methyl/butyl methacrylate. The resulting blocks were then sectioned using an Exakt system, producing 75-micron sections. Resulting sections were stained with Sanderons' Rapid bone stain counterstained with Van Gieson. Histomorphometry was completed using Image Pro Plus. Residual polymer, allograft bone, and new bone formation were quantified for three zones, including both edges of the implant and the center region.

Results

In vitro Release Study

Figure 5.1 shows an initial burst release of rhBMP-2 form the BVF scaffold between days 1 and 4. Subsequently, a steady release was observed after day 4 with a cumulative amount of 20% rhBMP-2 released by day 25.

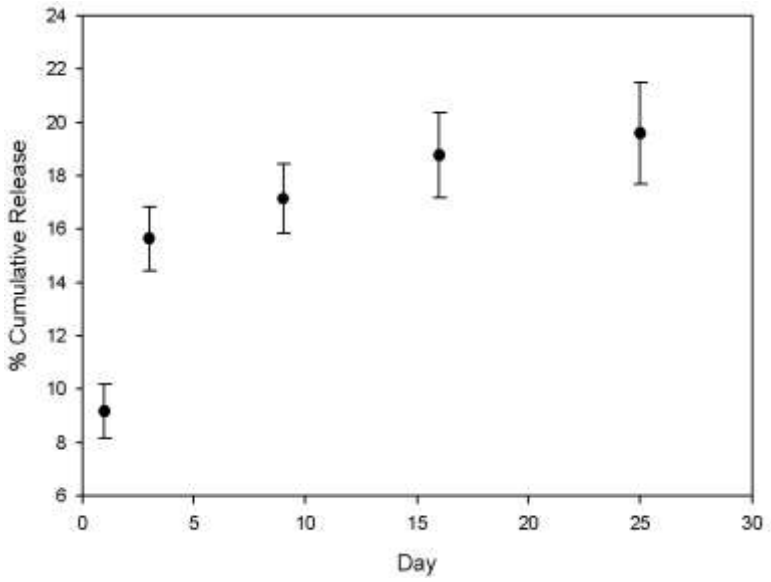

Figure V.1: In vitro release kinetics of rhBMP-2 from BVF composite with 50% porosity and 47% AMBP.

Animal Study

During the surgical procedure, either the Norian or BVF composite groups was injected in the defect, which had a volume of approximately 0.5 mL. A total of 0.25 mL of the AMBP/PUR bone void filler (BVF) composite was used to fill the defect as it doubled in size during curing. In contrast, the Norian group developed cracks as it hardened before closing the wound.

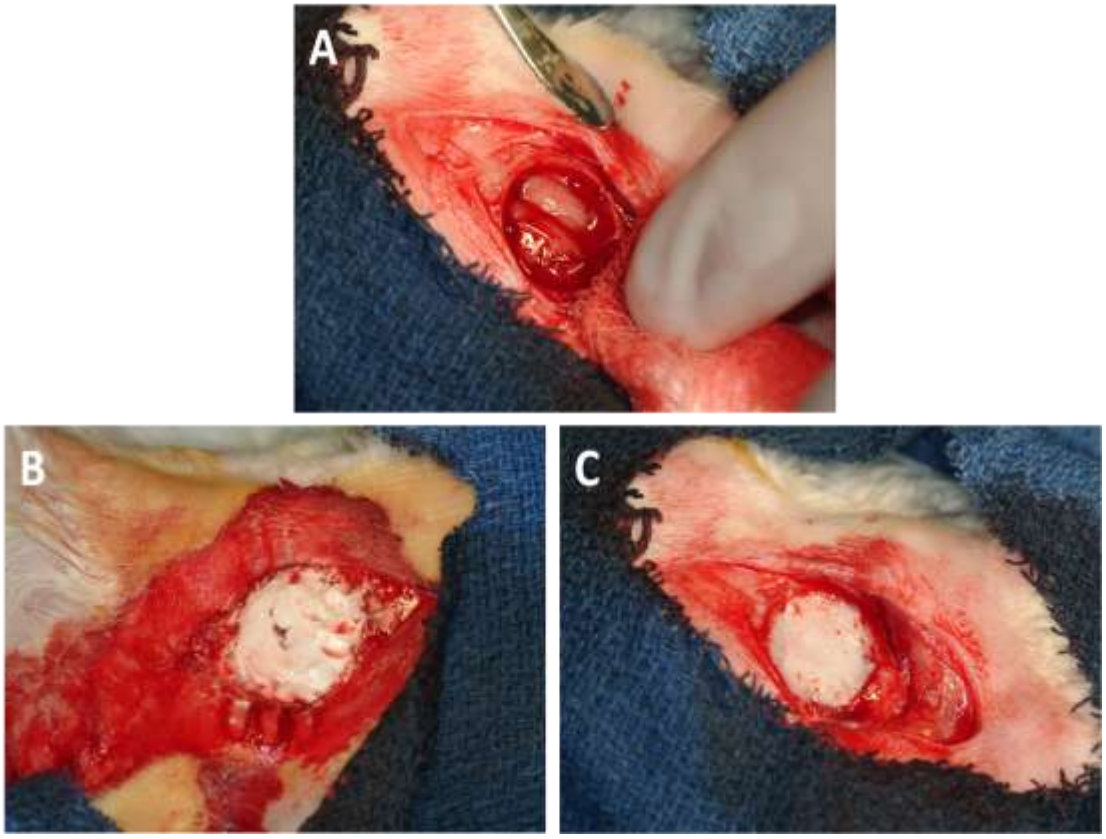

Figure V.2: Surgical photos from the NZW rabbit calvaria CSD study
(A: preparation of CSD, B: injection of Norian material showing material failure due to cracks, C: injection of BVF composite.)

X-ray Analysis

X-rays (Figure 5.2) of the negative control defects showed minimal bone formation in the defect at both 6 and 12 weeks, as anticipated for a CSD. Consistent with observations during surgery, x-rays of the Norian treatment group showed cracking of the material. Bone ingrowth was observed around the perimeter of the BVF treatment groups with traces of bone in the center. X-rays did not indicate any significant differences between the 6 and 12 week time points for the BVF composite treatment group. The x-rays of the BVF composite with rhBMP-2 showed a significant increase in new bone

formation within the defect. In contrast, the x-rays of the collagen/rhBMP-2 showed minimum bone growth in the defect.

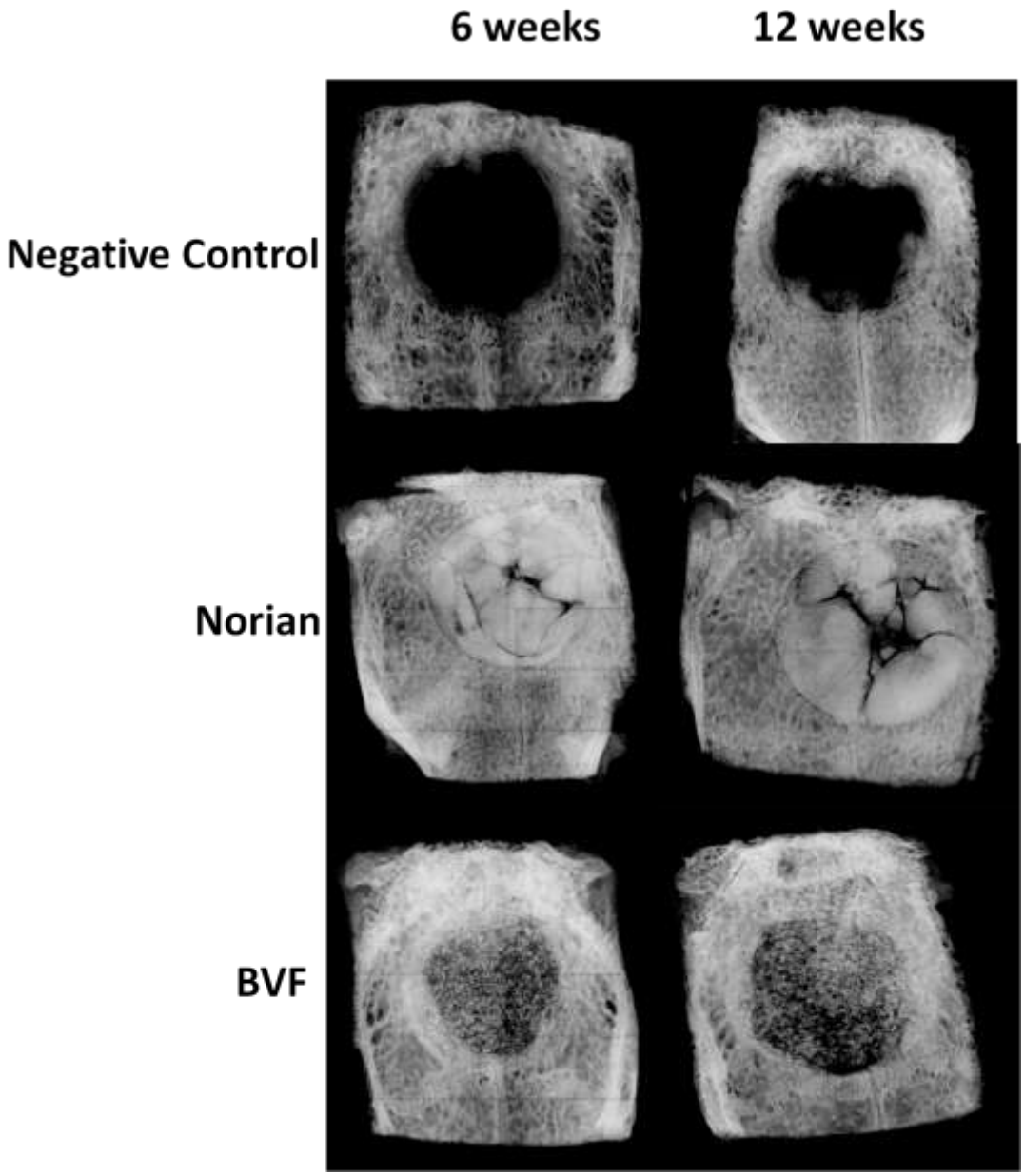

Figure V.3: X-rays of rabbit calvaria at 6 and 12 weeks.

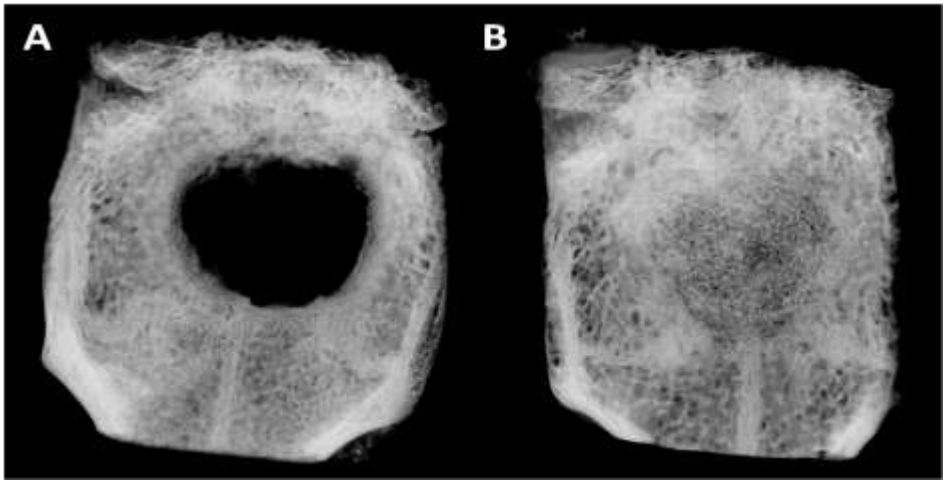

Figure V.4: X-ray of (A) collagen with rhBMP-2 and (B) BVF composite with the incorporation of rhBMP-2 at 6 weeks.

Figure 5.5 shows the results of the CTAn software analysis of the first three treatment groups. A majority of the mineral content measured for the Norian treatment group derived from residual calcium phosphate and not new bone formation. Therefore, little information could be inferred from CTAn analysis on the Norian groups. CTAn analysis confirmed that there were no significant differences between the 6 and 12 week groups for the BVF composite groups. The CTAn analysis included both new bone formation and allograft bone particles. As expected, there was a significant difference between the negative control and the BVF composite groups. There was no significant difference in the density of the mineral at 6 and 12 weeks for the BVF composite. Figure 5.6 compares the 6 week BVF and collagen groups in which AMBP were also included in the bone volume analysis. BVF composites with rhBMP-2 showed a significant amount of bone volume in the defect; however, there were no significant differences in bone density over all the BVF composite groups. As observed for the x-ray images, CTAn

analysis showed very little mineralization for the collagen/rhBMP-2 group. However, the mineral density of the regenerated bone in the collagen/rhBMP-2 was consistent with the other treatment groups.

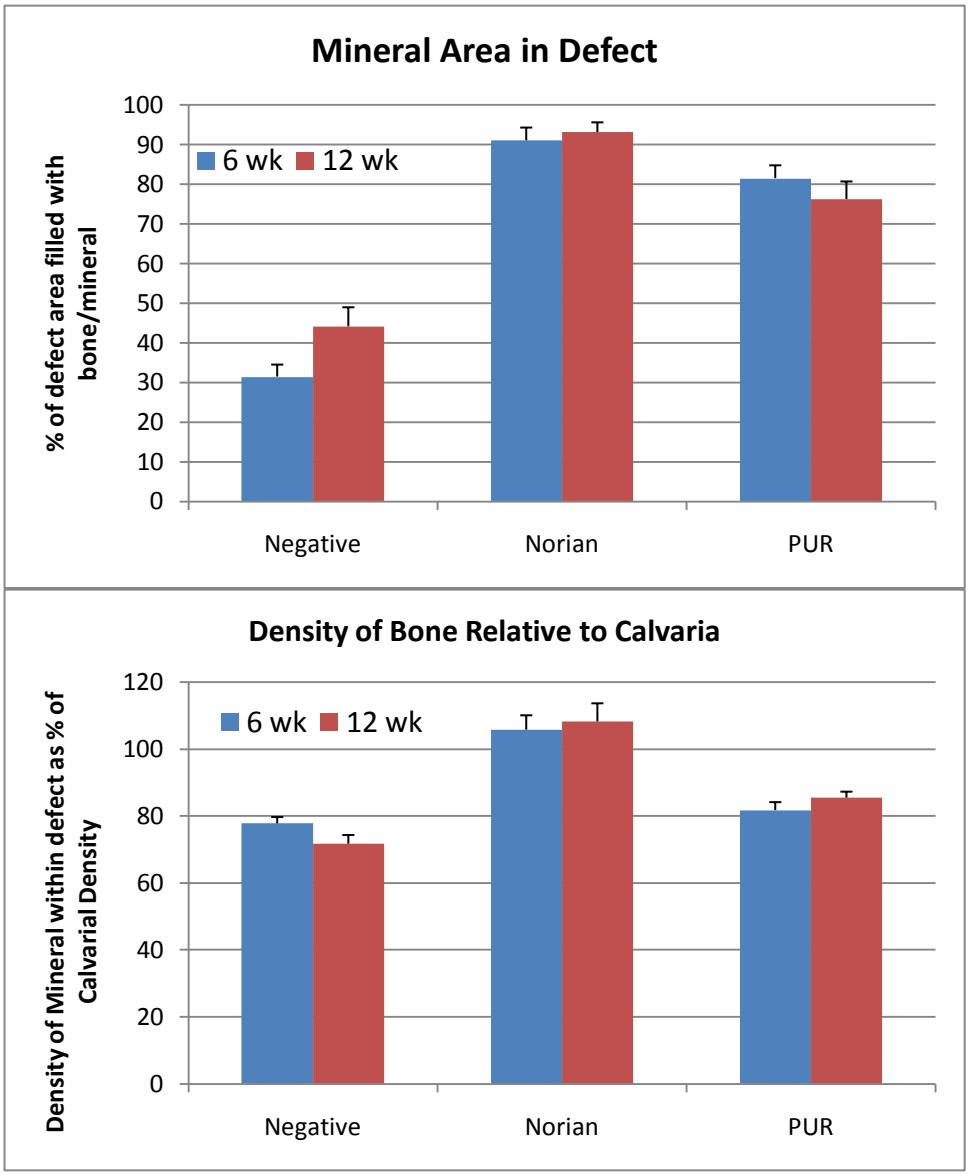

Figure V.5: Percent of defect area filled and density measurements as measure by CTAn software.

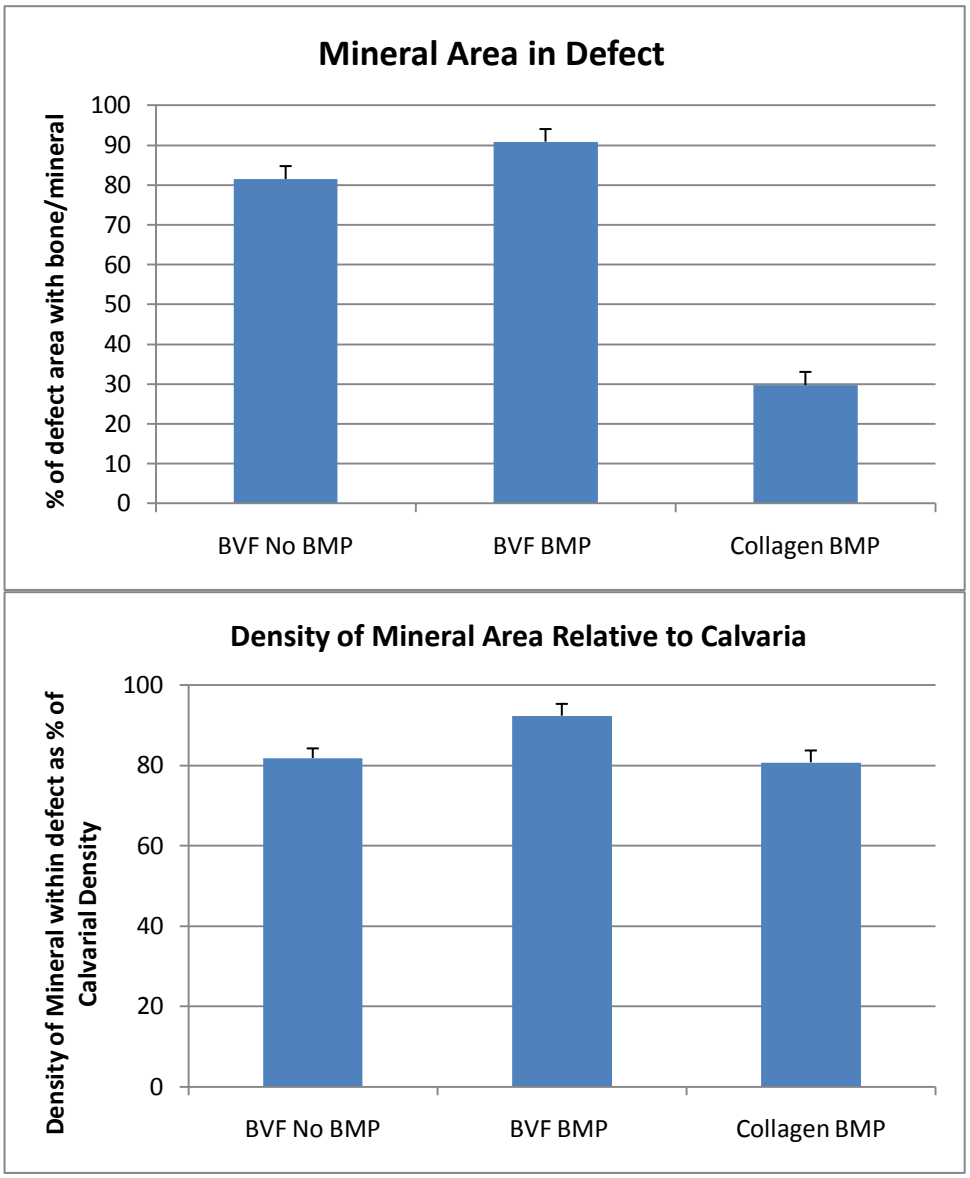

Figure V.6: Percent of defect area filled and density measurements as measure by CTAn software.

Histology

As expected, a fibrous scar filled the untreated defect at both time points (Figure 5.7). Histology indicates that there were no adverse responses to any of the treatment groups used in this study. The Norian treatment groups (Figure 5.8) show appositional bone growth around the surface and between the cracks of the material as evident by the

mineralization stained in pink. This pattern was the same for both the 6 and 12 week Norian groups. However, there was no cellular infiltration in the material as there was no pathway for invasion. Figure 5.9 shows histology of a BVF composite at the 6 week time point. Cells, stained light blue, invaded the BVF composite via the pores of the material. At the host bone/implant interface new bone formed within the pores of the implant lined with osteoid which is stained blue. There is a moderate amount of residual polymer, stained dark blue, within the implant cavity. There was a moderate amount of overexpansion and lifting of the BVF composites due to the carbon dioxide blowing reaction that occurs during curing[27]. Despite overexpansion, cells were still able to infiltrate the entire implant. In contrast, histology from the 12 week BVF composite (Figure 5.10) showed extensive polymer degradation as well as new bone formation. The BVF composite with rhBMP-2 showed extensive bone growth around the composite as well as throughout the pores of the material. The histology (Figure 5.12) of collagen/rhBMP-2 showed fibrous tissue and minimal new bone formation. High magnification images (Figure 5.13) show blood vessel formation within the implant cavity, as well as osteoclasts and osteoid.

Figure 5.14 shows the histomorphometry of the BVF treatment groups. As expected, there are significant differences in the amount of new bone and residual polymer between 6 and 12 weeks. Furthermore, the BVF incorporating rhBMP-2 exhibited the greatest bone formation and polymer degradation. The increased polymer degradation in the rhBMP-2 group is most likely due to development of blood vessels which deliver monocytes to the defect site. Surprisingly, there was not a significant difference in the amount of allograft bone remaining in all of the treatment groups. This

suggests that the AMBP is being resorbed at early time points to provide pathways of cellular infiltration.

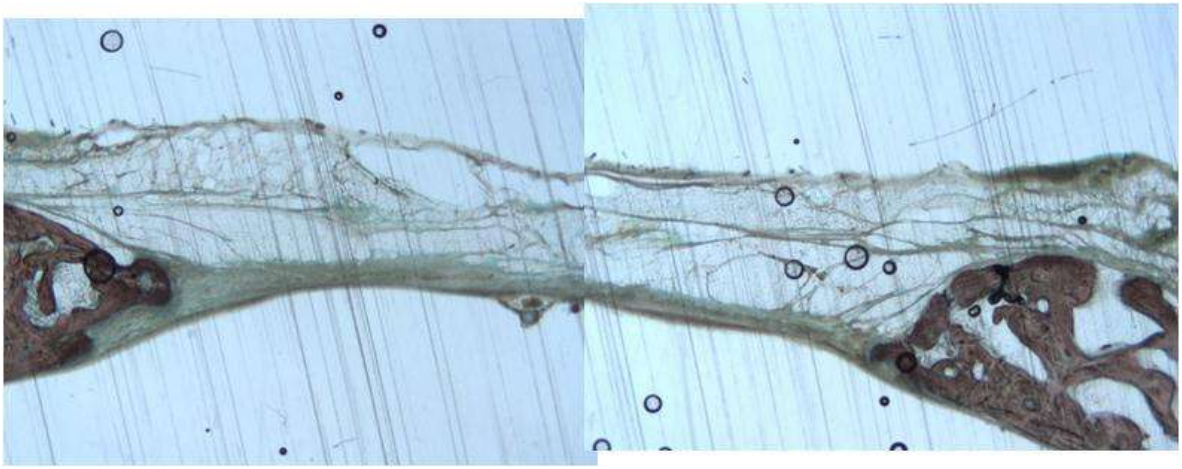

Figure V.7: Histology of untreated calvarium defect.

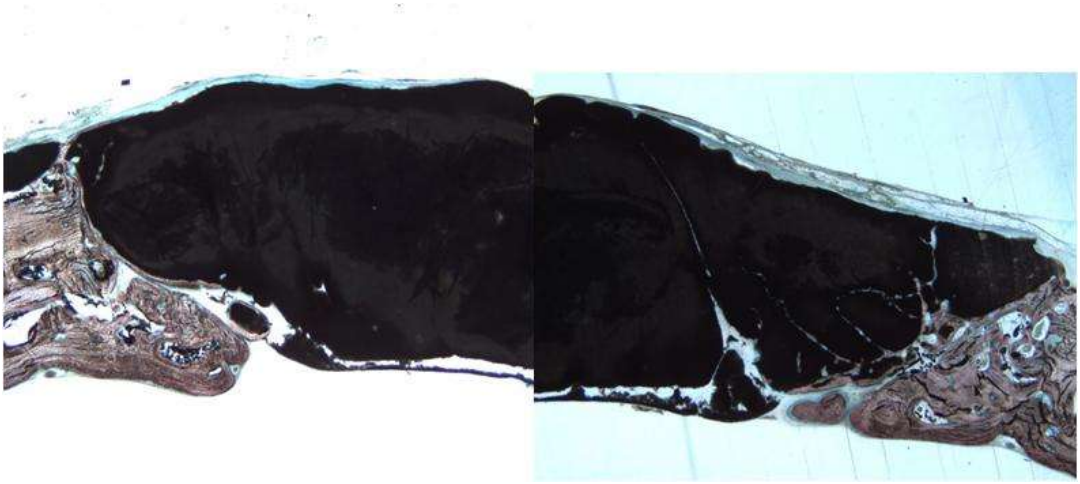

Figure V.8: Histology of Norain treatment group in the calvarium defect .

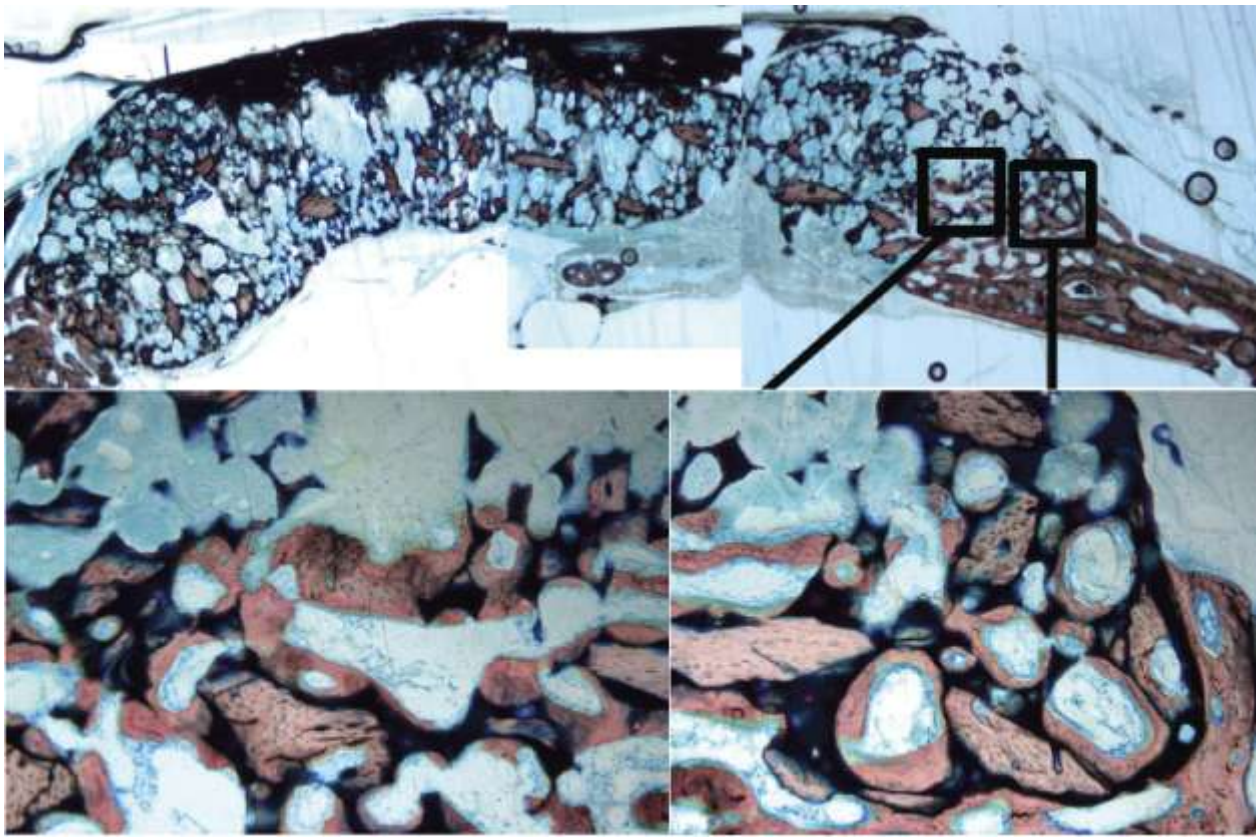

Figure V.9: Histology of BVF composite treatment group in the calvarium defect at 6 weeks.

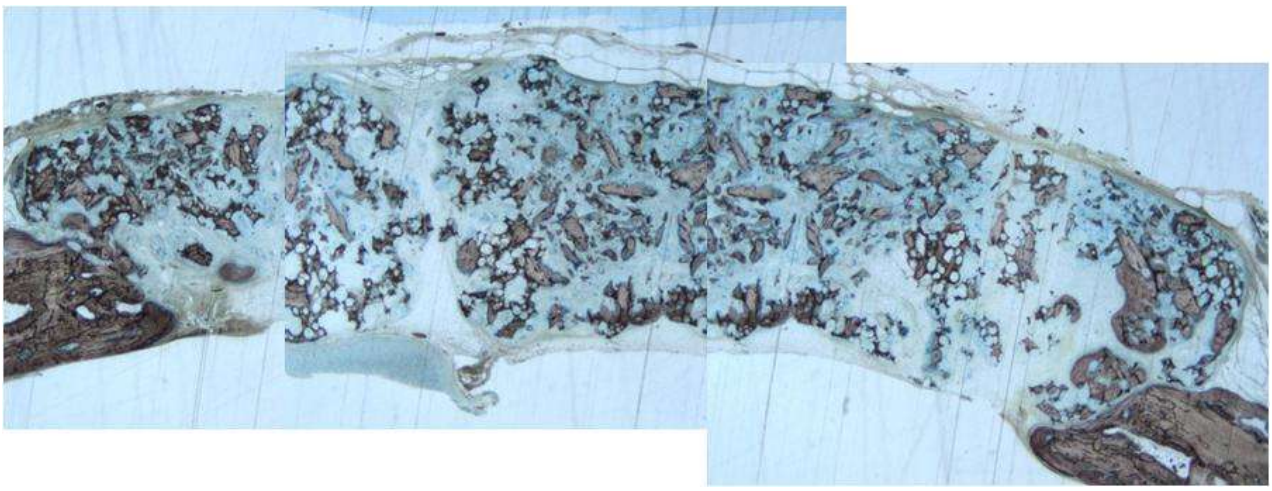

Figure V.10: Histology of BVF composite treatment group at 12 weeks.

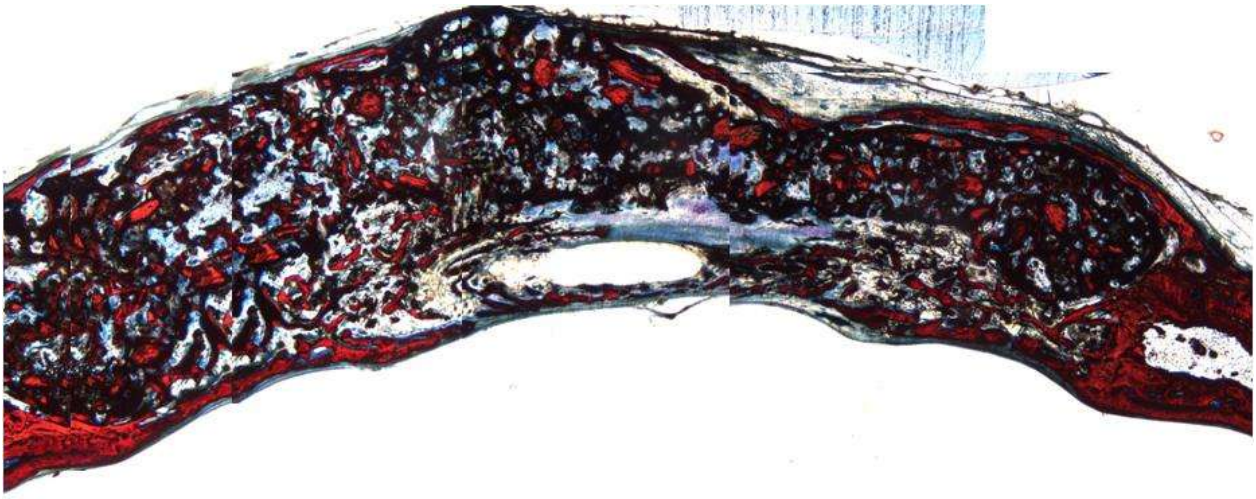

Figure V.11: Histology of BVF composite treatment group with the incorporation of rhBMP-2 at 6 weeks.

Figure V.12: Histology of collagen treatment group with the incorporation of rhBMP-2 at 6 weeks.

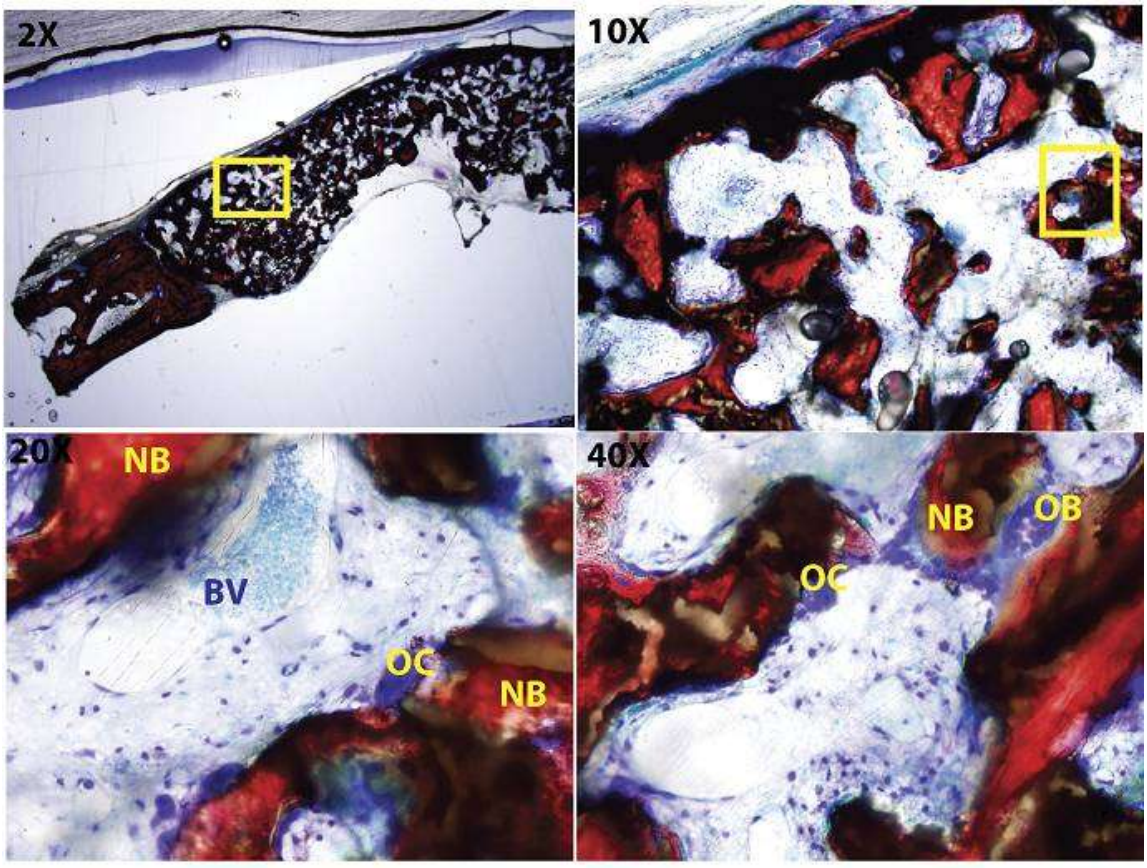

Figure V.13: High magnification histology of BVF treatment group with the incorporation of rhBMP-2 at 6 weeks.
(OB: old bone, OC: osteoclast, NB: new bone, BV: blood vessel.)

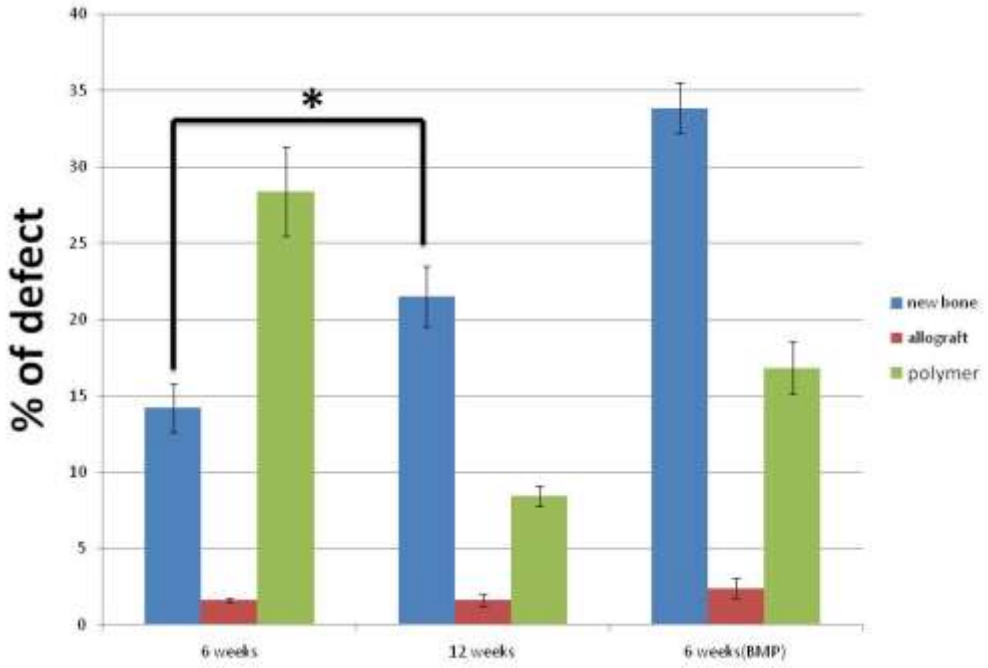

Figure V.14: Histomorphometry of the BVF treatment groups.

Discussion

There are several rhBMP-2 release strategies being studied as potential clinical applications[15,16,18,22]. These systems do not typically provide initial strength to the defect and require the support of an additional implant. Furthermore, the release kinetics of these systems can be difficult to control. The *in vitro* release kinetics of rhBMP-2 from the BVF composites shown a modest release (<10%) after 1 day. It has been reported that initial bursts of kinetics of greater that 30% is non-ideal as clinical complications such as hematomas of soft tissues can occur[18,28]. When implanted *in vivo*, it is expected that osteoclastic resorption of the AMBP phase provides an additional pathway for the release of rhBMP-2. With this attribute, BVF composites are anticipated to under cell-mediated release of rhBMP-2.

The *in vivo* curing attributes of the BVF composites were superior to the Norian biomaterials considering the cracking of the Norian cements before wound closure, which has been observed with calcium phosphate cements from previous studies[11]. This observation is expected as the pulsatile forces of the dura can have systolic normal and tangential stresses of 54.2 kPa and 345.4 kPa, respectively[29]. Both materials cured within 10 minutes of injection, providing early protection to the brain unlike DBM putties, which possess weak initial mechanical properties[12]. However, studies have shown that the stiffness of Norian (80 N/mm) does not match that of bone (~130 N/mm) after implantation for 8 weeks, but is still significantly greater than the Novabone/DBM mix (~30 N/mm) at the same time point[12].

Surprisingly, the collagen/rhBMP-2 group did not stimulate a substantial amount (<30% mineralized) of new bone in the defect. In a similar rabbit study,greater than 90% ossification after 6 weeks using collagen/rhBMP-2 was reported[7]. In a primate CSD calvarium model, greater than 70% ossification as observed after 6 months[30]. Both of these studies utilized a higher dose of rhBMP-2, greater than 400 μg/mL. However, it is anticipated that the defect would show more new bone formation than the untreated group. The histology from this study suggests that the collagen degraded too quickly. Without a scaffold to support the osteoblastic cells, new bone formation is hindered. As histology shows, Figure 5.12, the collagen implant was likely degraded prior to the onset of bone formation.

Histological sections showed extensive cellular infiltration for all of the BVF groups. In contrast, the Norian group did not support cellular infiltration and essentially acted as a barrier to bone formation over the 12 weeks. Bone was regenerated in all of

the BVF composite groups, as evidenced by the observation that new bone formation significantly progressed with time. Interestingly, there was minimum residual PUR remaining at 12 weeks, and rhBMP-2 accelerated PUR degradation, which is conjectured to result from an increased presence of blood vessels. Although there was a significant difference between new bone formation at 6 and 12 weeks, the amount observed was lower than expected, especially in the center of the implant. At this later time point, the degradation of the PUR is anticipated to diminish the structural integrity of the BVF composites, since the majority of the bone ingrowth was observed around the perimeter of the defect and not in the middle. Without new bone, allograft, or PUR remaining in the middle region of the implant, new bone formation could not progress due to the absence of a scaffold for new formation. Mechanical stability is a key characteristic of successful biomaterials[31], especially in the calvaria defect due to the pulsatile forces emanating from the dura[29]. In contrast, histological sections of the BVF/rhBMP-2 group show a bridge of new bone covering the upper surface of the implant as well as new bone formation throughout the implant, suggesting the adequate delivery of rhBMP-2 from the material. It is anticipated that this new bone formation would provide adequate support during the healing process as the PUR is degraded.

Extensive vascular formation in the defect was only observed in the BVF/rhBMP-2 composite groups. Several *in vitro* co-culture studies have shown that osteoblasts have the capability to regulate proliferation and differentiation of endothelial cells by changing pro-angiogenic cues such as VEGF via paracine signaling[32-34]. Furthermore, this vascularisation is essential for bone induction[34]. It is conjectured that the release of rhBMP-2 from the BVF composite acts to increase the population of osteoblasts, thereby

increasing the endothelial cell population creating vessel structures as shown in Figure 5.13. These vessel structures further supply the nutrients needed for cells to remodel in the interior of the implant. Since osteoclasts and osteoblasts are also coupled[35], the population of osteoclasts is anticipated to increase, thereby accelerating resorption of allograft bone particles and allowing for additional release of rhBMP-2.

As the typical rhBMP-2 dose for rabbits is 400 μg/mL[16], it is encouraging that there was extensive new bone formation and vessel formation at a fraction of the recommended dose (80 μg/mL). This finding further suggests that the BVF composite platform is an efficient carrier for rhBMP-2 *in vivo*. Improving the efficiency of the release of rhBMP-2 is a key factor in enhancing the cost-effectiveness of the growth factor[19], making rhBMP-2 a more attractive option for bone tissue engineering.

Conclusion

In vitro release studies have shown that rhBMP-2 has a sustained release from BVF composites. BVF composites had a cure and working time comparable to injectable, fast-setting Norian, while displaying mechanical integrity during wound closure. BVF composites were shown to facilitate the ingrowth of new bone around the perimeter of the rabbit calvaria CSD. Furthermore, the addition of a low dose of rhBMP-2 (80 μg/mL) accelerated new bone formation as new bone was observed throughout the implant while also increasing blood vessel formation. Injectable BVF composites are a promising injectable biomaterial capable of providing initial strength[27], while sustaining a release of rhBMP-2.

REFERENCES

1. Shermak MA, Wong L, Inoue N, Nicol T. Reconstruction of complex cranial wounds with demineralized bone matrix and bilayer artificial skin. J Craniofac Surg 2000;11(3):224-31.

2. Eppley BL. Craniofacial reconstruction with computer-generated HTR patient-matched implants: use in primary bony tumor excision. J Craniofac Surg 2002;13(5):650-7.

3. Khan Y, Yaszemski MJ, Mikos AG, Laurencin CT. Tissue Engineering of Bone: Material and Matrix Considerations. J Bone Joint Surg Am 2008;90(Supplement_1):36-42.

4. Tessier P. Autogenous bone grafts taken from the calvarium for facial and cranial applications. Clin Plast Surg 1982;9(4):531-8.

5. Smith DM, Cooper GM, Mooney MP, Marra KG, Losee JE. Bone morphogenetic protein 2 therapy for craniofacial surgery. J Craniofac Surg 2008;19(5):1244-59.

6. Wan DC, Aalami OO, Wang Z, Nacamuli RP, Lorget F, Derynck R, Longaker MT. Differential gene expression between juvenile and adult dura mater: a window into what genes play a role in the regeneration of membranous bone. Plast Reconstr Surg 2006;118(4):851-61.

7. Smith DM, Afifi AM, Cooper GM, Mooney MP, Marra KG, Losee JE. BMP-2-based repair of large-scale calvarial defects in an experimental model: regenerative surgery in cranioplasty. J Craniofac Surg 2008;19(5):1315-22.

8. Kauvar DS, Wolf SE, Wade CE, Cancio LC, Renz EM, Holcomb JB. Burns sustained in combat explosions in Operations Iraqi and Enduring Freedom (OIF/OEF explosion burns). Burns 2006;32(7):853-7.

9. Lew TA, Walker JA, Wenke JC, Blackbourne LH, Hale RG. Characterization of craniomaxillofacial battle injuries sustained by United States service members in the current conflicts of Iraq and Afghanistan. J Oral Maxillofac Surg;68(1):3-7.

10. Schmitz JP, Hollinger JO, Milam SB. Reconstruction of bone using calcium phosphate bone cements: a critical review. J Oral Maxillofac Surg 1999;57(9):1122-6.

11. Moghadam HG, Sándor GKB, Holmes HHI, Clokie CML. Histomorphometric evaluation of bone regeneration using allogeneic and alloplastic bone substitutes. Journal of Oral and Maxillofacial Surgery 2004;62(2):202-213.

12. Elshahat A, Shermak MA, Inoue N, Chao EY, Manson P. The use of Novabone and Norian in cranioplasty: a comparative study. J Craniofac Surg 2004;15(3):483-9.

13. Clokie CM, Moghadam H, Jackson MT, Sandor GK. Closure of critical sized defects with allogenic and alloplastic bone substitutes. J Craniofac Surg 2002;13(1):111-21; discussion 122-3.

14. Lindholm TC, Gao TJ, Lindholm TS. Granular hydroxyapatite and allogeneic demineralized bone matrix in rabbit skull defect augmentation. Ann Chir Gynaecol Suppl 1993;207:91-8.

15. Takaoka K, Koezuka M, Nakahara H. Telopeptide-depleted bovine skin collagen as a carrier for bone morphogenetic protein. J Orthop Res 1991;9(6):902-7.

16. Haidar ZS, Hamdy RC, Tabrizian M. Delivery of recombinant bone morphogenetic proteins for bone regeneration and repair. Part A: Current challenges in BMP delivery. Biotechnol Lett 2009;31(12):1817-24.

17. Yamamoto M, Takahashi Y, Tabata Y. Controlled release by biodegradable hydrogels enhances the ectopic bone formation of bone morphogenetic protein. Biomaterials 2003;24(24):4375-4383.

18. Haidar ZS, Hamdy RC, Tabrizian M. Delivery of recombinant bone morphogenetic proteins for bone regeneration and repair. Part B: Delivery systems for BMPs in orthopaedic and craniofacial tissue engineering. Biotechnol Lett 2009;31(12):1825-35.

19. Garrison KR, Donell S, Ryder J, Shemilt I, Mugford M, Harvey I, Song F. Clinical effectiveness and cost-effectiveness of bone morphogenetic proteins in the non-healing of fractures and spinal fusion: a systematic review. Health Technol Assess 2007;11(30):1-150, iii-iv.

20. McKay WF, Peckham SM, Badura JM. A comprehensive clinical review of recombinant human bone morphogenetic protein-2 (INFUSE Bone Graft). Int Orthop 2007;31(6):729-34.

21. Maire M, Chaubet F, Mary P, Blanchat C, Meunier A, Logeart-Avramoglou D. Bovine BMP osteoinductive potential enhanced by functionalized dextran-derived hydrogels. Biomaterials 2005;26(24):5085-5092.

22. Miyazaki M, Morishita Y, He W, Hu M, Sintuu C, Hymanson HJ, Falakassa J, Tsumura H, Wang JC. A porcine collagen-derived matrix as a carrier for recombinant human bone morphogenetic protein-2 enhances spinal fusion in rats. Spine J 2009;9(1):22-30.

23. Hollister S, Lin C, Saito E, Lin C, Schek R, Taboas J, Williams J, Partee B, Flanagan C, Diggs A and others. Engineering craniofacial scaffolds. Orthodontics & Craniofacial Research 2005;8(3):162-173.

24. Guelcher SA, Srinivasan A, Dumas JE, Didier JE, McBride S, Hollinger JO. Synthesis, mechanical properties, biocompatibility, and biodegradation of polyurethane networks from lysine polyisocyanates. Biomaterials 2008;29(12):1762-75.

25. Bonzani IC, Adhikari R, Houshyar S, Mayadunne R, Gunatillake P, Stevens MM. Synthesis of two-component injectable polyurethanes for bone tissue engineering. Biomaterials 2007;28(3):423-433.

26. Dumas JE, Davis T, Holt GE, Yoshii T, Perrien DS, Nyman JS, Boyce T, Guelcher SA. Synthesis, characterization, and remodeling of weight-bearing allograft bone/polyurethane composites in the rabbit. Acta Biomater;6(7):2394-406.

27. Dumas JE, Zienkiewicz K, Tanner SA, Prieto EM, Bhattacharyya S, Guelcher SA. Synthesis and characterization of an injectable allograft bone/polymer composite bone void filler with tunable mechanical properties. Tissue Eng Part A;16(8):2505-18.

28. Geiger M, Li RH, Friess W. Collagen sponges for bone regeneration with rhBMP-2. Adv Drug Deliv Rev 2003;55(12):1613-29.

29. Goldberg CS, Antonyshyn O, Midha R, Fialkov JA. Measuring pulsatile forces on the human cranium. J Craniofac Surg 2005;16(1):134-9.

30. Sheehan JP, Sheehan JM, Seeherman H, Quigg M, Helm GA. The safety and utility of recombinant human bone morphogenetic protein-2 for cranial procedures in a nonhuman primate model. J Neurosurg 2003;98(1):125-30.

31. Donath K, Laass M, Gunzl HJ. The histopathology of different foreign-body reactions in oral soft tissue and bone tissue. Virchows Arch A Pathol Anat Histopathol 1992;420(2):131-7.

32. Santos MI, Unger RE, Sousa RA, Reis RL, Kirkpatrick CJ. Crosstalk between osteoblasts and endothelial cells co-cultured on a polycaprolactone-starch scaffold and the in vitro development of vascularization. Biomaterials 2009;30(26):4407-4415.

33. Unger RE, Sartoris A, Peters K, Motta A, Migliaresi C, Kunkel M, Bulnheim U, Rychly J, James Kirkpatrick C. Tissue-like self-assembly in cocultures of endothelial cells and osteoblasts and the formation of microcapillary-like

structures on three-dimensional porous biomaterials. Biomaterials 2007;28(27):3965-3976.

34. Szpalski M, Gunzburg R. Recombinant human bone morphogenetic protein-2: a novel osteoinductive alternative to autogenous bone graft? Acta Orthop Belg 2005;71(2):133-48.

35. Suda T, Takahashi N, Udagawa N, Jimi E, Gillespie MT, Martin TJ. Modulation of osteoclast differentiation and function by the new members of the tumor necrosis factor receptor and ligand families. Endocr Rev 1999;20(3):345-57.

CHAPTER VI.

Low-porosity injectable allograft bone/polymer biocomposites incorporating rhBMP-2

Introduction

Autograft bone is the clinical standard of care for treatment of bone defects due to its osteoinductive and osteogenic properties. However, its limited supply has prompted a search for suitable alternatives. Numerous injectable biomaterials, such as calcium phosphate cements, have been developed as a substitute autograft, but they typically lack its osteogenic properties. Incorporation of growth factors, such as recombinant human bone morphogenetic protein-2 (rhBMP-2), is an attractive option used to enhance the osteogenic properties of synthetic biomaterials. However, the release of rhBMP-2 can be a challenge, as a sustained release is desirable to support bone healing during the initial stages.

The optimal delivery of rhBMP-2 has been widely studied[1-6] due to concerns regarding biosafety and cost-effectiveness[1,7]. Collagen and hydrogels have been extensively investigated as delivery systems for rhBMP-2[1,3,4,6]; however, there are few injectable weight-bearing platforms for recombinant human bone morphogenetic protein (rhBMP-2). Allograft bone mineralized particle (AMBP)/polyurethane (PUR) systems have exhibited both biocompatibility as well as remodeling capabilities *in vivo*[8,9]. An allograft bone particle/polyurethane (PUR) composite non-porous putty with a release mechanism of rhBMP-2 that is more responsive to the surrounding cellular environment

would aid in the efficient delivery of rhBMP-2. Both non-porous and porous platforms have been studied. In the rabbit distal femur model, compression molded AMBP/PUR with allograft loadings approaching the random close-packing limit (64 vol%) showed rapid osteoclast-mediated resorption of the AMBP phase, thereby providing a pathway for cellular infiltration. However, due to the relatively slower rate of new bone formation, large resorption gaps were observed near the host bone/implant interface[8]. In the rabbit calvaria critical size defect (CSD) model, injectable AMBP/PUR bone void filler (BVF) composites (~50% porosity) demonstrated modest new bone formation around the perimeter of the implant. When an 80 μg/mL dose of INFUSE (rhBMP-2) was added to the composite, new bone formation was enhanced throughout the interior of the composite. This dose was significantly lower than the recommended dose for rabbits (400 μg/mL[1]). To study the effects of higher doses, two studies are currently being completed incorporating two doses of rhBMP-2 (100 μg/mL and 400 μg/mL) at 6 and 12 weeks.

Materials and Methods

Materials

LTI-PEG prepolymer and polyester polyol were obtained from Ricerca (Concord, OH), Tegoamin 33 was received from Goldschmidt (Hopewell, VA), and recombinant human bone morphogenetic protein (rhBMP-2) was purchased from R&D systems (Minneapolis, MN). Trehalose dehydrate, heparin sodium salt, acetonitrile, and trifluoroacetic acid (TFA) was purchased from Sigma Aldrich(St. Louis, MO). Rabbit

allograft mineralized bone particles (100-500 microns) were received as a gift from Osteotech, Inc. (Eatontwon, NJ).

Preparation of rhBMP-2

The rhBMP-2 was supplied as a solution which comprised 35% acetonitrile and 0.1% TFA. A separate acetonitrile/TFA solution was prepared containing a ratio of 10:1 of trehalose dehydrate:heparin sodium. The rhBMP-2 and trehalose mixtures were combined such that the ratio of rhBMP-2 to trehalose was 1:125. The resulting mixture was distributed in glass vials and frozen at -80 C in preparation for freeze-drying, which produced a powder.

Synthesis of AMBP/PUR Putty

The polyester polyol backbone comprised 60% caprolactone, 30% glycolide, and 10% lactide and had a molecular weight of 900 g mol^{-1} (6C3G1L900). The appropriate amounts of polyol, AMBP, and LTI-PEG prepolymer were added to a mixing cup and mixed for 90 seconds. The target index was 130 and catalyst concentration of Tegoamin 33 was 5500 ppm. The resulting paste was then added to the rhBMP-2 vial and mixed for 60 seconds. The filler content (AMBP and rhBMP-2 powder) was kept at constant 70 wt% for each putty treatment group (Table 6.1). The resulting reactive paste had a tack-free (i.e., cure) time of approximately 10 minutes.

Mechanical Properties

Cylindrical samples of each treatment group were prepared for mechanical testing. The reactive paste was transferred into cylindrical plastic cups and a 1 pound weight (20.7 psi) was placed on the material for 10 minutes. The resulting cylinders were

placed in a vacuum oven at 37°C overnight and removed from the plastic cups. After cure, the cylinders were removed from the cups and cut using a Buehler saw to produce 6 mm x 12 mm cylinders. Three different formulations were synthesized as summarized in Figure 6.1. After 24 hours of hydration in phosphate buffered saline (PBS), the rods were tested using a MTS 898 using compression.

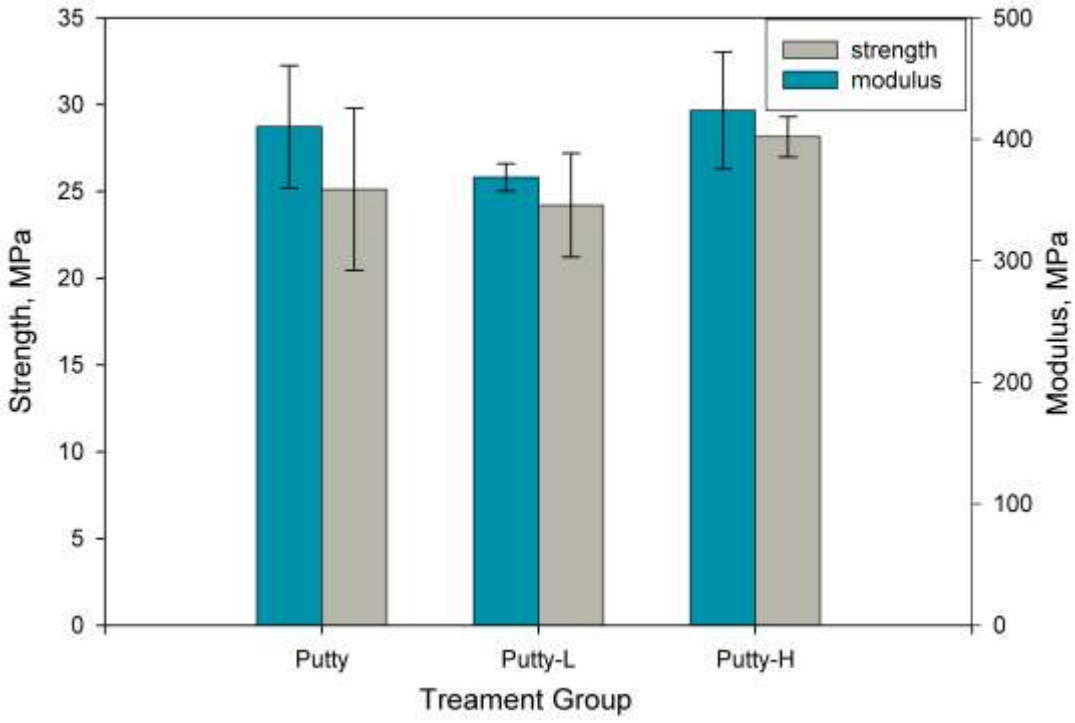

Figure VI.1: Mechanical properties of AMBP/PUR putty system.

Animal Study

Forty-two New Zealand White (NZW) rabbits weighing between 3.8 and 4.1 kg were used in this study. All surgical and care procedures were carried out under aseptic conditions per the approved IACUC protocol. The AMBP/PUR putty components were gamma irradiated using a dose of approximately 25 kGY. Glycopyrrolate was

administered at 0.01 mg/kg IM followed by ketamine at 40 mg/kg IM. Bilateral defects of approximately 6 mm diameter by 11 mm in depth were drilled in the metaphysis of the distal femurs of each rabbit. AMBP/PUR plugs from each treatment group, Table 6.1, were subsequently injected into each defect using a 1 mL syringe. Treatment groups for each composite were dispersed randomly among the rabbits. The rabbits were euthanized at both 6 and 12 week time points using Fatal-plus (2.2 mL/10 kg) intra-venously.

Table VI.1: Treatment groups of *in vivo* rabbit study.

	rhBMP-2 (μg/mL)	6 weeks	12 weeks
empty	0	n=6	n=6
AMBP putty	0	n=10	n=10
AMBP putty-L	100	n=10	n=10
AMBP putty-H	400	n=10	n=10

μCT Data

A μCT40 (SCANCO Medical, Basserdorf, Switzerland) was used to acquire images of the extracted femurs.

Histology

After fixation, the femurs were embedded in Technovit 7200 and 200-μm sections were cut from the resulting blocks using an Exakt band saw. The sections were then ground and polished using an Exakt grinding system to less than 100 μm and stained with Sanderson's rapid bone stain counterstained with van Gieson. Old allograft bone stained

light brown, while new bone stained pink with dark blue osteocytes within the matrix. The polymer was stained dark blue, while cells were stained light blue.

Results

Mechanical Properties

There were no significant differences between the mechanical properties of each treatment group as the strength and modulus values ranged from 24.2-28.1 MPa and 357.3-503.0 MPa, respectivley. These compressive strength is comparable to that of trabecular bone, which ranges from 4-12 MPa[10].

μCT Data

The μCT images of the AMBP/PUR treatment groups are presented in Figure 6.2. The absence of a resorption front was observed for all of the AMBP/PUR treatment groups without rhBMP-2 (Figure 6.2A). However, remodeling for this group was the slowest and least extensive when compared with the groups that incorporated rhBMP-2. Approximately 10% of the AMBP/PUR group incorporating low rhBMP-2 exhibited resorption gaps. In comparison, 30% of the high rhBMP-2 group exhibited resorption gaps as shown in Figure 6.2D.

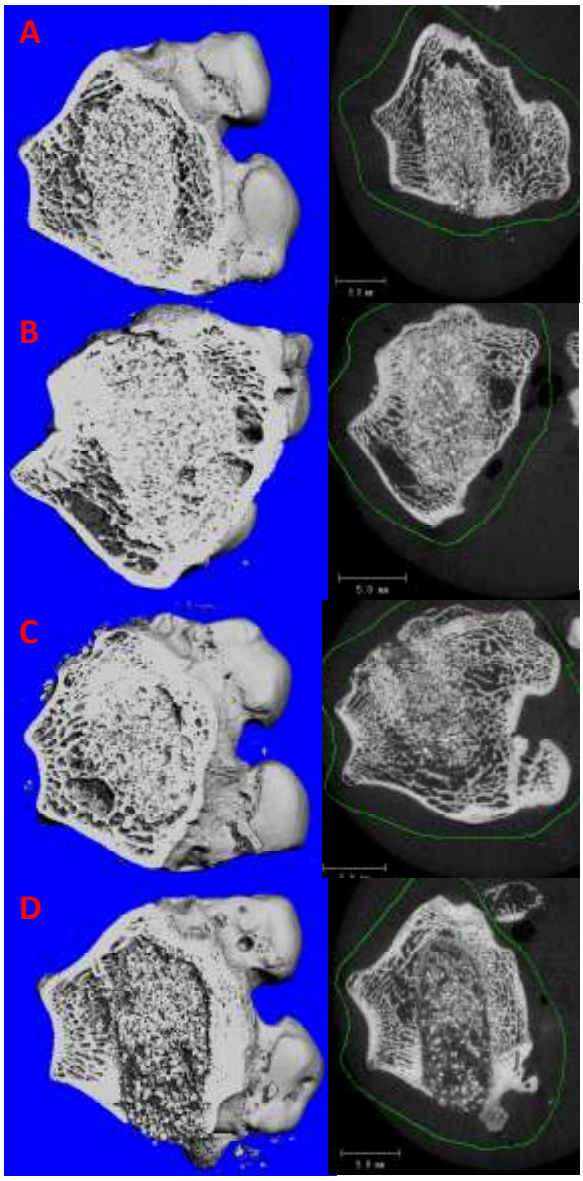

Figure VI.2: μCT images of AMBP/PUR composites.
(A: μCT images show extensive remodeling of AMBP/PUR composites at twelve weeks (A: 0 μg/mL, B: 110 μg/mL, C: 440 μg/mL,) and six weeks (D: 440 μg/mL).)

Histology

Histological sections (Figure 6.3) of the AMBP/PUR putty treatment group showed extensive new bone formation and cellular infiltration throughout the implant. The original border between the host bone and implant is indistinguishable. The high

magnification view (Figure 6.3B) shows connectivity between new bone and allograft bone particles and suggests a creeping substitution remodeling mechanism.

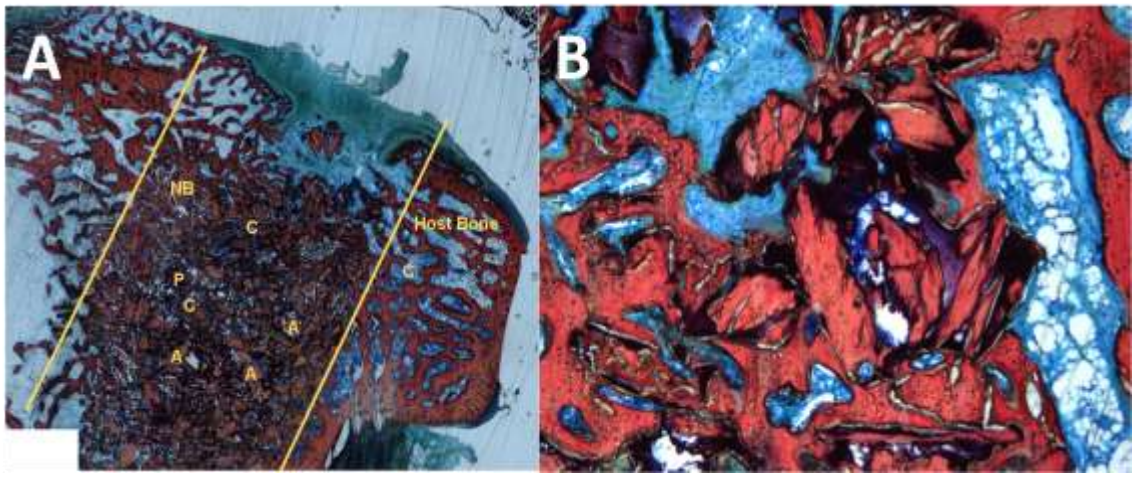

Figure VI.3: Histology from the ABMP/PUR putty treatment group with no rhBMP-2. (A: low magnification (A: allograft bone, NB: new bone, C: soft tissue, P: residual polymer), B: high magnification view at implant-host bone boarder.)

Discussion

AMBP/PUR biocomposites exhibited compressive strengths ranging from 27.2-33.2 MPa, which are comparable to trabecular bone strength. Figure 1 shows μCT images for all treatment groups. The μCT image for the biocomposite at 12 weeks without rhBMP-2 is shown in Figure 1A, and is characterized by extensive remodeling with negligible resorption gaps. A similar pattern was observed at 6 weeks, although the fraction of residual allograft particles that had not been remodeled was higher. These observations contrast with a previous study where compression-molded biocomposites incorporating 79 wt% allograft showed substantial resorption after 6 weeks in a rabbit femoral condyle plug model.[8] As reported previously, cells infiltrated the biocomposite

by creeping substitution, wherein the allograft component is first resorbed by osteoclasts, followed by infiltration of cells and new bone formation.[8] The rhBMP-2 is conjectured to be released from the polymer into the newly formed pores resulting from allograft resorption. Incorporation of rhBMP-2 (Figure 6.2B-D) enhanced new bone formation at 12 weeks relative to the biocomposite without rhBMP-2, as evidenced by the presence of fewer allograft bone particles (irregularly shaped white particles). Similar results were observed at 6 weeks. However, approximately 30% of the samples incorporating a high dose of rhBMP-2 displayed extensive areas of resorption at 6 or 12 weeks, as shown in Figure 6.2D. Similar regions of osteoclast-mediated resorption have been reported for doses of rhBMP-2 exceeding by a factor of 3 the recommended dose delivered on an ACS sponge in a sheep femoral condyle plug model.[11] Figure 6.4 is a diagram of the proposed mechanism of remodeling. The initial release of rhBMP-2 from the AMBP/PUR composites stimulates the differentiation of osteoprogenitor cells to osteoblasts, which subsequently regulate osteoclast differentiation through production of Receptor Activator for Nuclear Factor κB ligand (RANKL).[12,13] The increased osteoclast population results in accelerated resorption of the AMBP filler, which consequently increases rhBMP-2 release through the creation of pores. In addition to its role of indirect regulation of osteoclasts through RANKL, rhBMP-2 can also directly stimulate osteoclast differentiation[11,14-16], and the concentration of rhBMP-2 must be maintained below a threshold to prevent excessive resorption. The results from this study suggest that the high dose of rhBMP-2 (400 μg/mL) is near this threshold, as evidenced by the relatively high frequency (~30%) of samples showing resorption gaps.

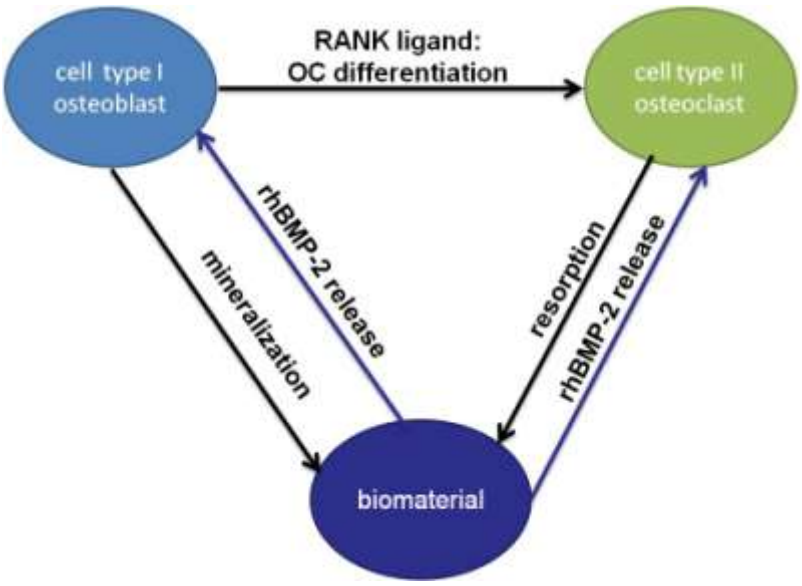

Figure VI.4: Critical interactions of AMBP/PUR putty.
An analogous "control loop" summarizing the critical interactions that occur during the remodeling of the AMBP/PUR putty with rhBMP-2 incorporation.

Interestingly, in this study the high dose was the typical dose for rabbits, suggesting that the release mechanism of rhBMP-2 from the biocomposite may reduce the minimum effective dose required to enhance bone healing.

Conclusions

Injectable allograft bone biocomposites supported bone remodeling with minimal resorption gaps in a rabbit femoral condyle plug model. Release of rhBMP-2 corresponding to 25% of the typical dose enhanced remodeling of the biocomposite, while some of the composites showed resorption gaps at the high dose of rhBMP-2 corresponding to the typical dose. These results suggest that the release efficiency of rhBMP-2 from the AMBP/PUR composites can reduce the dose of rhBMP-2 that yields optimal bone formation. Thus the allograft/polymer biocomposites may be a promising

approach for developing an injectable biomaterial that maintains its initial weight-bearing properties during remodeling.

REFERENCES

1. Haidar ZS, Hamdy RC, Tabrizian M. Delivery of recombinant bone morphogenetic proteins for bone regeneration and repair. Part A: Current challenges in BMP delivery. Biotechnol Lett 2009;31(12):1817-24.

2. Gautschi OP, Frey SP, Zellweger R. Bone morphogenetic proteins in clinical applications. ANZ J Surg 2007;77(8):626-31.

3. McKay WF, Peckham SM, Badura JM. A comprehensive clinical review of recombinant human bone morphogenetic protein-2 (INFUSE Bone Graft). Int Orthop 2007;31(6):729-34.

4. Han D, Liu W, Ao Q, Wang G. Optimal delivery systems for bone morphogenetic proteins in orthopedic applications should model initial tissue repair structures by using a heparin-incorporated fibrin-fibronectin matrix. Med Hypotheses 2008;71(3):374-8.

5. Smith DM, Cooper GM, Mooney MP, Marra KG, Losee JE. Bone morphogenetic protein 2 therapy for craniofacial surgery. J Craniofac Surg 2008;19(5):1244-59.

6. Miyazaki M, Morishita Y, He W, Hu M, Sintuu C, Hymanson HJ, Falakassa J, Tsumura H, Wang JC. A porcine collagen-derived matrix as a carrier for recombinant human bone morphogenetic protein-2 enhances spinal fusion in rats. Spine J 2009;9(1):22-30.

7. Garrison KR, Donell S, Ryder J, Shemilt I, Mugford M, Harvey I, Song F. Clinical effectiveness and cost-effectiveness of bone morphogenetic proteins in the non-healing of fractures and spinal fusion: a systematic review. Health Technol Assess 2007;11(30):1-150, iii-iv.

8. Dumas JE, Davis T, Holt GE, Yoshii T, Perrien DS, Nyman JS, Boyce T, Guelcher SA. Synthesis, characterization, and remodeling of weight-bearing allograft bone/polyurethane composites in the rabbit. Acta Biomater;6(7):2394-406.

9. Dumas JE, Zienkiewicz K, Tanner SA, Prieto EM, Bhattacharyya S, Guelcher SA. Synthesis and characterization of an injectable allograft bone/polymer composite bone void filler with tunable mechanical properties. Tissue Eng Part A;16(8):2505-18.

10. Bonzani IC, Adhikari R, Houshyar S, Mayadunne R, Gunatillake P, Stevens MM. Synthesis of two-component injectable polyurethanes for bone tissue engineering. Biomaterials 2007;28(3):423-433.

11. Smoljanovic T, Bojanic I, Bicanic G, Delimar D. Short-term osteoclastic activity induced by locally high concentrations of recombinant human bone morphogenetic protein-2 in a cancellous bone environment. Spine (Phila Pa 1976);35(5):597; author reply 597-8.

12. Suda T, Takahashi N, Udagawa N, Jimi E, Gillespie MT, Martin TJ. Modulation of osteoclast differentiation and function by the new members of the tumor necrosis factor receptor and ligand families. Endocr Rev 1999;20(3):345-57.

13. Marina IS, Rui LR. Vascularization in Bone Tissue Engineering: Physiology, Current Strategies, Major Hurdles and Future Challenges. Macromolecular Bioscience;10(1):12-27.

14. Kaneko H, Arakawa T, Mano H, Kaneda T, Ogasawara A, Nakagawa M, Toyama Y, Yabe Y, Kumegawa M, Hakeda Y. Direct stimulation of osteoclastic bone resorption by bone morphogenetic protein (BMP)-2 and expression of BMP receptors in mature osteoclasts. Bone 2000;27(4):479-86.

15. Itoh K, Udagawa N, Katagiri T, Iemura S, Ueno N, Yasuda H, Higashio K, Quinn JM, Gillespie MT, Martin TJ and others. Bone morphogenetic protein 2 stimulates osteoclast differentiation and survival supported by receptor activator of nuclear factor-kappaB ligand. Endocrinology 2001;142(8):3656-62.

16. Jensen ED, Pham L, Billington CJ, Jr., Espe K, Carlson AE, Westendorf JJ, Petryk A, Gopalakrishnan R, Mansky K. Bone morphogenic protein 2 directly enhances differentiation of murine osteoclast precursors. J Cell Biochem;109(4):672-82.

CHAPTER VII.

Conclusions

Polyurethane (PUR) composites derived from a lysine triisocyanate and polyester polyols have provided a versatile platform for a family of novel biomaterials for bone tissue engineering. Through the manipulation of system parameters such as filler, polyol molecular weight, porosity, and growth factor incorporation, these PUR composites displayed an array of both mechanical and *in vivo* remodeling properties. Furthermore, PUR composites can be utilized as either a prefabricated implant or an injectable two component system. Table 7.1 summarizes the platforms described in this work.

Table VII.1: Summary of PUR Composites

platform	porosity	filler	filler wt%	strength (Mpa)	modulus (Mpa)
implant	< 5%	HA/TCP	79%	107-172	3000-6000
implant	<5%	AMBP	79%	59.6-87	2500-3600
injectable	40-50%	AMBP	47%	1-13	7-400
injectable	<5%	AMBP	70%	24.2-28.1	357.3-503.0

Fabricated non-porous implants utilized a particulated phase of filler by meeting the random closed packing (RCP) limit of spheres (64 vol%). Compression molded calcium phosphate (CaP)/PUR composites exhibited mechanical properties suitable for weight-bearing applications and were shown to be biocompatible in both *in vitro* and *in vivo* studies. In a more extensive study on compression molded allograft mineralized

bone particle (AMBP)/PUR composites, mechanical properties were tuned by varying the molecular weight of the polyol used during synthesis. Furthermore, osteoclast-mediated resorption was shown to provide a pathway for cellular infiltration *in vivo*.

Injectable, porous, weight-bearing AMBP/PUR bone void filler (BVF) composites were synthesized by utilizing the carbon dioxide blowing reaction that occurs when isocyanates are exposed to water. Mechanical properties were tuned in this system with the ability to control porosity. Furthermore, working time and cure time were controlled by manipulating catalyst concentration. *In vivo* studies demonstrated that the pores in the AMBP/PUR BVF composite system provided a primary pathway for cellular infiltration while the AMBP provided a secondary pathway via osteoclast-mediated resorption. AMBP/PUR BVF composites demonstrated remodeling potential in the rabbit calvaria critical sized defect (CSD) model with a modest amount of new bone formation. When recombinant human bone morphogenetic protein (rhBMP-2) was incorporated in the AMBP/ PUR BVF composite, the amount of new bone formation was enhanced in the rabbit CSD calvaria model, suggesting that the system is an adequate delivery vehicle for growth factors.

Injectable AMBP/PUR putty supported bone remodeling with minimal resorption in a rabbit femoral condyle plug model. Release of rhBMP-2 corresponding to 25% of the typical dose enhanced remodeling of the biocomposite. Thus, the AMP/PUR putty could make a profound impact on the delivery strategies rhBMP-2 and other growth factors. The AMBP/PUR putty may be a promising approach for developing an injectable biomaterial that maintains its initial weight-bearing properties during remodeling.

The data from this work supports the use of lysine-based PUR as a treatment for craniofacial and orthopaedic defects. As it is injectable, this platform is attractive because it is minimally invasive. *In vivo* studies have demonstrated that they are osteoconductive. Furthermore, they exhibit osteoinductive properties with the incorporation and release of rhBMP-2. This platform could be used to fulfill the clinical need for treating challenging fractures in which traditional grafts fail to facilitate healing.

There are several opportunities for the continued evolution of this platform. The mechanical properties can be enhanced by the comminuted study of the interaction between the allograft bone and PUR phase of the composites since there are a myriad of agents that can be grafted on the surface of the bone. Also, a further investigation of the *in vivo* release kinetics of rhBMP-2 from the PUR composite platform could lead to further optimization of the material. Implantable PUR scaffolds without AMBP have been fabricated successfully as a dual delivery system for rhBMP-2 and antibiotics. Thus, the dual delivery of such biologics from the AMBP/PUR composites would be a significant accomplishment in the treatment of wounds that are infected (e.g., battlefield injuries), which compromises the normal healing.